Forty-Year "Drift" and Change of the SAA

E.G. Stassinopoulos, M.A. Xapsos, C.A. Stauffer

NASA STI Program ... in Profile

Since its founding, NASA has been dedicated to the advancement of aeronautics and space science. The NASA scientific and technical information (STI) program plays a key part in helping NASA maintain this important role.

The NASA STI program operates under the auspices of the Agency Chief Information Officer. It collects, organizes, provides for archiving, and disseminates NASA's STI. The NASA STI program provides access to the NASA Aeronautics and Space Database and its public interface, the NASA Technical Report Server, thus providing one of the largest collections of aeronautical and space science STI in the world. Results are published in both non-NASA channels and by NASA in the NASA STI Report Series, which includes the following report types:

- TECHNICAL PUBLICATION. Reports of completed research or a major significant phase of research that present the results of NASA Programs and include extensive data or theoretical analysis. Includes compilations of significant scientific and technical data and information deemed to be of continuing reference value. NASA counterpart of peer-reviewed formal professional papers but has less stringent limitations on manuscript length and extent of graphic presentations.

- TECHNICAL MEMORANDUM. Scientific and technical findings that are preliminary or of specialized interest, e.g., quick release reports, working papers, and bibliographies that contain minimal annotation. Does not contain extensive analysis.

- CONTRACTOR REPORT. Scientific and technical findings by NASA-sponsored contractors and grantees.

- CONFERENCE PUBLICATION. Collected papers from scientific and technical conferences, symposia, seminars, or other meetings sponsored or co-sponsored by NASA.

- SPECIAL PUBLICATION. Scientific, technical, or historical information from NASA programs, projects, and missions, often concerned with subjects having substantial public interest.

- TECHNICAL TRANSLATION. English-language translations of foreign scientific and technical material pertinent to NASA's mission.

Specialized services also include organizing and publishing research results, distributing specialized research announcements and feeds, providing help desk and personal search support, and enabling data exchange services. For more information about the NASA STI program, see the following:

- Access the NASA STI program home page at http://www.sti.nasa.gov

- E-mail your question via the Internet to help@sti.nasa.gov

- Fax your question to the NASA STI Help Desk at 443-757-5803

- Phone the NASA STI Help Desk at 443-757-5802

Forty-Year "Drift" and Change of the SAA

Epaminondas G. Stassinopoulos, Emeritus
NASA's Goddard Space Flight Center, Greenbelt, MD

Michael A. Xapsos
NASA's Goddard Space Flight Center, Greenbelt, MD

Craig A. Stauffer
AS and D, Llc., AS and D- Inc Beltsville, MD

National Aeronautics and
Space Administration

Goddard Space Flight Center
Greenbelt, Maryland 20771

Decemember 2015

Forty-Year "Drift" and Change of the SAA

E.G. Stassinopoulos
M.A. Xapsos
C.A. Stauffer

Abstract

1.   A comprehensive study was conducted to evaluate the change in the location and size of the South Atlantic Anomaly (**SAA**) as a function of time, primarily in relation to trapped Van Allen Belt proton populations. The study was limited to one altitude only (800 km), which is still within the Earth's atmosphere but is removed from the atmospheric cut-off level located at about 100-200 km.

Introduction

2.   Since its recognition and acknowledgement as an area of great importance to the space program, particularly for Low Earth Orbits (**LEO),** the **SAA** has been the subject of much published research. Studies in the literature have dealt with the **SAA**'s drift, size, area, strength, and change. However, most of these publications have been based on data generated by diverse instruments, designed for research projects unrelated to the **SAA** and demonstrating varying degrees of sensitivity, accuracy, reliability, and efficiency. Most of the observations have therefore been peripheral and incidental and could not be expected to correctly and precisely define the size, form, area, strength, motion, or drift of the **SAA**, or to have solved the problem of its existence, evolution, variability, and future.

3.   Incidental information about the anomaly that can be gleaned from these sources, should be taken into account, but cannot be considered a full or valid definition, description, or model of the **SAA,** as is aptly demonstrated by the significant variations and discrepancies in the reported results and conclusions. Additionally, many **SAA** related publications have shown inconsistencies in reference to the geomagnetic field, the trapped particle models, and the relationship between them.

4.   The **SAA** is really not an "anomaly" at all, but an apparent local depression of the Earth's magnetic field. When first observed, the **SAA** was considered an "anomaly" of the field, an aberration [1]. Later, the **SAA** was defined as stemming from the tilt, the eccentricity, and the displacement of the dipole axis from the center of the Earth i.e. the **SAA** is determined by **(a)** the tilt of the magnetic dipole axis to the axis of rotation (approximately ~11 degrees), **(b)** and is considered eccentric because it does not pass through the center of the planet, and **(c)** is displayed (by about 500 km) away from the center towards the North Pacific, thus producing a weaker magnetic field over Brazil and a stronger field over the North Pacific. As a result of these conditions, the Earth-size magnetic unit-sphere lies outside the northern physical Earth over the Pacific, which is closer to the magnetic center, resulting in a higher local field strength at the surface of the globe, and inside the physical Earth over the south Atlantic, which is farther away from the magnetic center, with a lower field strength at the local surface of the globe. A uniquely different explanation for the existence of the SAA was given in one of the reviewed papers.[1]

---

[1] Quote from APPENDIX A [4b]: "*The anomaly arises from the eccentric displacement between* **the magnetic and geographic poles** *of the Earth ....*"

5.   The Earth's magnetic field is a combination of **(a)** a major dipole term, and **(b)** of minor quadrupole and higher order components. The major dipole term of the magnetic field has a strong radial dependence, dropping off inversely with the cube of the distance, as $\mathbf{B_r = B/r^3}$, whereas the non-dipole terms drop off inversely with the fourth power of the distance, and the dipole potential drops off as $1/r^2$. The currently most widely used standard model for the magnetic field, globally, is the officially established "*International Geophysical Reference Field*" (**IGRF**), that is issued every five years by the "International Association of Geomagnetism and Aeronomy" (**IAGA**) [2]. The **IGRF** models contain first and second order time derivatives for temporal extrapolations, and are limited to a maximum of 5 years, because longer extrapolations introduce unacceptable errors and uncertainties in the results. Each new 5-year model is based on current global measurements, correctly accounting for the changes in the magnetic field for the 5-year period. A striking example of calculations, which vastly exceed the limits of the field model projection-validity by several decades, is given in the frequently- cited publications in the Footnote.[2,3,4]

6.   The Earth's magnetic field experiences two slow but important variations with time: **(1)** the drift of the magnetic poles and **(2)** the secular variation of the field, a gradual, continuous, long range trend of decreasing strength. The rate of change, of both variations, is not constant. Thus, the drift of the north Magnetic Pole has increased over the last century and may change again in the near future. It is currently moving at about 40 km per year towards Siberia.

7.   As mentioned in paragraph #6 above, the secular variation, expressed by the first and second derivatives of the standard **IGRF** models, has been on a decreasing trend in terms of field strength for several centuries [3] (Figures 1-9). This decreasing trend, with a varying rate, expressed as the magnetic moment of the field, is plotted as a function of time in Figure 10 for the period of interest of this study, i.e. 1970 to 2010.

---

[2] **Quote** from APPENDIX A [12a]: *"The calculations presented here will be based on the IGRF for 1975 and fluxes of protons with energies above 30 MeV as represented by AP8MIN.------- Figure 1 shows B and L contours in the SAA at 500 km altitude for epochs 1965(a), 1995(b), and 2025(c)."*

[3] **Quote** from APPENDIX A [14b]: *"The most likely secular variation of the geomagnetic field is estimated and used to extrapolate the geomagnetic field to the year 2100."*

[4] **Quote** from APPENDIX A [14e]: *"If the map of secular change from the IGRF coefficients (Figure 6) is used to extrapolate from 1995 to 1922 the charts compare favorably in the South Atlantic."*
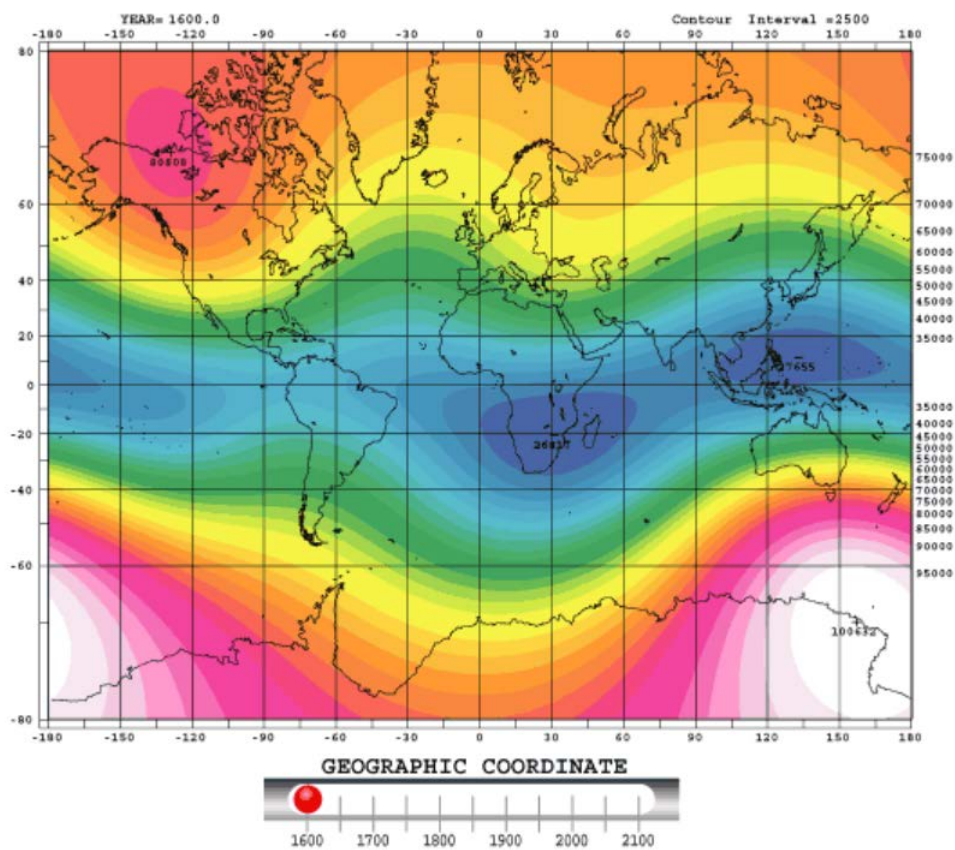
Figure 1: Year 1600.
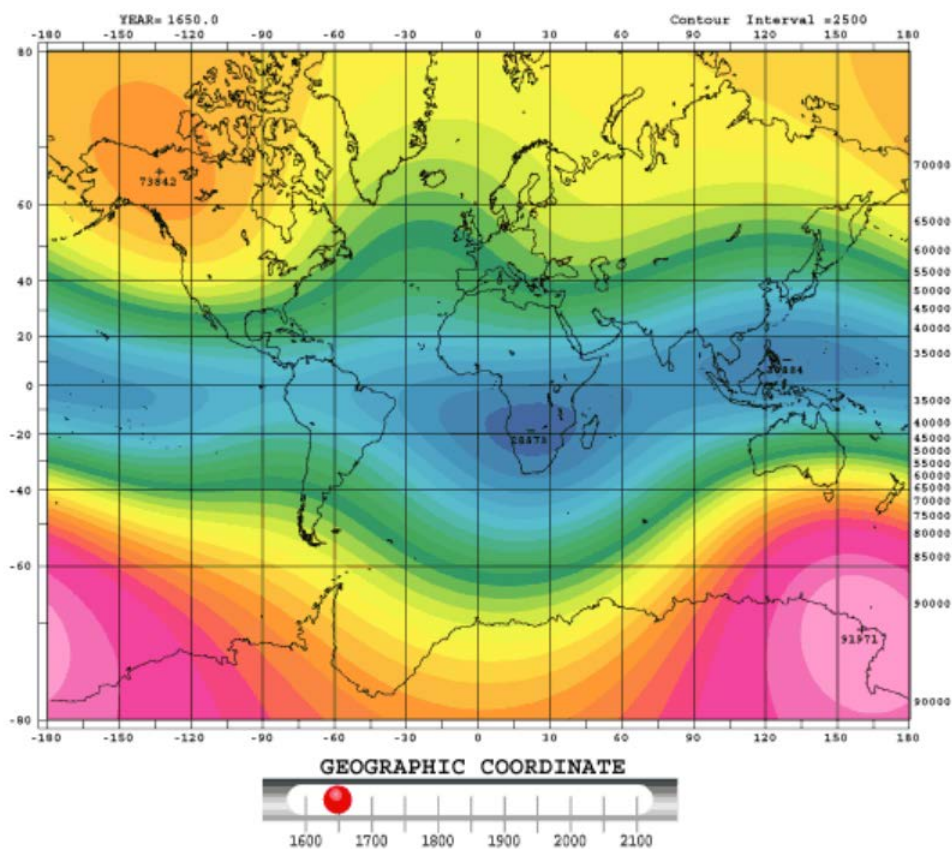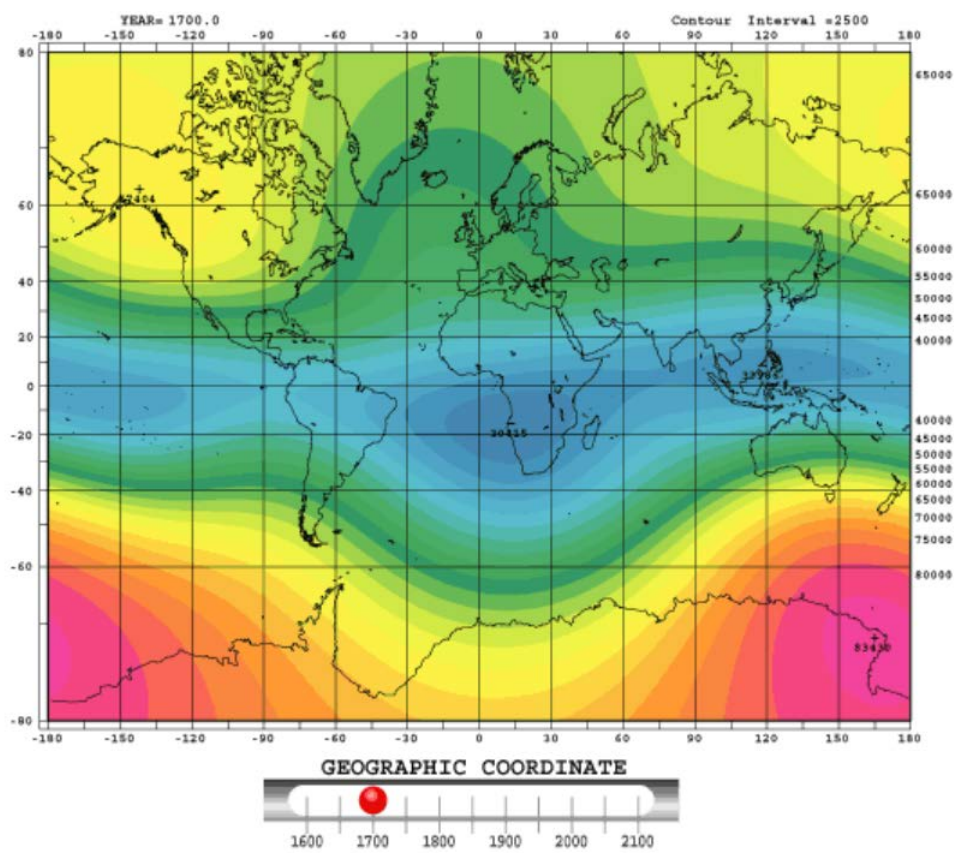

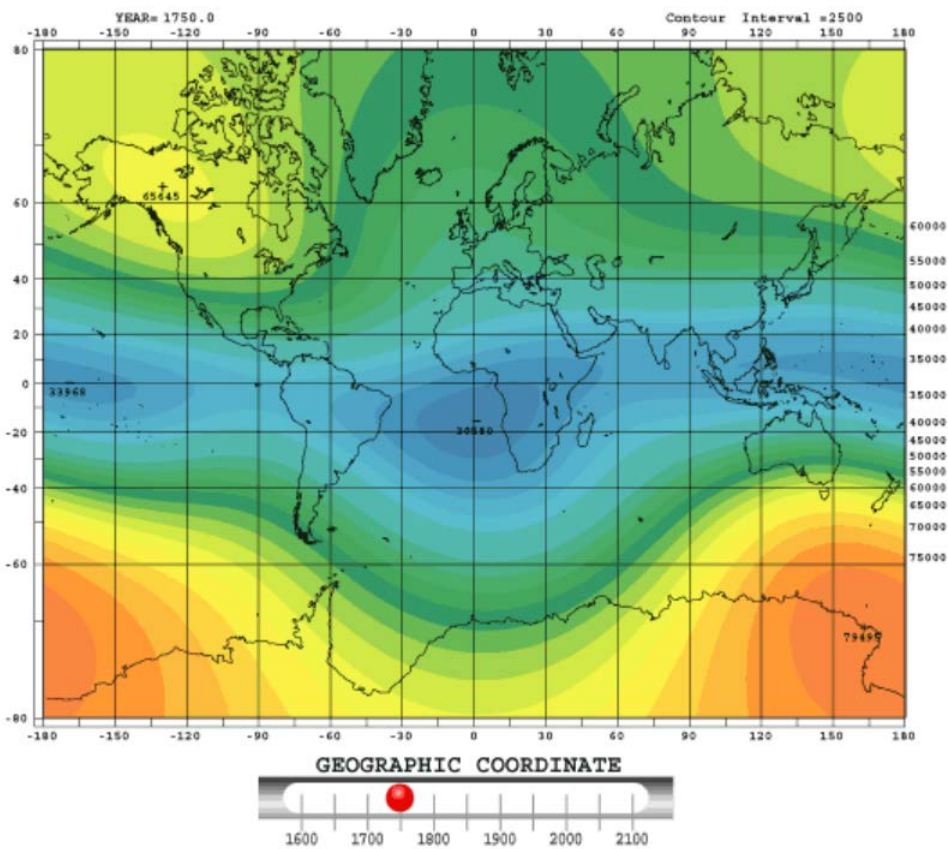
Figure 2: Year 1650.
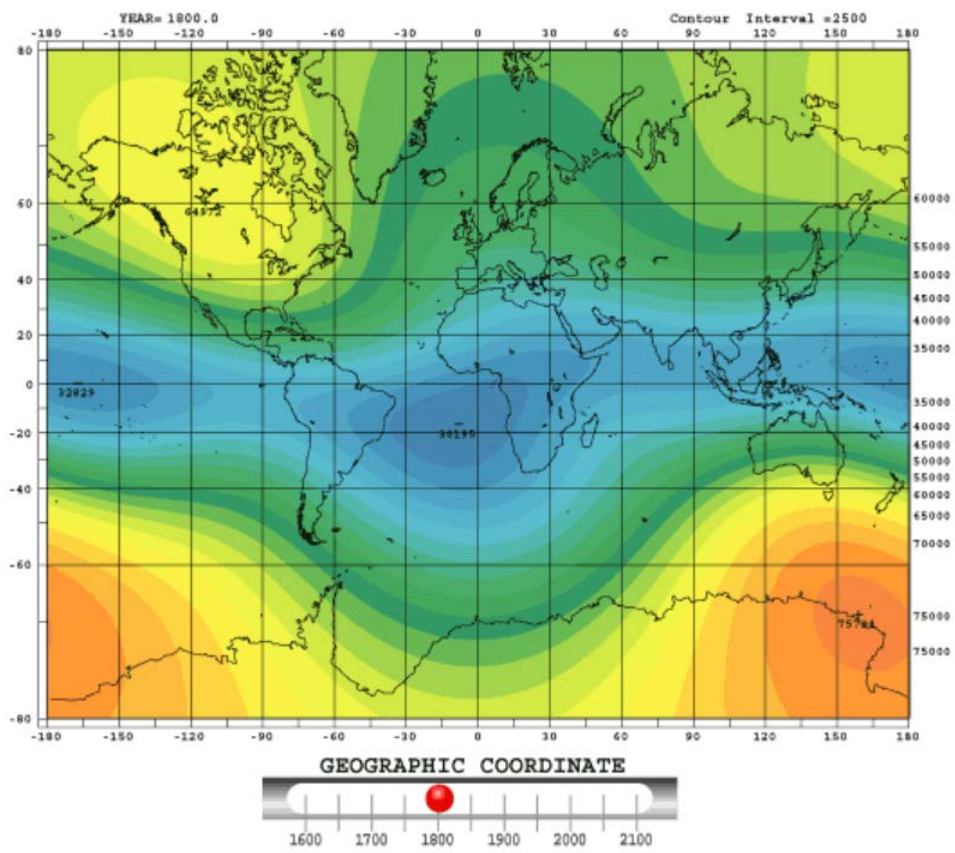
3

Figure 3: Year 1700.
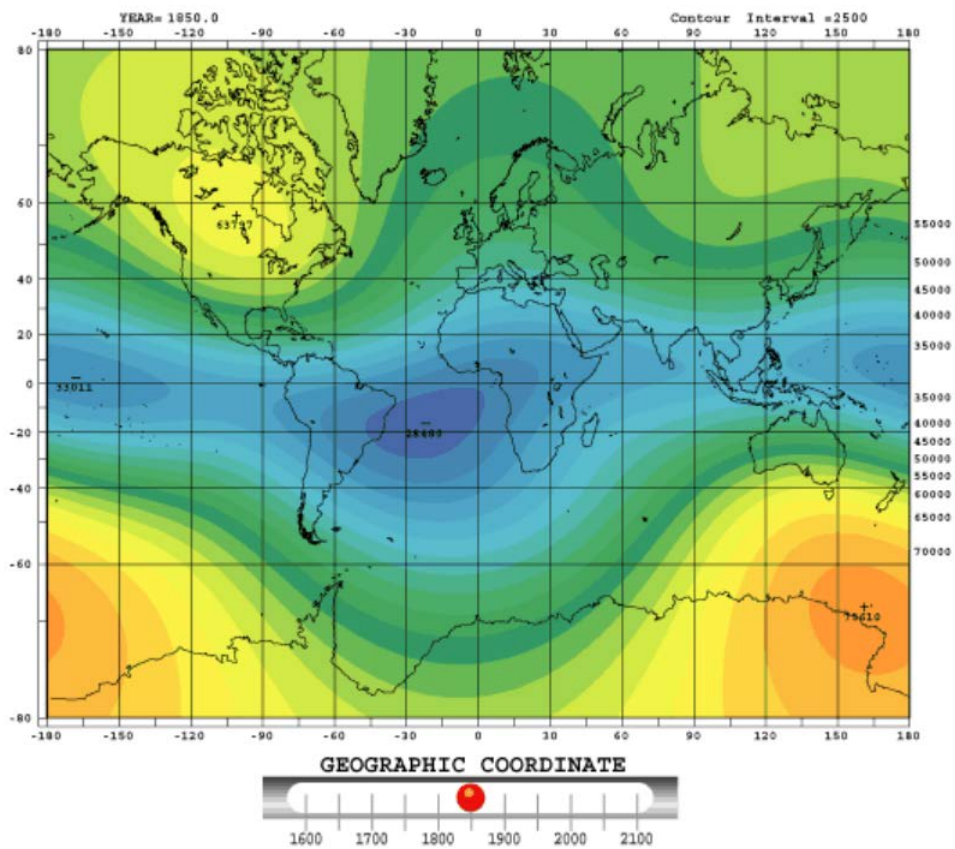

Figure 4: Year 1750.

4

Figure 5: Year 1800.
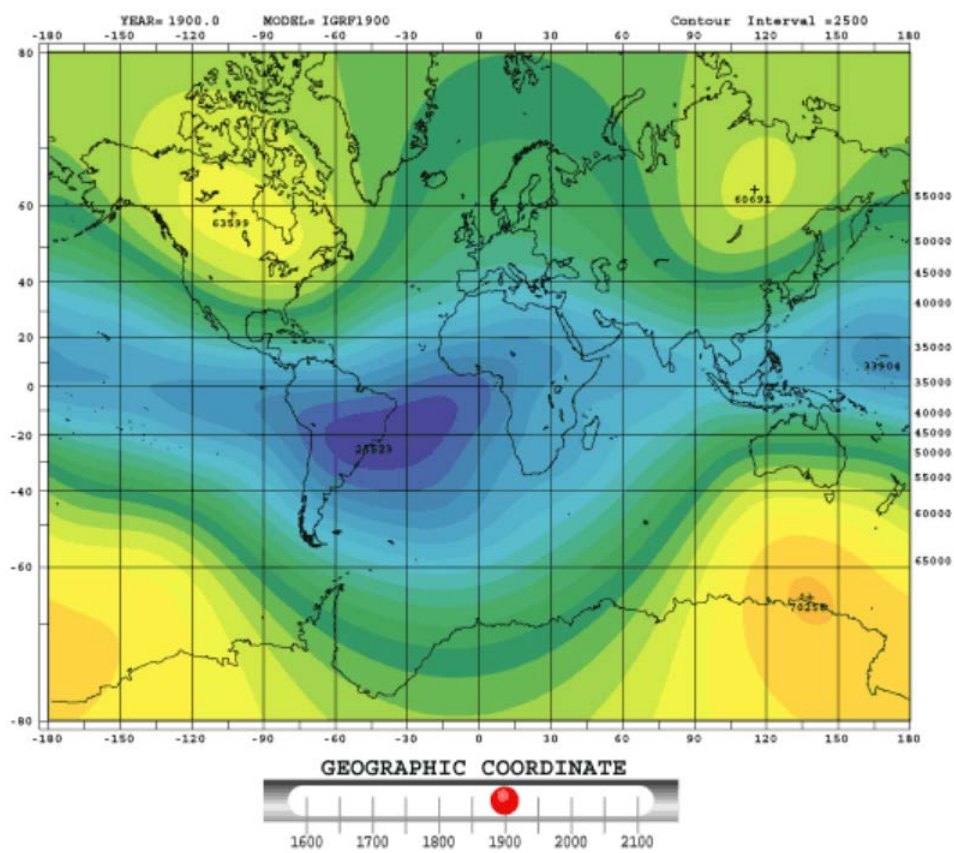

Figure 6: Year 1850.
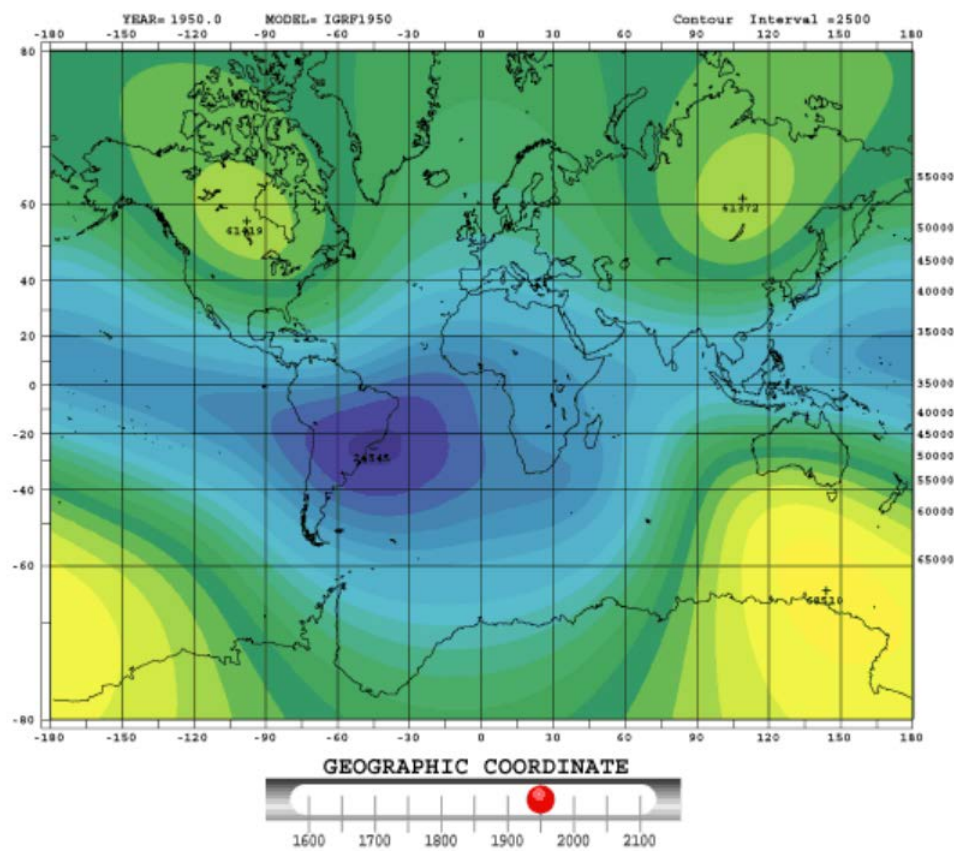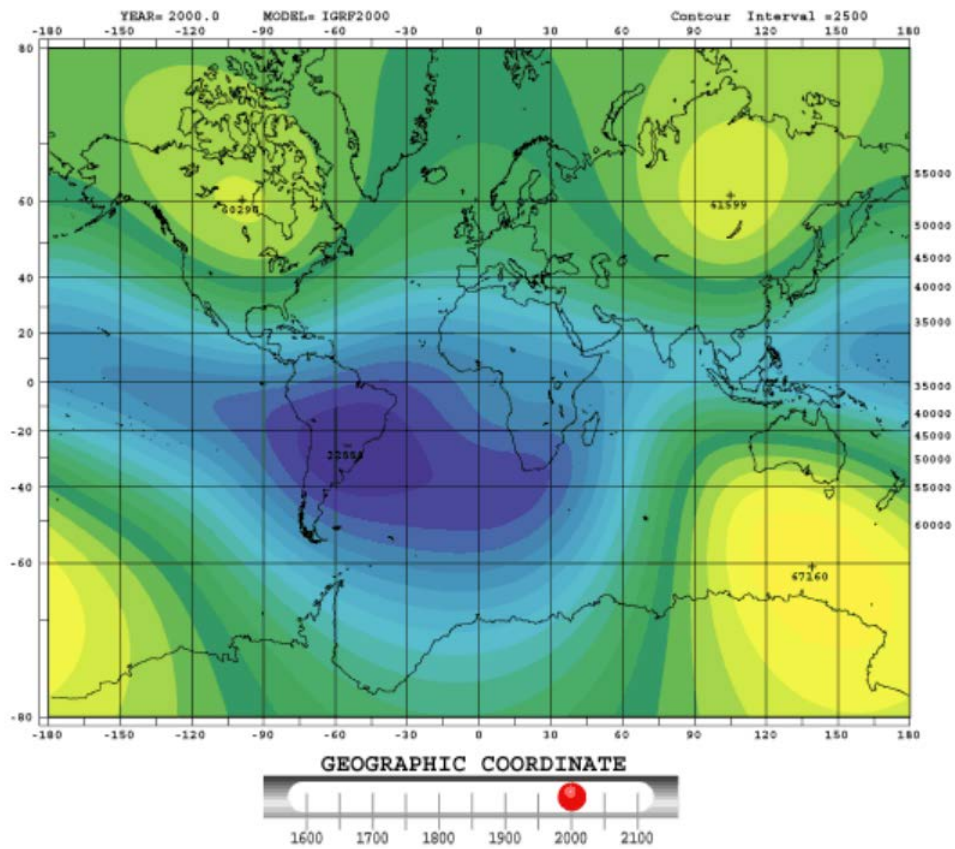
Figure 7: Year 1900.

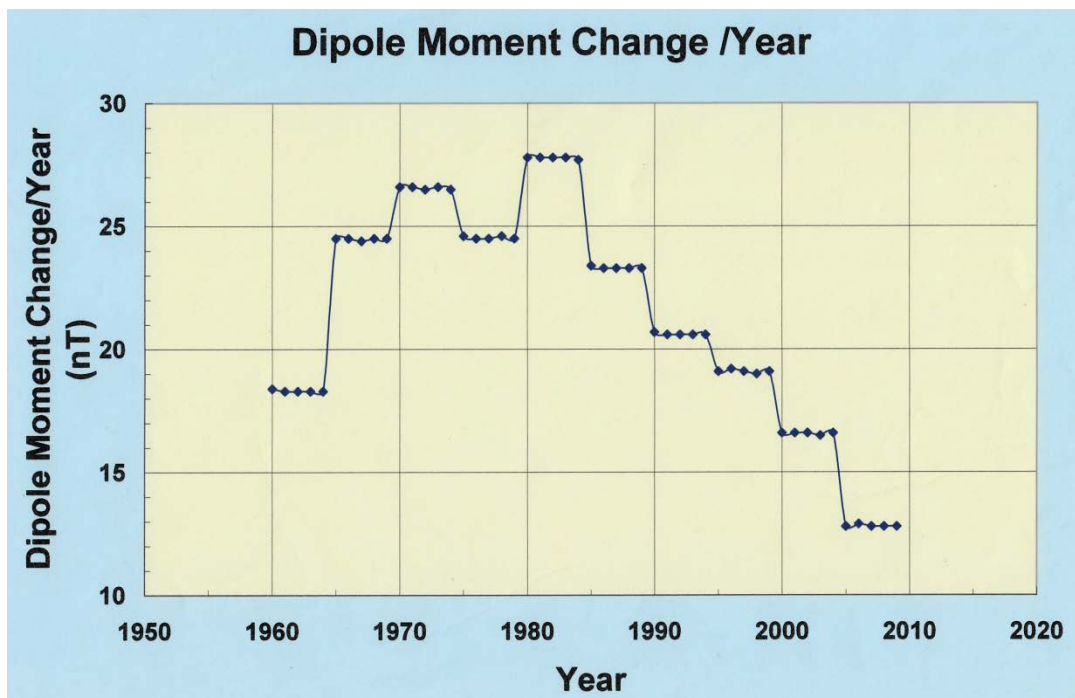Figure 8: Year 1950.

Figure 9: Year 2000.

Figure 10: The change/year of the Earth's dipole moment.

8.   Based on calculations performed with the **IGRF** models, the **SAA** has "drifted" primarily west-northwest and to a lesser extent north-northeast, over the four decades considered in this analysis. From these calculations, though, the **SAA** appears to have only "expanded" in area into those directions, at all altitude levels and for all proton energies, and not drifted in totality. The **SAA** has also extended a narrow pointed protrusion toward the east, centered at about 20 degrees south geographic latitude, i.e. in the opposite direction from the "drift". What has actually "drifted" is the peak proton flux position within the frame of the **SAA**, which, of course, is of major importance to Low-Earth Orbiting missions (**LEO**).

9.   Before addressing in more detail the issue of the "drift" of the **SAA**, some helpful background information and definitions are in order, which may provide explanations for some of the varied questions, assumptions, and conclusions encountered frequently in the referenced literature.

10.   Several papers have been published, dealing with the "*Drift of the SAA*". Most of these reports were based on measurements obtained from instruments not specifically designed or dedicated to: **(a)** the study of trapped radiation levels (electrons and/or protons) within the **SAA**, **(b)** systematically evaluate the effects of these particles on electronic systems, instruments, or components, or **(c)** focusing on identifying the causes of the changes in the size, area, and drift of the South Atlantic Anomaly. Nevertheless, single event effects and total doses experienced in the **SAA** have been frequently mentioned in many of these papers

11.   Such usually unrelated measurements of opportunity, however, may not accurately reflect the actual and correct shape and location of the **SAA**. The most important parameter that defines the domain of the **SAA** and the changes in its location with the passing of time, is the main dipole field, which has frequently been neglected, overlooked, or ignored, while this role has been assigned, in some publications, to the minor non-dipole field. In addition, the existence, shape, size, and drift of the **SAA** are not controlled or influenced by the presence, absence, distribution, or intensity of the particle radiation within its domain. Particles don't define the **SAA**, which as a local magnetic depression, would still exist and change with time, even if there were no particles present at all.

12.   Another comment frequently encountered in the reviewed literature is the reference to the effect of the non-dipole field on the **SAA**, which by some is considered to be a major force driving the changes. But in regards to the existence and evolution of the **SAA** and the corresponding trapped radiation levels, the non-dipole field is, at best, of small significance, in comparison to the main dipole field. All of the **SAA's** trapped particles are part of the inner zone of the Van Allen belts, and are hundreds to thousands of kilometers removed from the Earth's surface, whereas most non-dipole field measurements are made on or near the surface. Non-dipole field values decline rapidly as altitude increases, dropping off with a rate inversely related to the fourth power of the distance, whereas the dipole field changes as $1/r^3$. Hence the effects of the non-dipole field are of minimum importance to the intensity level and location of the trapped, as well as the transiting, particle radiation, within the magnetosphere and the inner zone of the Van Allen belts.

13.   Other causes, such as, Space Weather events, solar flares, coronal mass ejections, magnetic storms, atmospheric conditions, and geomagnetic jerks, could briefly affect the **SAA**'s particle population and the magnetic field, and could produce small, short, and mostly localized variations in the field strength. But such brief, minor, and locally-restricted excursions, although scientifically valuable and important, do not significantly affect the prevailing basic shape and position of the **SAA**, or its long-range evolution, and therefore have been ignored for the purpose of this study.

14.   A review of several dozen published papers dealing with the anomaly, indicated that the measurements (i.e. the data) which were used in the attempts to describe the **SAA**, were obtained from a variety of instruments, detectors, or parts, each of which had a different sensitivity, resolution, and accuracy in performance and calibration, These data were also obtained over different epochs and time intervals (duration), for missions with varying trajectories (inclination, altitude, eccentricity, etc.). It is to be expected that this variety of conditions, produces numerous results and conclusions that may not reflect accurately the true shape and position of the **SAA**, nor to effectively predict and describe the dynamics of its existence, which remains mainly a function of the dipole field. In addition, many instances have been noticed, in which problems have been identified relating to **(a)** instruments and their calibration, **(b)** detectors and their sensitivity or performance, **(c)** orbital trajectory generation, **(d)** data contamination, **(e)** data analysis and processing issues, **(f)** field model selection and coordinate conversion, **(g)** flux calculations from models, **(h)** drift of the **SAA**, **(i)** origin of the **SAA**, etc. Some examples of these problems are provided in **Appendix A**.

The Magnetic Field and its Effects

15.   The solar wind encounters the Earth's magnetic field and creates the geomagnetic cavity that defines the terrestrial magnetosphere (Figure 11). The interaction of the solar wind with the magnetosphere sets up a multitude of currents. The sum of those currents represents the external magnetic field of the Earth. The external field is vectorially superimposed onto the internal field of the Earth. The combination of the two then becomes the total field which experiences:
  * slow changes in the internal field (long-term effects), and
  * fast changes in the external field (short-term effects).
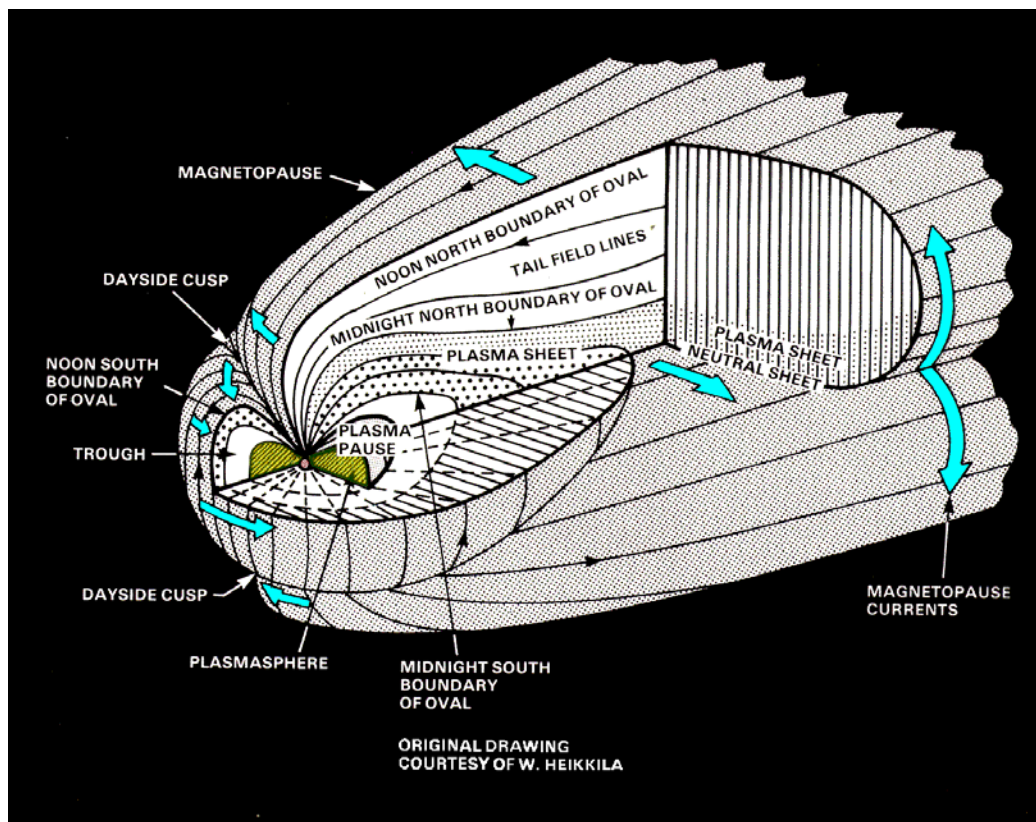
Figure 11: The Earth's magnetosphere as sculpted by the solar wind.

9
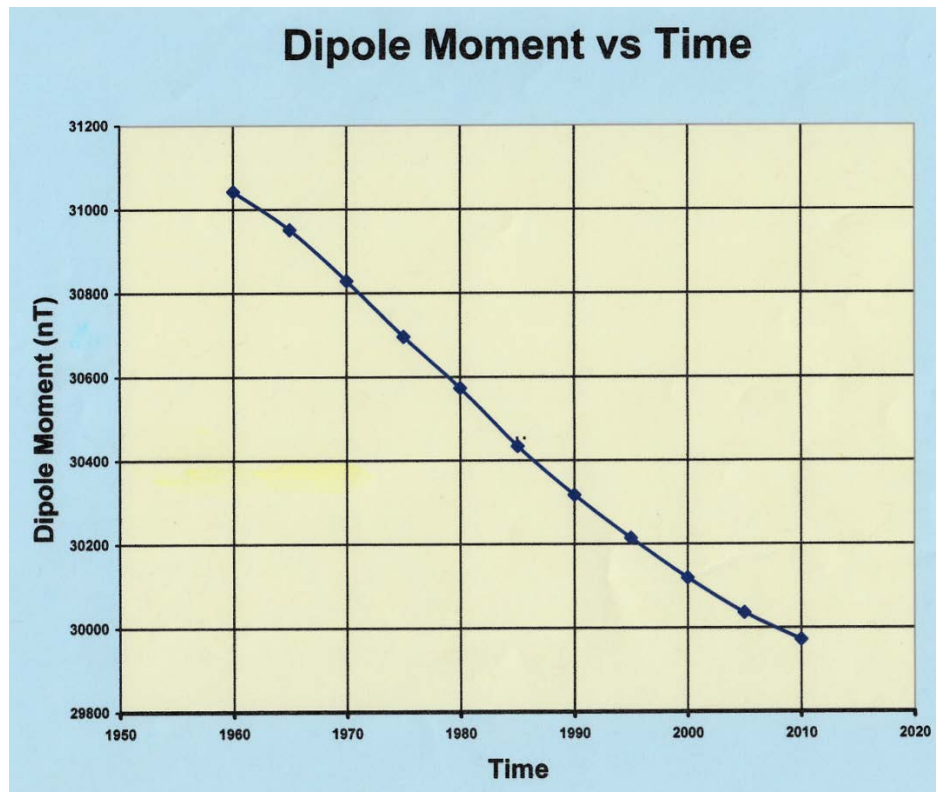
Figure 12: The long-term change of the Earth's dipole moment

16.   The fact that the internal field is slowly changing, can be observed in two important ways:
  • the drift of the magnetic poles and
  • the shrinking of the field strength.
The rate of change of both of these variation is not constant in time,
The rate at which the internal field changes is called the "Secular Variation". If the shrinking were to continue at the present rate, the Earth could experience another magnetic reversal in about two thousand years (see **Appendix D** for calculations). Short and rare disturbing events, such as geomagnetic jerks, can alter prevailing normal conditions, and cause minor magnetic reversals, which cannot be predicted in terms of frequency or intensity, and which, like **CME'**s, solar flares, and earthquakes, cannot be modeled easily or reliably, so as to be of practical use to scientists, engineers, and managers of the space program.

17.   The trend of the secular variation of the internal field, mentioned earlier in paragraph #7, is indicated in Figure 10 by the magnetic moment, plotted as a continuous function of time for the period of interest to this study. The corresponding rate-change per year is shown in Figure 12, where the magnetic moment obtained from the **IGRF** models, is plotted versus time.

18.   Several external field models also exist. Two of the earliest and most popular models were the Mead-Fairfield [4] and the Olson-Pfitzer [5] versions. These were later superseded by the more sophisticated and improved Tsyganenko models [6, 7] that are now being widely used by the international scientific community.[5]

---

[5] External field model effects were not considered in this review as they have no impact on the field strength in the domain of the SAA. Their impact is only significant at distances greater than 4 Earth radii (at **L**-shells >4).

19.   Fast changes of the <u>total field</u> are caused by strong and rapid modulations of the external field, resulting from three dynamic and complex processes that cause rapid short-term changes in the orientation and magnitude of the external field.

    a.   The first process pertains to the interplanetary medium in which *convection* transfers solar wind mass, energy, and electric field into the magnetosphere,

    b.   The second process deals with the magnitude and orientation of the interplanetary field which *induces* dynamic changes in the magnetosphere, resulting in magnetic storms, and

    c.   The third process involves diurnal rotation and yearly orbital motion (dipole wobbling).

20.   The gradual and slow secular-variation changes of the internal field are accompanied by a long term movement (drift) of the magnetic poles. This is shown for the "**N**orth **M**agnetic **P**ole" (**NMP**) in Figure 13, in which the path of the **NMP**, since its discovery in 1831, has been plotted. During the last century, the pole has moved a remarkable 1000 km. Since 1970, the **NMP** movement has accelerated and is now drifting at more than 40 km per year. Furthermore, superimposed on the polar drift and on the secular variation of the field, is the diurnal motion in the position of the magnetic pole. Figure 14 shows the 24-hour path of such a motion.

Figure 13: Term movement of the north magnetic pole.

11

Figure 14: Diurnal variation of the north magnetic pole.

21.   A further concern of high altitude balloon projects, which have to deal with atmospheric or space radiation, is the effect of a diurnal variation in the value of the magnetic shell parameter **L**, particularly at high latitudes and/or high altitudes. An example of the range of this variation, at a sample position, is shown in Figure 15 for a quiet environment (**Kp = 0.0**), at a high latitude and an altitude of 36 km, for epoch 2001. The variation in **L** is significant, ranging from 7.8 to 10.5 r_e.
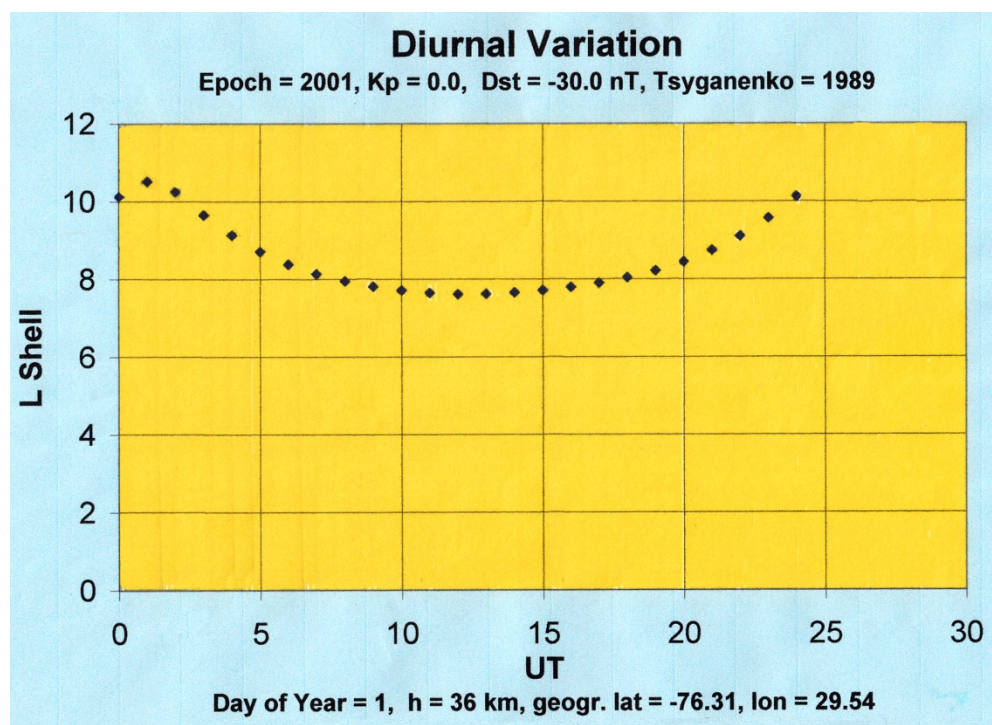
Figure 15: Diurnal variation of magnetic shell parameter **L**.

Dose Calculation Methods

22.   In dealing with radiation measurements, another area of concern and source of possible errors and discrepancies may be the method by which dose levels on sensitive targets within near-Earth orbiting satellites, frequently mentioned in the referenced literature regarding the **SAA**, are calculated from the spacecraft surface-incident space radiation. A quick and simple method, widely used in the past, is the popular **SHIELDOSE** code [8], which does not involve elaborate solid angle sectoring or 3-D ray tracing techniques, and considers only "slab" and "spherical" geometries (Figure 16). More elaborate codes such as **NOVICE** [9] or **GEANT-4** [10], have also been widely used to obtain results with greater accuracy and detail.

CASE 1.   SEMI-INFINITE MEDIUM; ABSORBED DOSE IN DETECTOR DENOTED AS $D_{\infty}^{det}(z)$

CASE 2.   FINITE-THICKNESS SLAB; ABSORBED DOSE IN DETECTOR DENOTED AS $D_s^{det}(z)$

CASE 3.   SOLID SPHERE; ABSORBED DOSE IN DETECTOR DENOTED AS $D_\bullet^{det}(z)$
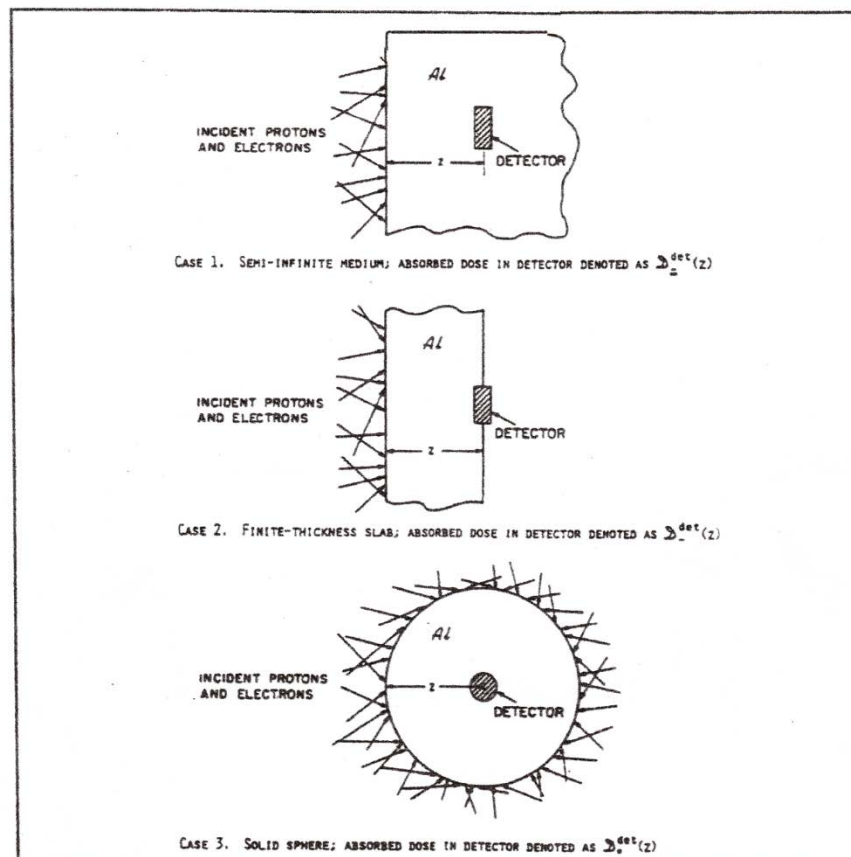
Figure 16: Geometries used for dose calculations.

23.   It should be noted that dose calculations for both slab and spherical shields (for a 4-pi exposure) performed with the same given set of radiation data, will typically yield different results. The spherical shield dose will be larger than the slab dose. For example, at a shield thickness of 200 mils, the difference for electrons will be a factor of approximately 6, as shown in Figure 17 [8]. Since spacecraft geometries are neither slabs nor spheres, the actual dose on a target inside the vehicle will be greater than slab but less than sphere predictions. In any given case, the reality will usually lie between these two extremes, as shown in Figure 18 for the polar orbit of the **NPOESS** (**NPP**) mission through the **SAA,** at approximately 800 km altitude
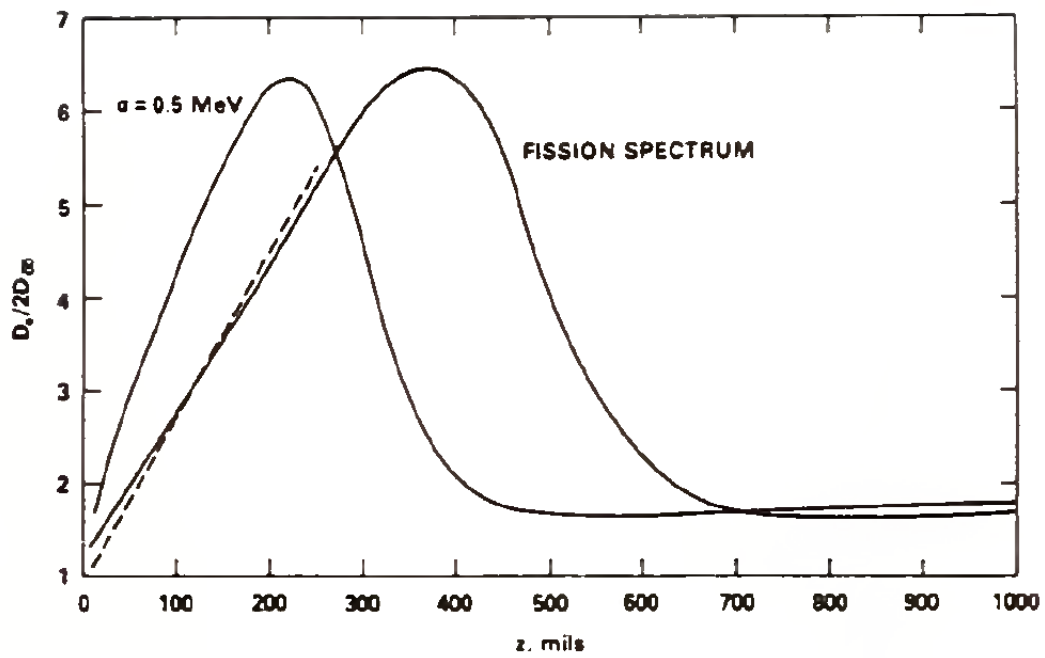
Figure 17: Ratio of electron dose at center of aluminum sphere to twice the dose in a semi-infinite aluminum medium.
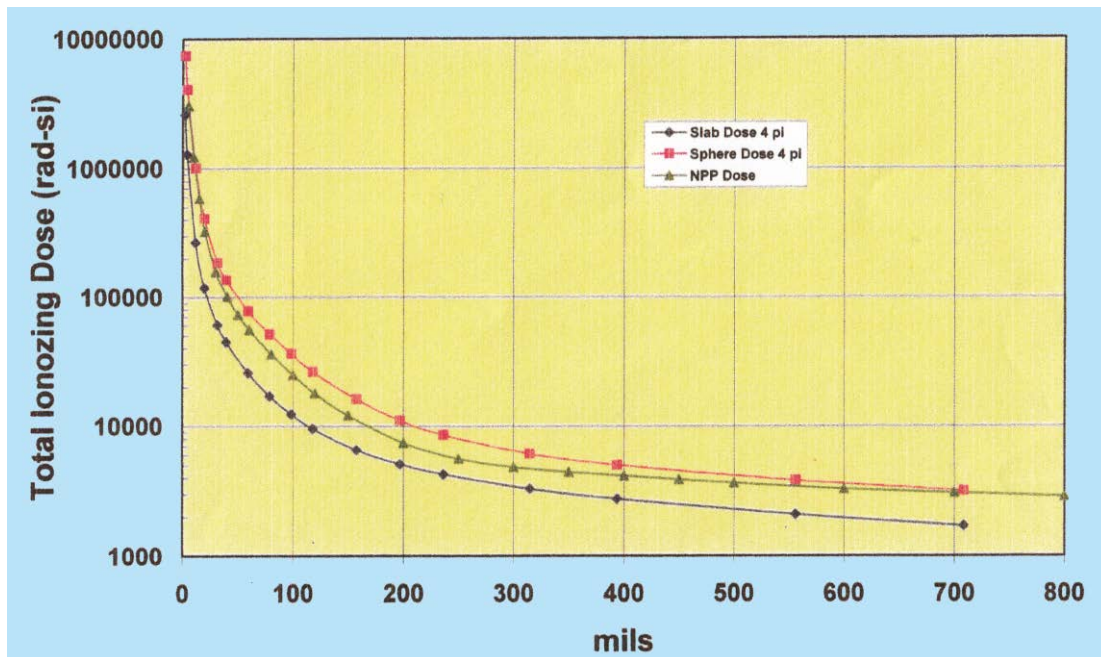
Figure 18: Total dose vs Al shield thickness.

Quality of Dose Data

24.	With the great variety of instruments involved in measurements some data from the SAA show noticeable variations for equivalent positions and times. This can happen for many reasons, such as: **(a)** varying sensitivity and response of detectors, **(b)** their calibration, **(c)** their geometric factor, **(d)** their threshold energy, **(e)** interference or contamination, **(f)** data analysis and processing method, etc. However, when evaluating sets of data for the same target and for the same conditions, particularly when comparing dose data with similar results obtained from other sources, small differences of up to 50%, or even factors of two or more, are quite common, because they reflect mostly minor variations in initial conditions, parameter definitions, accuracy of computations, and a multitude of other causes. Examples include:

1. The quality of the orbit generator that was used to obtain the trajectory of the spacecraft [11].[6]
2. The applied orbit integration step-size; that is, the density of trajectory positions used to evaluate the satellite's radiation exposure.
3. The magnetic field model used to convert positional geographic to magnetic coordinates.
4. The reference epoch of the field model (year) and the updating to the mission date (with the secular variation terms of the model).
5. The influence of solar cycle activity.
6. The efficiency, sophistication, and complexity of the radiation transport code that propagates the energetic particles through the shield(s) to the target.
7. The shield geometry, for example: spherical vs. slab (see the comments in paragraph #17)
8. Minor variations in shield composition, e.g. pure aluminum vs. aluminum alloy.
9. Minor variations in target composition, e.g. pure Si vs. SiO_2.
10. A small difference in the slab shielding results if the target is assumed to be embedded within the slab (e.g.: Case 1, in Figure 16, [8] vs. behind the slab (e.g.: Case 2, in Figure 16, [8].
11. The inclusion (or omission) of the smaller contribution to the total doses from the penetrating Bremsstrahlung (braking radiation) that is generated by the slowing of the electrons in the material surrounding the target.
12. Solar proton contributions that have been included in the calculations, by the confidence level considered: the probability that the predictions will not be exceeded by actual events.
13. The uncertainty factor of the standard radiation models which may or may not have been applied to the results.
14. The fact that margins are occasionally applied to the results of calculations for projects or missions with sensitive components.

However, in some cases, data concerning the **SAA**, collected from a variety of different instruments, can be **significantly** different, even for similar basic conditions. This may be due to detector: **(a)** sensitivity and response, **(b)** calibration, **(c)** geometry factor, and **(d)** contamination [noise, interference], as well as the data processing and analysis efforts.

---

[6] **Quote** from APPENDIX A [1a]: *"The position of RHESSI in latitude, longitude, and altitude is calculated via two different algorithms. The first algorithm has three faults: (a) <u>sometimes no numerical value is given at all</u>, (b) on other occasions, the derived altitude is suggested to be constant, equal to 6378.13 km for a while, <u>being obviously wrong</u>, and (c) the third defect is more delicate: <u>the satellite seems to jump occasionally from its orbit</u> at 540 km to 600 km to less than 500 km and back again within short time, <u>which is rather unrealistic behavior for a spacecraft</u>"*.

Space Radiation Models

25.   In all the **SAA** studies reviewed, for comparison with on-orbit measurements, frequent references are made to the standard **NASA AP8** (proton) and/or **AE8** (electron) Van Allen Belt radiation models [11], that have been used for many years to calculate satellite exposure predictions. Both types are published in two versions: for solar minimum and solar maximum conditions. These series have been the best available models since the mid-1960s. However, the modeling of space radiation data is not an exact science. The static models are commonly constructed by combining a number of measurements obtained from different spacecraft, and acquired with different instruments, at different times, and at different locations. These data are then combined to produce an approximation of the environment at a specific period of time, as determined by the range of the measurements. It is not uncommon to have data sets of electrons or protons that fortuitously share similar basic times and locations of acquisition, but diverge significantly in the magnitude of their measurements (by factors of 2 to 10), due to instrument sensitivity, calibration, or efficiency factors.

26.   These differences may also be due to many other factors, including variations in instrument design, positional inaccuracy, and data processing conditions. Some of the challenges include:
   1.   correctly defining the location of each measurement in magnetic or geographic coordinates
   2.   the selection of the magnetic field model used in the specific process
   3.   the instrument calibration and efficiency factors, and
   4.   the data analysis efforts.

27.   Comparing calculated space radiation data from several sources, whether in the form of fluxes, of accumulated doses, or effects on electronic systems, may often show large differences that cannot easily be reconciled. These differences may sometime be due to the omission or the application of the intrinsic "Uncertainty Factors", attached to the radiation models (x2 for protons and x2-5 for electrons).

28.   A new set of trapped radiation models, AP9 and AE9, is available for use while being further developed (Ginet [23]). The fundamental approach of these models is different in that it is Monte Carlo based and represents the radiation belt dynamics in a statistical way, thus allowing results to be calculated for different confidence levels. Another improvement is the quantification of uncertainties due to both space weather and instrument uncertainties. A feature not yet included that would have significant impact for LEO calculations is the solar cycle dependence of trapped protons (Houston [24]). Comparisons of AP8 to the mean environment of AP9 at 800 km altitude show the new model generally predicts higher fluxes, particularly at low proton energies and low orbital angles of inclination.

Ground Irradiation Tests and Calibration Shortcomings

29.   The comments and conclusions expressed in the reviewed publications about the "drift" of the **SAA**, are exclusively based on the unrelated mission-specific data collected by the large variety of special instruments used, which were not designed or intended to measure the magnetic field or the trapped/transient radiation in the **SAA**. To what degree these data are correct, accurate, and reliable is another question. It was appropriately noted in some papers, that the instruments of old are not as sophisticated as modern instruments. A constant area of concern for instruments is the process of test and calibration, which may be negatively affected by a number of shortcomings. For example, particle radiation facilities are restricted to providing only **(a)** a single source at a time, **(b)** a single energy at a

time, **(c)** a single (standard) beam direction, **(d)** a single species at a time, and **(e)** very high rates of accelerated exposures. In contrast to these artificial conditions, the natural radiation in space consists of a simultaneous, continuous, mostly isotropic incidence of all particle species populating a given region, i.e. a breath of energies (complete spectral distributions), and of low rates *arriving instantaneously from all directions*.

30.   Consequently, because of these limitations, ground test simulations may not be equivalent to space effects, and may lead to potentially inaccurate results and conclusions. Protons, electrons, cosmic rays, and solar flare particles (intermittent only, if applicable), are simultaneously incident on a satellite, and continuous over the duration of an entire mission, but usually at a much lower rate than the separate high-rate partial exposures at the irradiation test facilities. In an attempt to mimic space conditions, the facilities may adjust particle species, energy, intensity, and micro-macro dose rates, at any time, but can do so only for a single discreet value in each case.

The B and L Parameters and their Application

31.   In order to obtain spacecraft encountered radiation levels for trapped Van Allen Belt protons or electrons, orbital flux calculations were, until recently, being performed with the standard **NASA AP8** and **AE8**, solar-min and solar-max models [11], which were constructed from space measurements on the basis of the two magnetic parameters: **B** (the field strength in gauss or nano-tesla) and **L,** the McIlwain drift shell parameter in Earth radii [12]. **L** is defined as the distance to the equatorial crossing of the field line (line of force), passing through the position where the **B** measurement is made. The concept of the **B-L** coordinate system is illustrated in Figure 19.
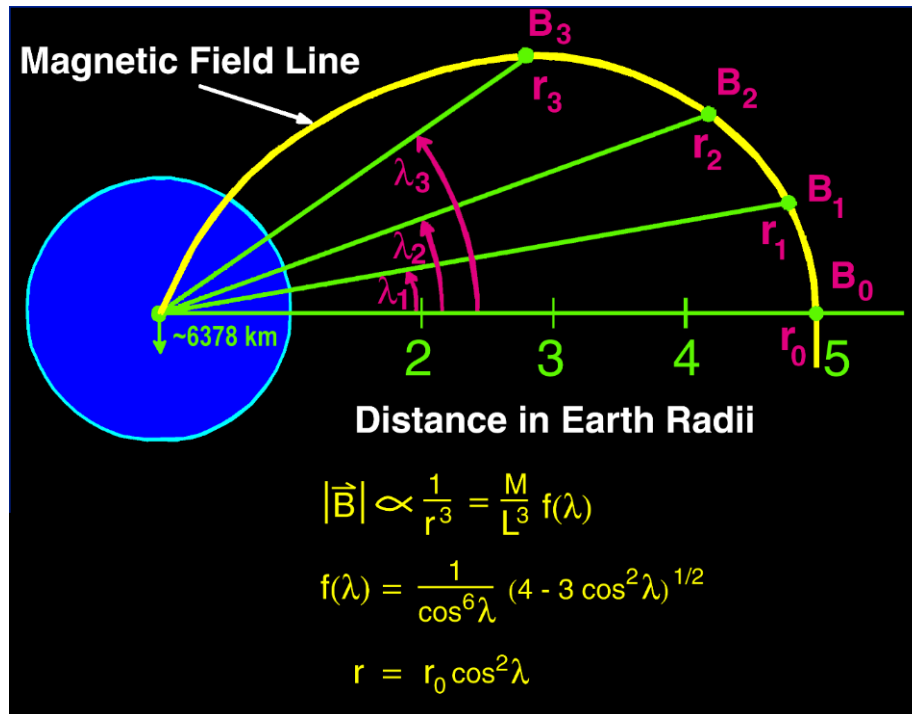

Figure 19: B-L Magnetic coordinate system. B=Magnetic field strength; L=Distance at equatorial crossing of field line.

32.   However, in many applications, when using the **AP8** to predict proton satellite radiation exposures, calculations were mostly performed with a **1970's** magnetic field model, even for a much later mission epoch (e.g. **2010**). This was being done because the **AP8** was constructed in the **1970** epoch on the basis of the two magnetic parameters, **B** and **L**, that were valid for that year, as well as because the orbital flux integrations, when performed for later missions with more recent field models, would yield increasingly higher fluences, especially at lower orbit altitudes (200-1000 km). These results were considered incorrect by some workers.

> Note: Low altitude near-Earth space missions (below an altitude of about 1000 km) experience only intermittent exposures to Van Allen belt radiations. That is, out of about **15-16** orbits per day, **5-6** do not intersect the **SAA**, but bypass it completely, whereas **7-9** revolutions cross through it, encountering the corresponding radiation. In addition, orbits with inclinations smaller than 45^0 will not usually experience solar flare proton encounters, as these protons generally do not penetrate to the low altitude orbits.

33.   In an effort to prevent or minimize these occurrences, modifications were implemented in 1986 by Vette [13], which recommended that the radiation models not be accessed with the 1970 **B** and **L** values, but with a new parameter **B/B$_0$** (obtained for the actual date of the mission) replacing **B**. **B$_0$** is the field strength of the **L**-line at the magnetic equator. The use of **B/B$_0$** has been widely preferred since the 1980's, by domestic and international research communities. [7]

34.   Developing satellite exposure predictions based on the assumption that no changes in the radiation levels at a specific position in space occurred between **1970** and **2010**, and that no changes in their magnetic field value should therefore be considered, did not solve the problem.

Special Calculations

35.   In order to evaluate the trend and the magnitude of the time-dependent variation of the **B-L** and **B/B$_0$-L** parameters within the **SAA** at the 800 km altitude level of this study, three pivotal positions were selected along the 23 degree south geographic latitude line: one in the approximate center of the **SAA** and one each at the west and east periphery. Table 1 lists the geographic coordinates of these points.

Table 1: Geographic coordinates of selected test positions.

Point	Longitude	Latitude
West	- 90°	- 23°
Center	- 30°	- 23°
East	+ 30°	- 23°

36.   In Figures 20 and 21, the changing magnetic coordinate values of these three points are plotted for the five epochs specifically selected: 1970, 1980, 1990, 2000, and 2010, in terms of the **B-L** and **B/B$_0$-L** parameters, respectively. All calculations were performed with the **IGRF** models relating to the above dates. It appears, that with both sets of parameters, the positions of the test points have moved magnetically, during the 40 years, mostly towards higher proton intensity regimes.

---

[7] It should be noted that on a given field line (of any L value), B$_0$ may not be the minimum field value, which may be located off the magnetic equator.
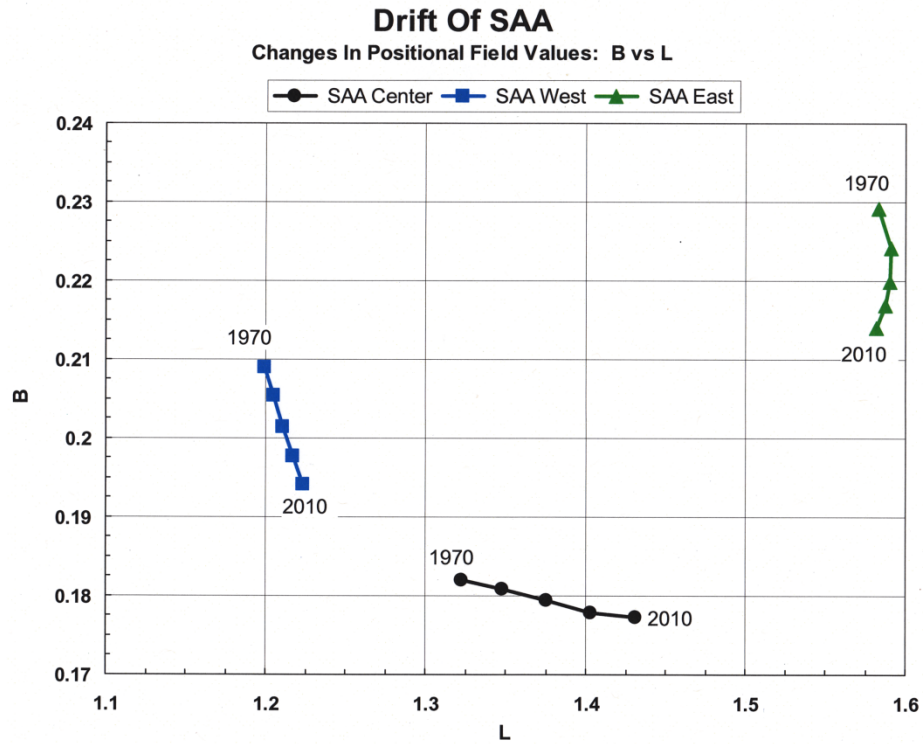
Figure 20: Changes in positional field values of **B** and **L** parameters.
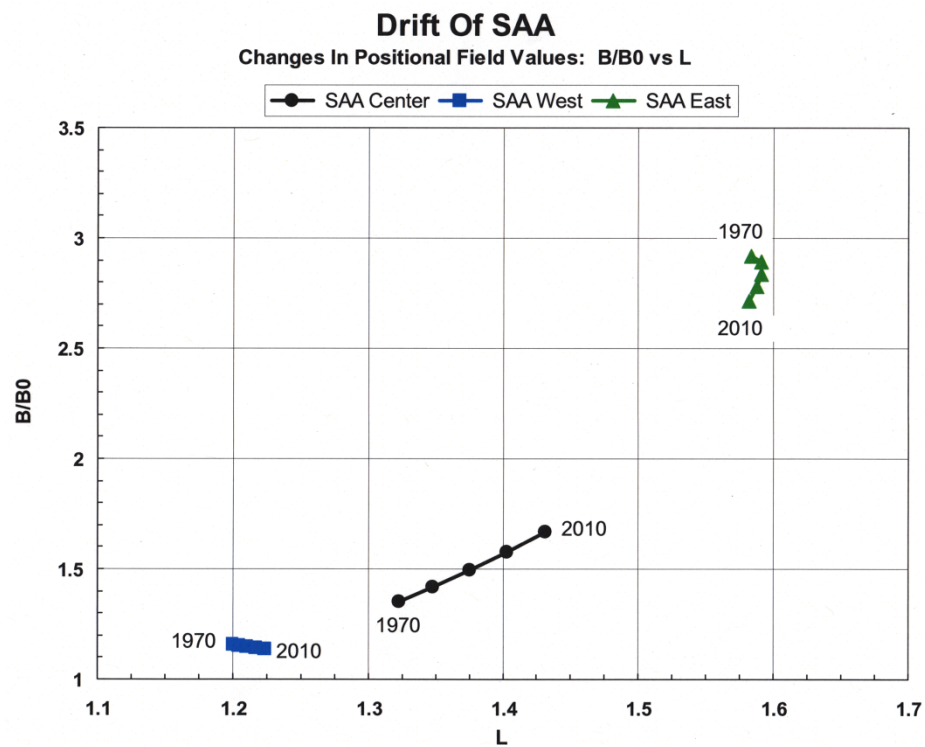
Figure 21: Changes in positional field values of **B/B₀** and **L** parameters.

37.   In Figures 22 (west), 23 (central), and 24 (east), the corresponding instantaneous **AP8-Max** integral omnidirectional proton fluxes, are plotted for the three test position, for energies > 30, >50, >100, and >200 MeV. They were obtained with the recommended **B/B$_0$** field parameter. These figures show significant increases-with-time in the positional proton fluxes, particularly at the lower energies (<200 MeV). Energies >200 MeV experience the smallest increases. It is interesting to note that at the central position, at the epoch 2000, there occurs a reversal in the rising trend, which results in lower flux predictions towards the epoch 2010. Figure 25 is a map, in **B-L** space, of constant intensity contours for E>50 MeV protons from the **AP8** model, in which the 40-year change in the magnetic location of the three test points has been indicated. The composition and distribution of the inner-zone Van Allen belt proton population, is likely not the same today, as it was in 1970, when the **AP8** was constructed; the present calculations may not represent correctly the real changes that have occurred, but serve only to indicate and approximate the possible trend in the temporal evolution of the belt.
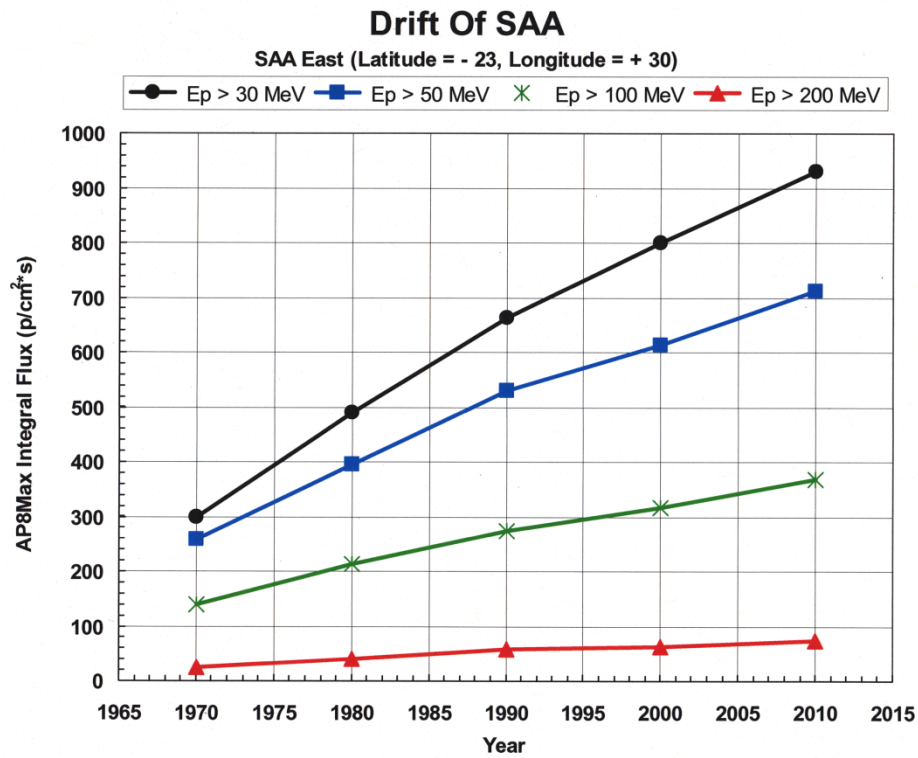
Figure 22: Variations of integral flux with time at indicated position.
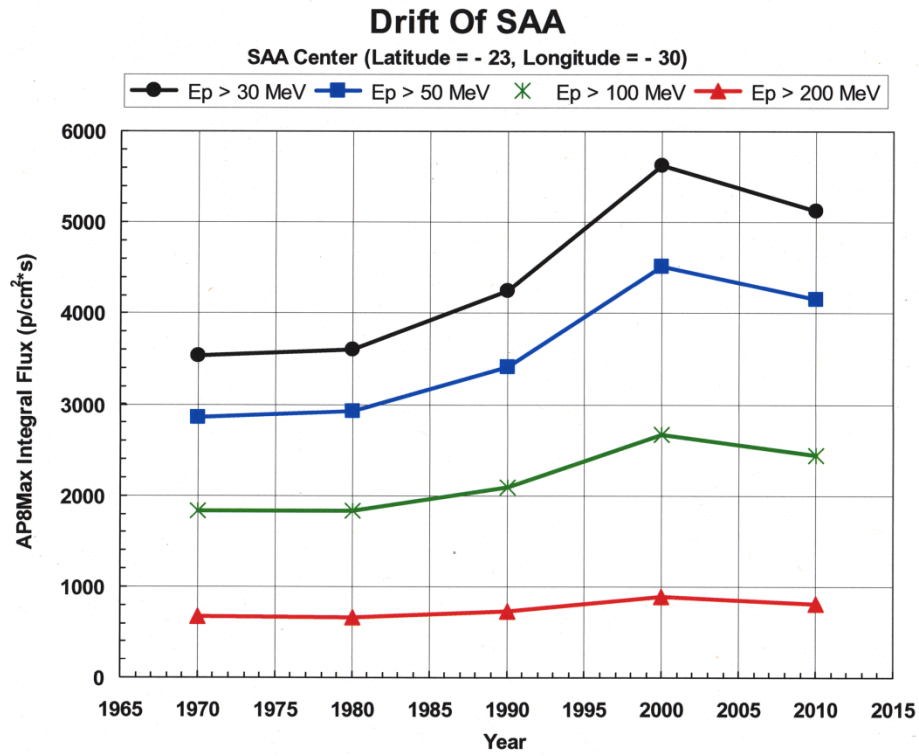
Figure 23: Variations of integral flux with time at indicated position.
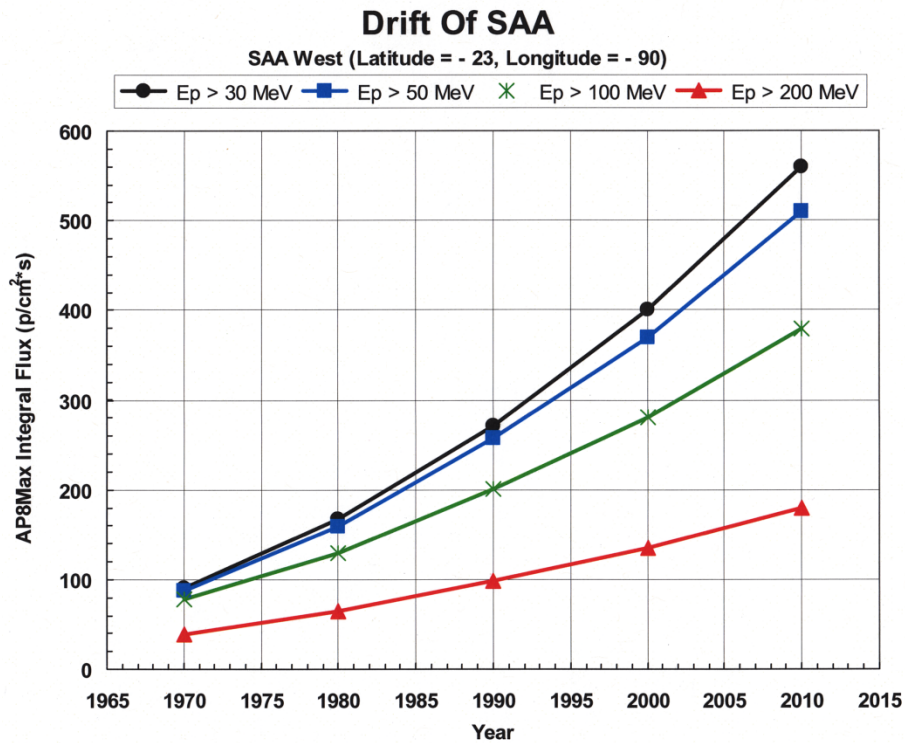
Figure 24: Variations of integral flux with time at indicated position.
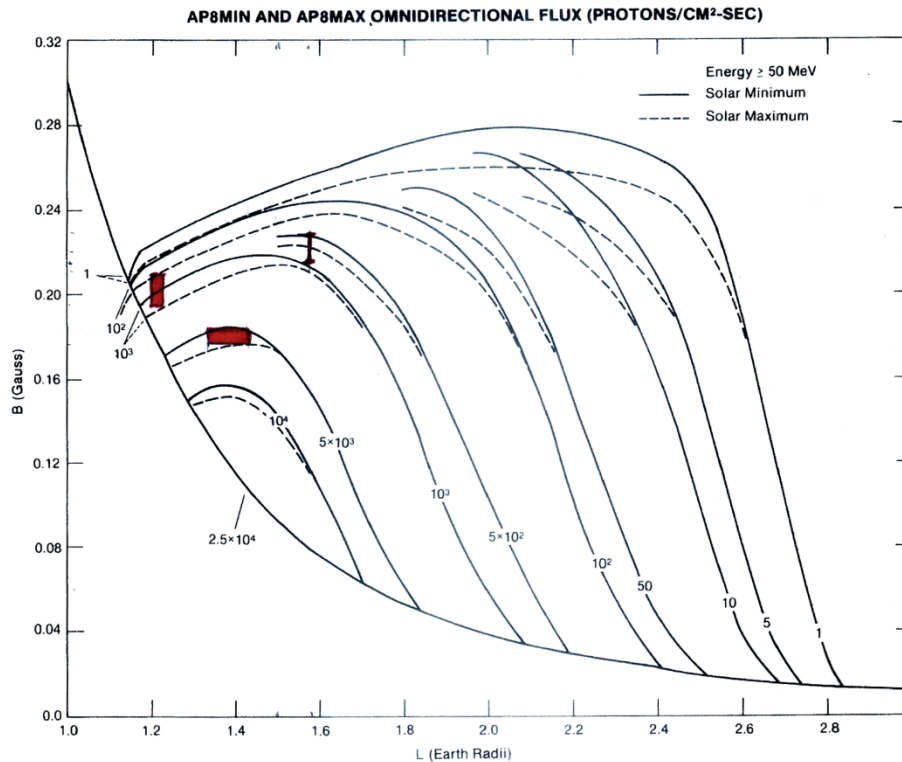
Figure 25: **B-L** space map of **AP8** proton model indicating the 40-year change in the magnetic location of the test positions.

38.   Therefore, the **B/B₀** approach, devised to avoid obtaining larger fluxes for epochs later than 1970, did not solve the problem. For that reason, in popular and widely used computer codes (e.g. **SPENVIS**), which calculate the orbit integrated vehicle encountered radiation belt fluxes, a simpler and more practical, but limited method, was adopted to achieve that goal: assigning the original 1970 fluxes to all later epochs, regardless of the changes in the **B** or **B/B₀** values, and ignoring the fact that the increase in the radiation levels is real, and is the result of the shrinking magnetic field, which brings down the larger fluxes from the higher altitudes. A comparison of sample calculations with the **SPENVIS** method for a position near the center of the **SAA** (23^0 south, 270^0 east) over 5 decades from 1960 to 2010, is given in Table 2. Several interim measurements, reported increased flux levels at formerly tested positions, indicating better agreement with model predictions that use the **B/B₀** approach.[8,9,10,11]

---

[8] **Quote from APPENDIX A [5a]:** *"Heinderickx's (1996) calculations of high-energy proton flux in the SAA region [with SPENVIS] do not coincide with experimental results obtained on the MIR station."*

[9] **Quote from APPENDIX A [7c]:** *"Trapped proton results: It was noted that certain SAA passes (e.g. orbit 23 of STS-48 and orbit 40 of STS-44) were not predicted when using the recommended technique of employing the field model pertaining to the data from when the models were created (i.e. 1970). However use of the 1991 geomagnetic field does predict peaks for these orbits as it accounts for the steady drift of the SAA contours to the west due to evolution of the geomagnetic field.*

[10] **Quote from APPENDIX A [7d]:** *"Trapped proton results: encouraging agreement is obtained between the three experiments despite the different design. For the region of the SAA, the LET spectra observed from KITSATA and POSAT have been compared with each other and with predictions based on the AP8 model for solar minimum, allowing for proton stopping and slowing in the detector. Figure 4 shows that agreement is good considering the uncertainties of a factor of two are inherent in allowing for spacecraft shielding and particle atmospheres."*

[11] **Quote from APPENDIX A [8a]:** *"The AP8 model predictions were found to be in good agreement with the flight data".* **[computed with B/B₀]**

22

Table 2: Comparison of proton calculations for the indicated test position by two methods: SPENVIS (mission time independent) and time-dependent on Vette's B/B_0 approach.

	Input			SPENVIS		AP8 Model Calculations				SPENVIS AP8-MAX			
	B1	**L1**	**B/B$_0$**	**B2**	**L2**	**>30**	**>50**	**>100**	**>200**	**>30**	**>50**	**>100**	**>200**
1960	0.23370	1.5743	2.9260	0.22939	1.5784	1.656^2	1.434^2	8.423^1	1.505^1	3.2683^2	2.7804^2	1.588^2	2.9033^1
1970	0.22918	1.5833	2.9185	"	"	2.922^2	2.531^2	1.378^2	2.515^1	"	"	"	"
1980	0.22412	1.5907	2.8944	"	"	5.015^2	4.029^2	2.182^2	4.022^1	"	"	"	"
1990	0.21984	1.5904	2.8376	"	"	6.510^2	5.224^2	2.691^2	5.295^1	"	"	"	"
2000	0.21683	1.5871	2.7816	"	"	7.988^2	6.133^2	3.161^2	6.377^1	"	"	"	"
2010	0.21398	1.5817	2.7166	"	"	9.048^2	6.934^2	3.594^2	7.242^1	"	"	"	"

Calculations for position: Latitude = -23°, Longitude = -90°, Altitude = 800 km

39.   The consequence of miscalculating the radiation levels on spacecraft traveling through the inner radiation belt, may not only jeopardize the success of a mission, but may also be hazardous to biological systems on board (including humans). The most common effects of underestimating the radiation exposure of a satellite, which may subsequently experience higher radiation levels than expected, include: **(a)** damage to electronic components, circuits and systems, **(b)** parts failure, **(c.)** data corruption, and **(d)** equipment malfunction.

40.   What appears to occur in the lower magnetosphere, is that the shrinking field draws the larger areas-of-occupation and the greater intensities from the higher altitudes to the lower altitude levels. This poses the question whether these greater trapped particle fluxes are sustained at the lower altitudes or, if not, by what mechanism they are depleted, particularly in the 300-1000 km altitude domain.

41.   An example of that process is shown in Figure 26, where **(a)** the 900 km fluxes of the year 1970 **[IGRF-1970]** and **(b)** the 800 km fluxes of the year 2010 **[IGRF-2010]**, are superimposed for the 1000-particle intensity contours of E>100 MeV protons, as obtained from the A**P8-MAX** model with the B/B_0 variable. These contours are almost identical in shape and size but the 2010 contour is shifted towards the west-northwest direction, probably due to the drift of the magnetic poles.
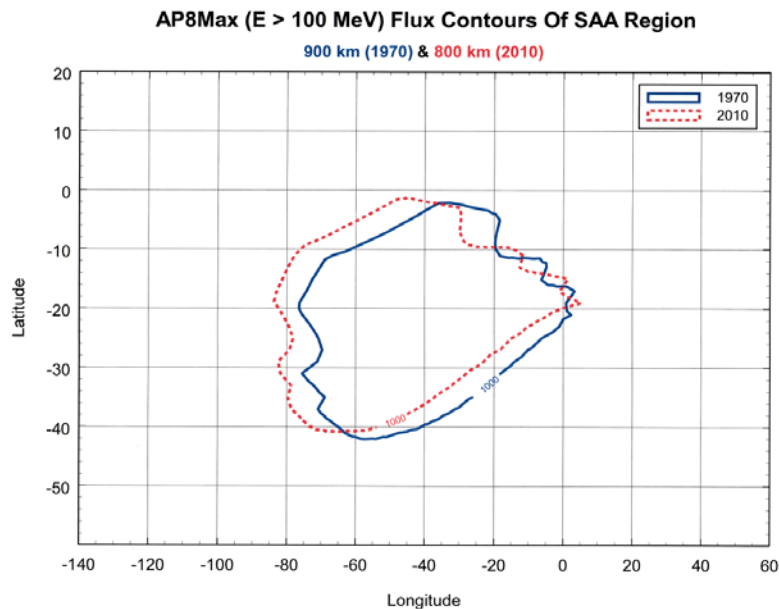
Figure 26: **AP8-MAX** flux contours (E>100 MeV) in **SAA** for epoch 1970 (at 900 km altitude) and for

42.   It is likely, that the shrinking magnetic field lowers the mirror-points of the trapped particles and that some mirror-points may drop into the atmospheric cut-off region, in which the particles will be lost due to coulomb scattering by the atmospheric constituents, thus depleting the larger intensities coming down from above. However, a quantitative evaluation of such a process, to determine the magnitude and extent of the depletion, is not possible without detailed pitch-angle information, which is not available for the **AP8** data that have been used in the construction of the model. An answer to this problem may be provided, after a new trapped particle model is constructed with current measurements and field models.

43.   An additional area of confusion and misunderstanding has been noted in some papers, regarding the trapped particle mirror points, particularly in reference to the **SAA**. This issue applies to all trapped particles, including those in the outer zone of the Van Allen belts[12]. Mirror point positions are determined by equations that predict their location as a function of their pitch angle, which can have any value $<90^0$. The predicted positions could be at any altitude, including on the surface of the Earth or even at subterranean locations. The atmospheric cutoff would prevent particles from reaching their mirror point below approximately 100 km in altitude. A relative display of the dip of the associated magnetic field lines, guiding the particles to the lower altitudes, is presented in Figure 27 by McIlwain [12], showing the drop observed below the Earth's surface.

---

[12] **Quote from APPENDIX A [12c]:** *"Since the gradient within the geomagnetic cutoff is very steep, within a short time period the order of magnitude flux increases and <u>even subterranean fluxes are predicted</u>." ---- "Not only does the flux increase with time, but also increases <u>disproportionally</u> at low altitudes and <u>even below the Earth's surface. If</u> real, such an increase would have implications far <u>beyond any one's imagination</u>."*
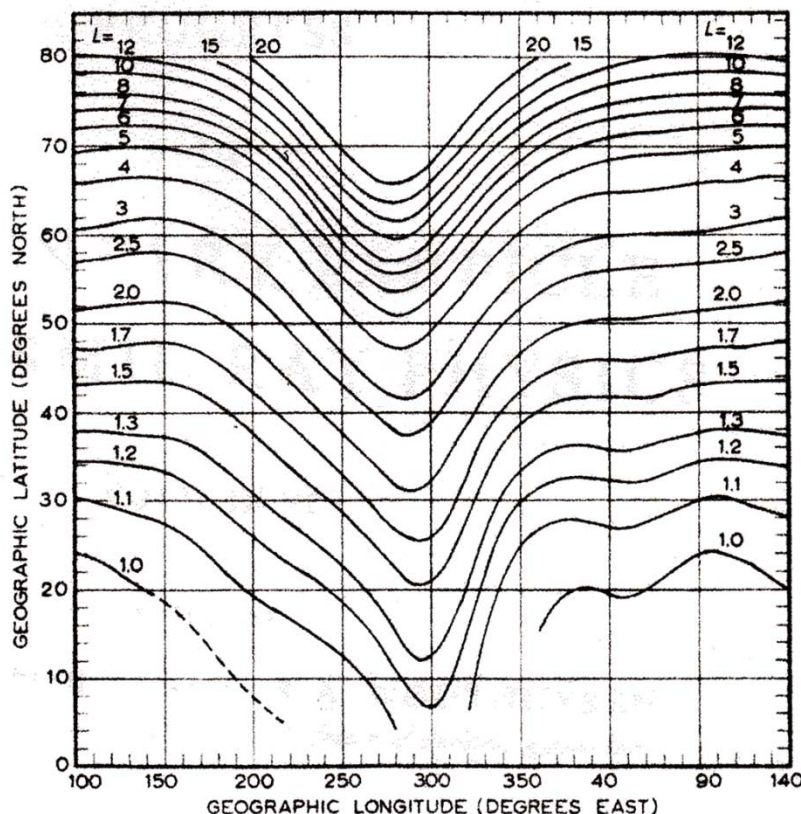
Figure 27: Intersections of shells of constant **L** with the surface of the Earth.

44.   It is difficult to evaluate correctly, for protons and electrons, the conditions of the atmospheric cutoff prevailing at any given time, in the inner zone of the Van Allen belt, without considering the significant changes in the atmospheric density that occur with time and that are not fully identified. These temporal variations are believed to reach about a factor of 200 between solar-max and solar-min periods. In addition, diurnal variations are estimated to reach a factor of 10. These effects, however, have no impact on the size, drift, and area of the **SAA,** and vice-versa, although in some papers the opposite has been suggested.

44.   Misconceptions regarding the "atmospheric cutoff" were noted in a few of the referenced publications, which claimed that a dependent relationship exists between the cutoff and the magnetic field, that is, that the cutoff and the field mutually affected each other. The atmospheric cutoff is in essence a function of density, which in turn is a function of altitude and of solar activity conditions, and not of the magnetic field. Therefore, a corresponding attempt to indirectly evaluate the "drift" of the **SAA** based on these assumptions would be inaccurate.

45.   Considering the dynamic nature of the Earth's main dipole field, concerns about the validity of the three adiabatic invariants, the foundation of the **B-L** system being used in ordering the particle data, are justified. However, in the case of the **IGRF**, each new updated model issued, includes and accounts for all changes in the field, so that within its 5-year period, the expressed field is considered **static**, and hence, all three adiabatic invariants are valid, and the use of the **IGRF** is safe, correct, and appropriate. This observation may not be well understood in the community.[13]

46.   Independent of any "drift" of the **SAA**, the **SAA** exhibits <u>a very real and unavoidable increase in size with time</u> **that implies longer transit times for spacecraft, and hence longer radiation exposures.** The accumulation of larger fluences, which is actually the major contribution to the higher radiation doses predicted for orbits in the **SAA**, is in addition to the substantial increase of the flux in the areas of highest energy particles. This is well illustrated in Figures 28, 29, 30, in which >10 MeV proton intensities of 1000, 3000, and 5000 particles per centimeter square per second, are compared for the years 1960 to 2010.
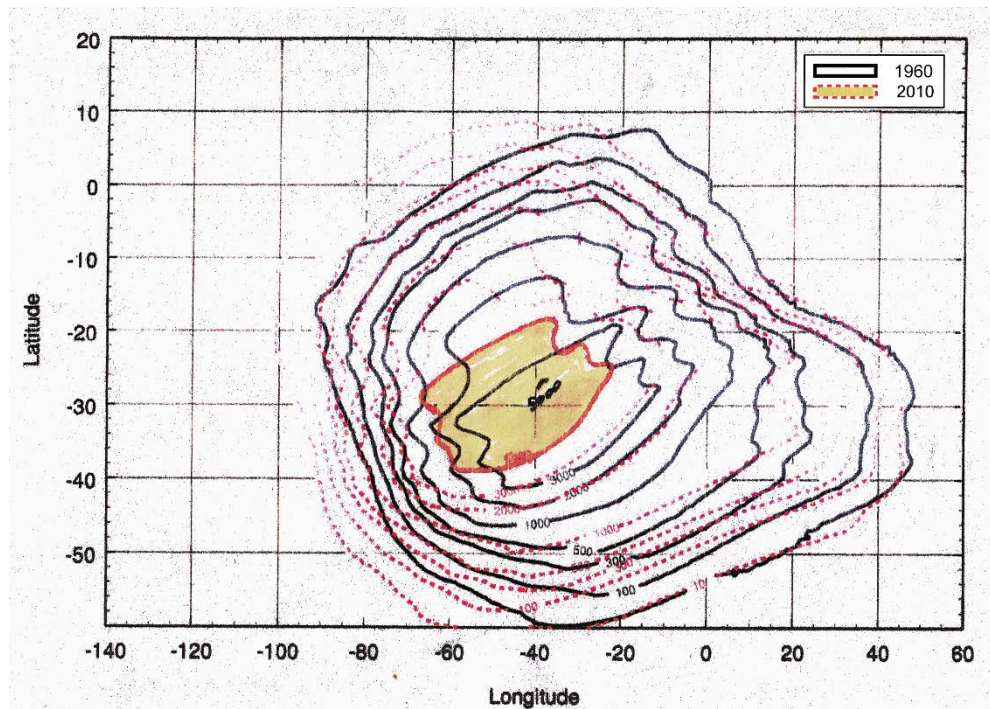
Figure 28: High intensity area of 1000 particle E>10 MeV proton flux for epochs 1960 and 2010.

---

[13] <u>**Quote**</u> **from APPENDIX A [12b]: "***The above described use of the trapped radiation environment models is also based on the <u>assumption that B and L, being derived from the first and second adiabatic invariants,</u> are themselves invariant. In a <u>static magnetic field</u>, this is certainly true and this coordinate system is very successful in ordering particle data and is, therefore, incorporated into the models of the Earth's trapped radiation environment. However, <u>since the Earth's dipole is decreasing</u> with a characteristic time of about 1000 years, when calculating particle flux transformations, <u>all three adiabatic invariants have to be taken into account properly.</u>*
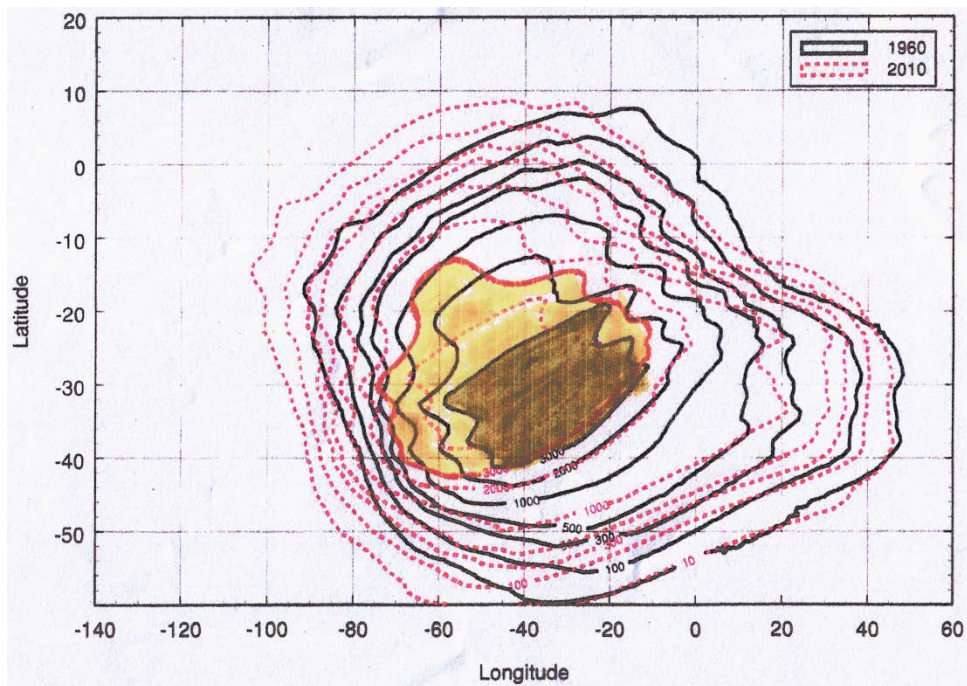
Figure 29: High intensity area of 3000 particle E>10 MeV proton flux for epochs 1960 and 2010.
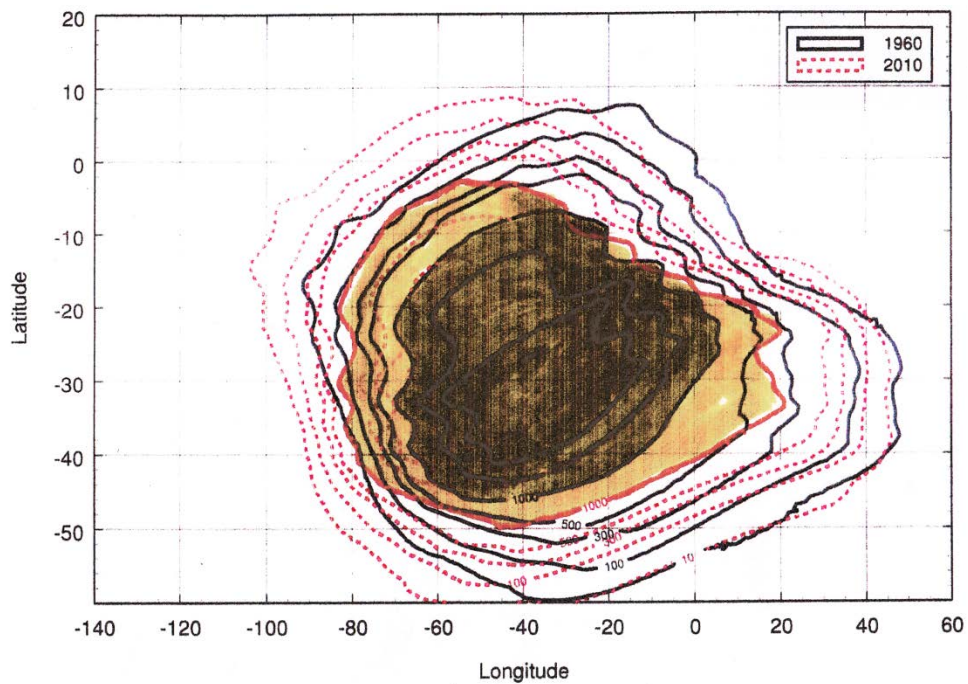
Figure 30: High intensity area of 5000 particle E>10 MeV proton flux for epochs 1960 and 2010.

47.   A more detailed comparison of the **SAA**'s location and area at 800 km altitude, as outlined by the proton population between the years 1970 and 2010, is shown in Figures 31-38 for energies E>50 MeV, 39-45 for E>100 MeV, 46-50 for E>200 MeV, and 51-53 for E>300 MeV, for integral proton flux contours of 10, 100, 300, 1000, 3000, and 5000 particles per centimeter square per second. This arrangement is illustrated in Table 3.
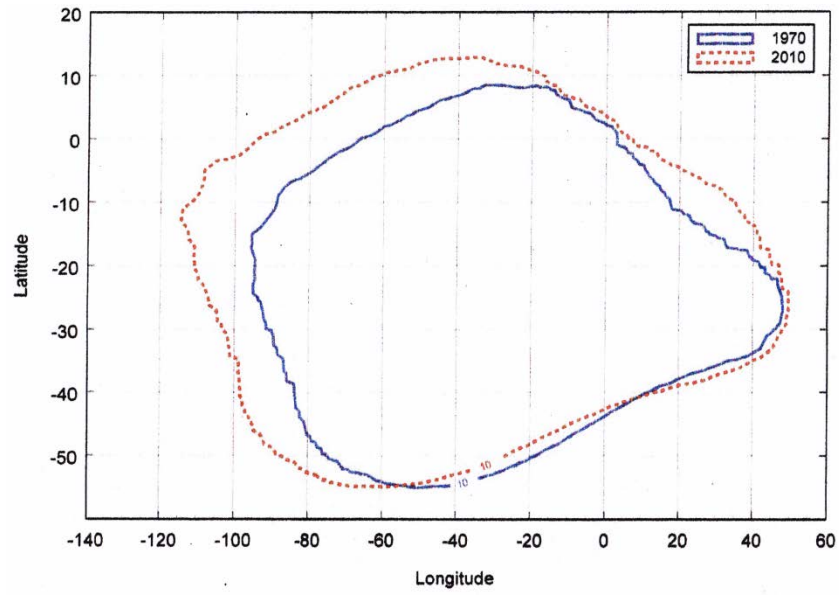
Figure 31: Location of E>50 MeV flux of 10 protons at 800 km altitude for epochs 1960 and 2010.
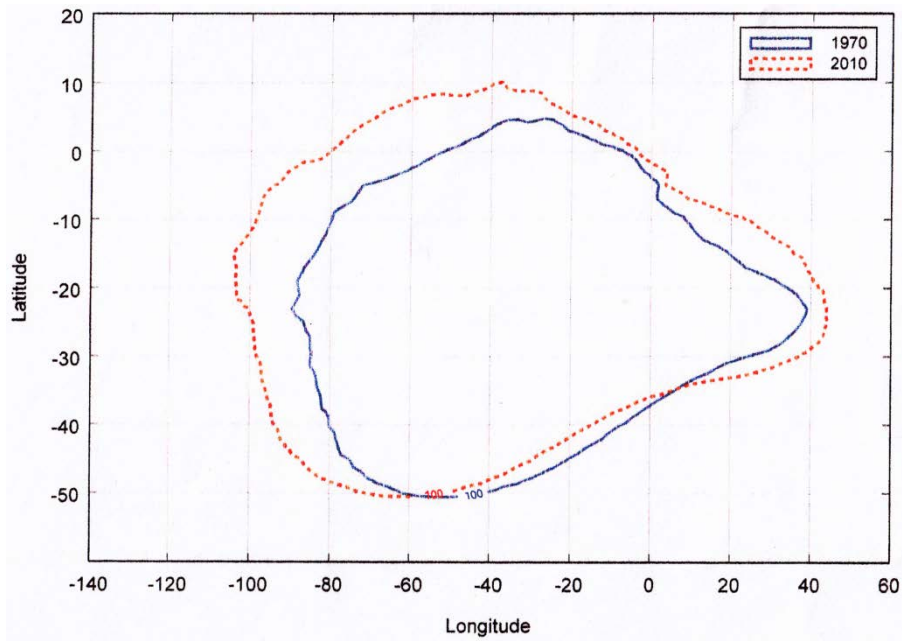
Figure 32: Location of E>50 MeV flux of 100 protons at 800 km altitude for epochs 1960 and 2010.

28
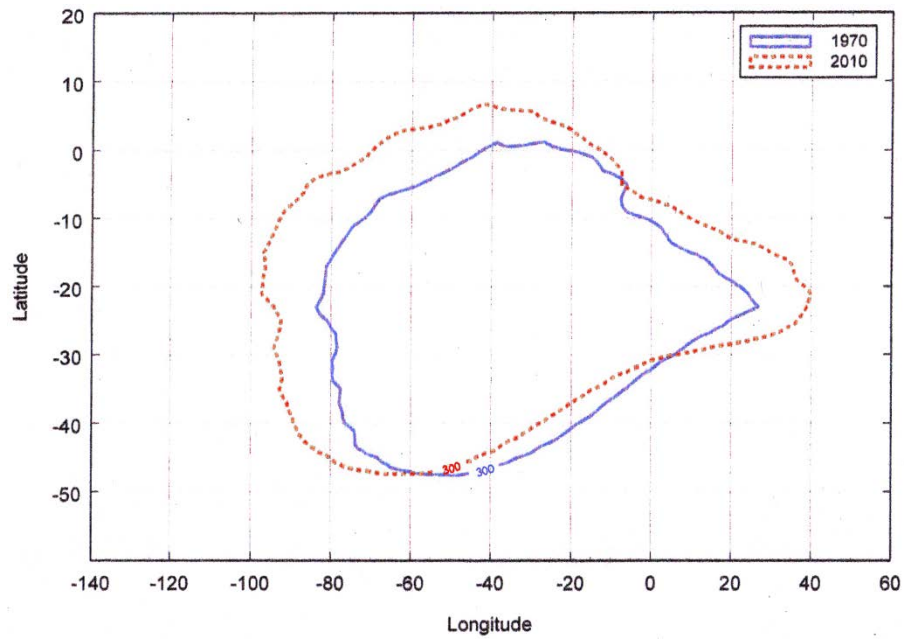
Figure 33: Location of E>50 MeV flux of 200 protons at 800 km altitude for epochs 1960 and 2010.
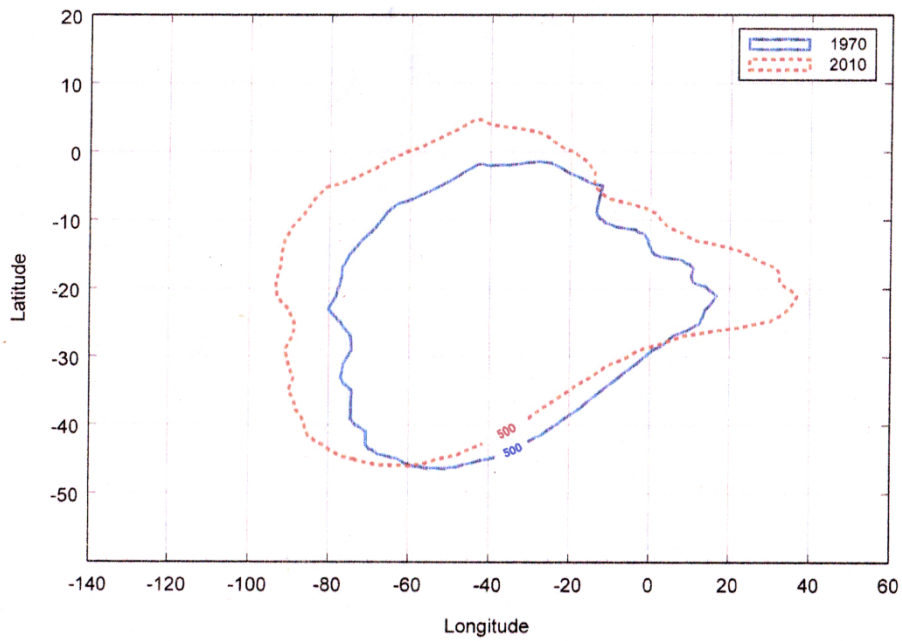
Figure 34: Location of E>50 MeV flux of 500 protons at 800 km altitude for epochs 1960 and 2010.
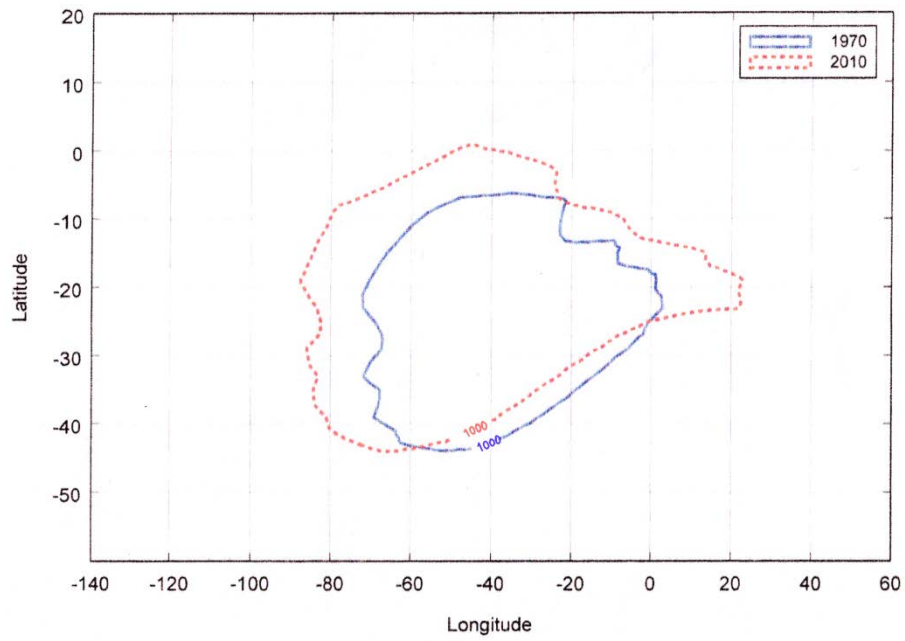
Figure 35: Location of E>50 MeV flux of 1000 protons at 800 km altitude for epochs 1960 and 2010.
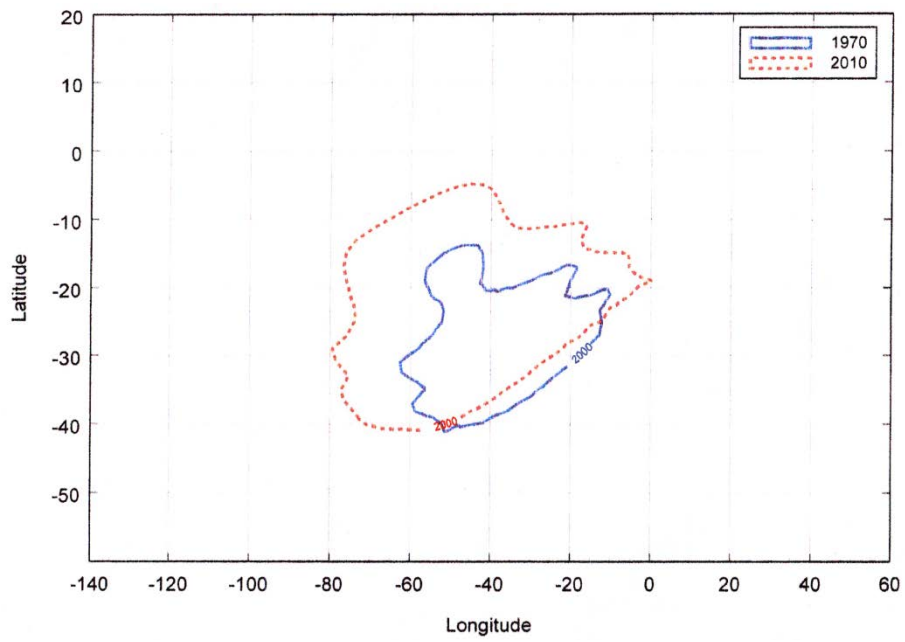
Figure 36: Location of E>50 MeV flux of 2000 protons at 800 km altitude for epochs 1960 and 2010.
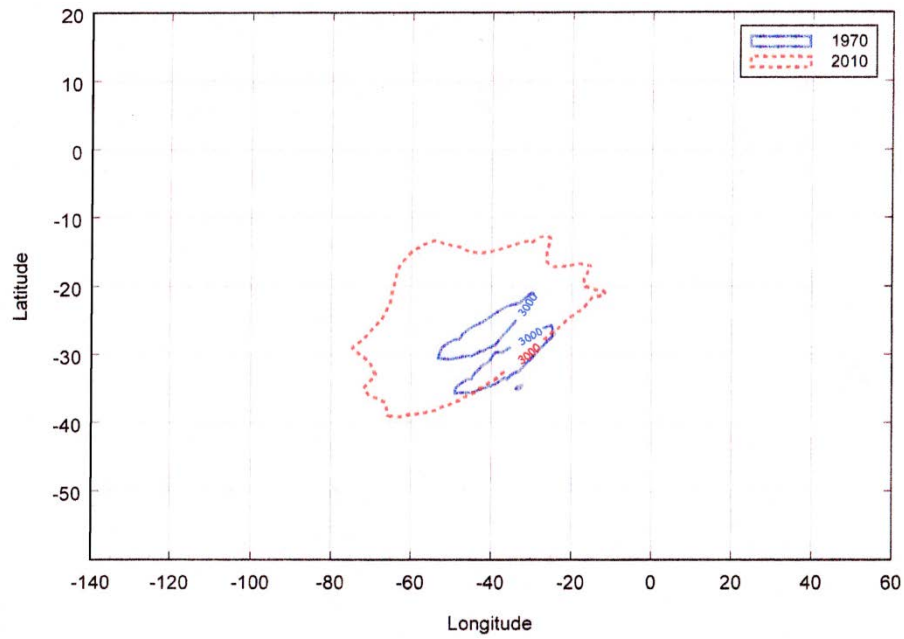
Figure 37: Location of E>50 MeV flux of 3000 protons at 800 km altitude for epochs 1960 and 2010.
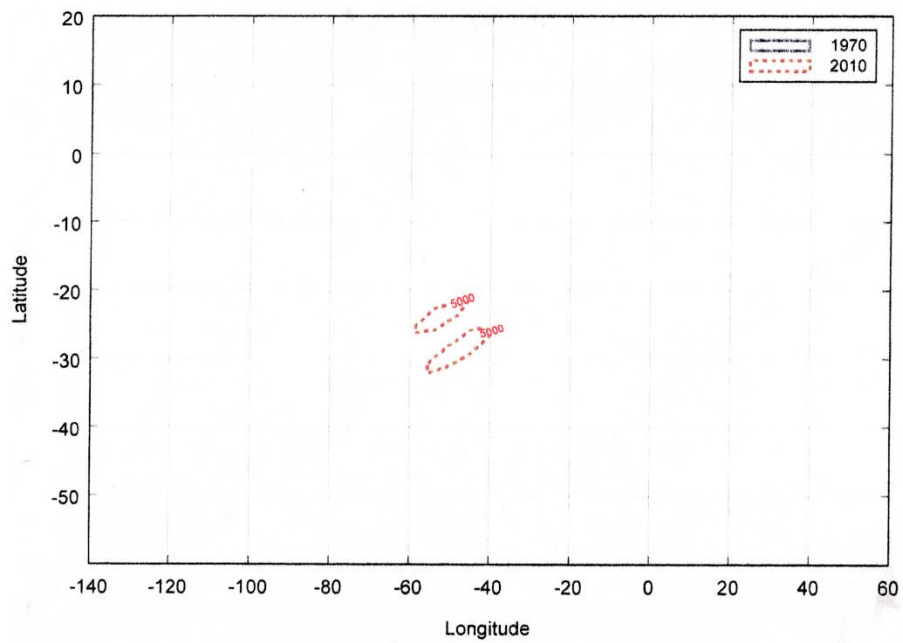
Figure 38: Location of E>50 MeV flux of 5000 protons at 800 km altitude for epochs 1960 and 2010.
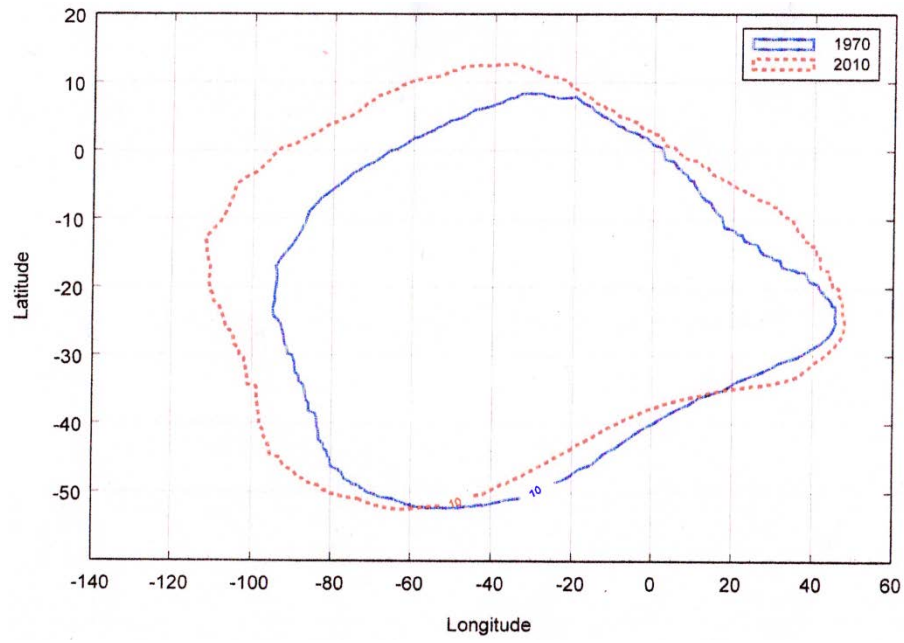
Figure 39: Location of E>100 MeV flux of 10 protons at 800 km altitude for epochs 1960 and 2010.
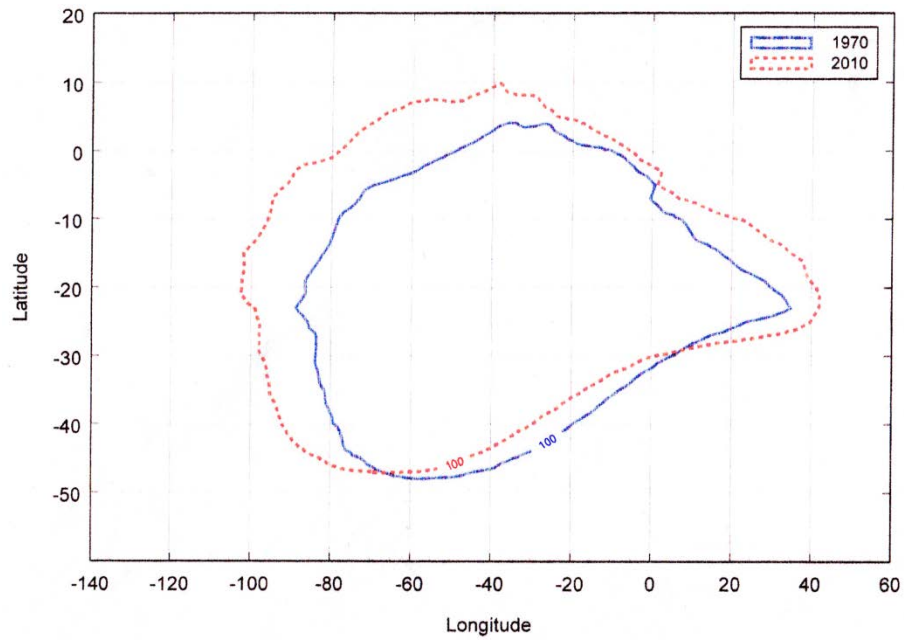
Figure 40: Location of E>100 MeV flux of 100 protons at 800 km altitude for epochs 1960 and 2010.

32
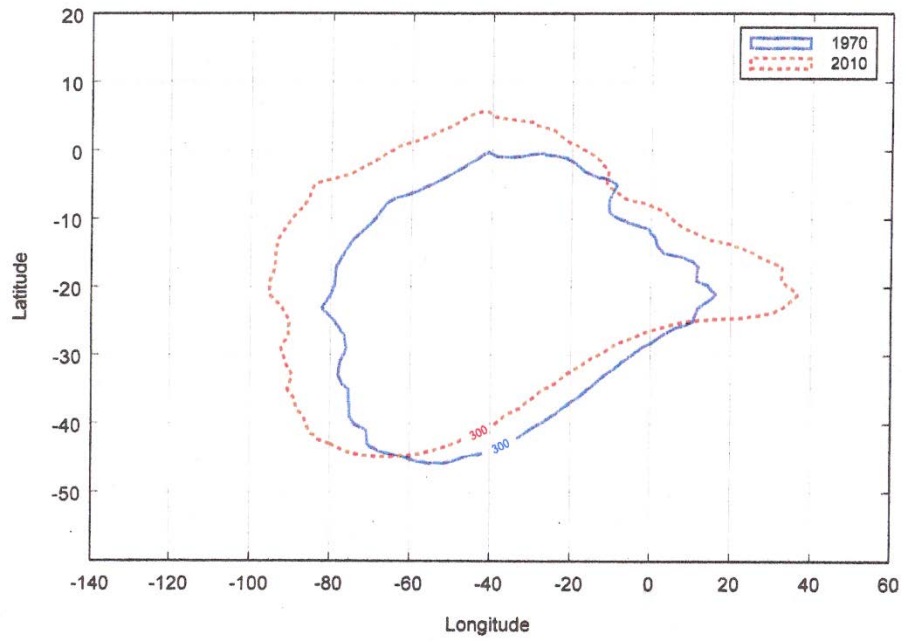
Figure 41: Location of E>100 MeV flux of 300 protons at 800 km altitude for epochs 1960 and 2010.
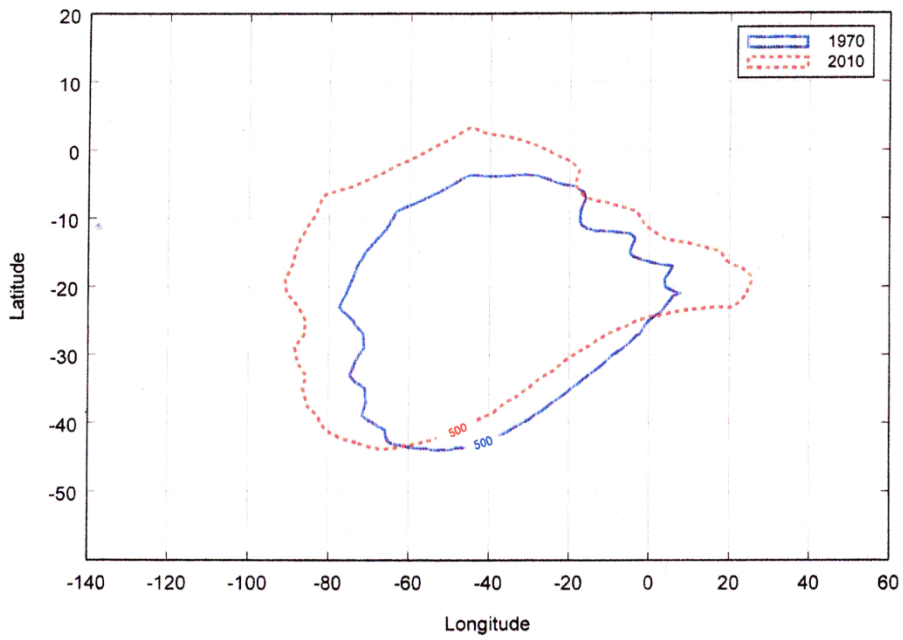
Figure 42: Location of E>100 MeV flux of 500 protons at 800 km altitude for epochs 1960 and 2010.
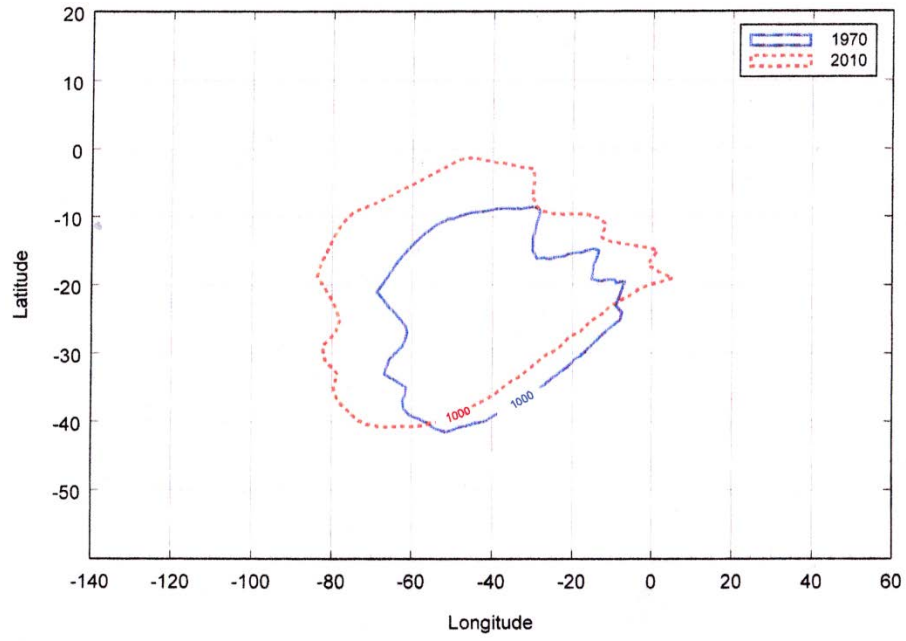
Figure 43: Location of E>100 MeV flux of 1000 protons at 800 km altitude for epochs 1960 and 2010.
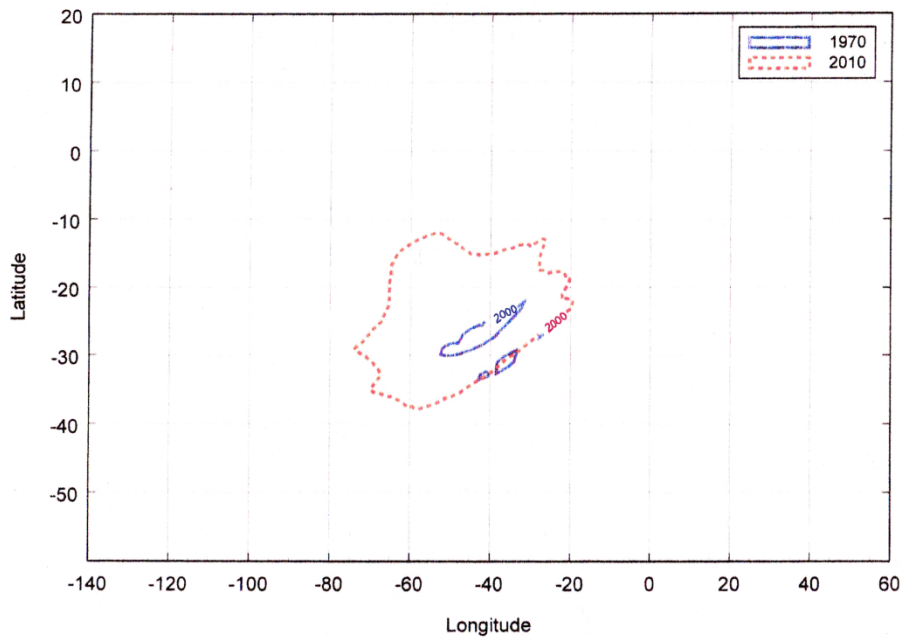
Figure 44: Location of E>100 MeV flux of 2000 protons at 800 km altitude for epochs 1960 and 2010.
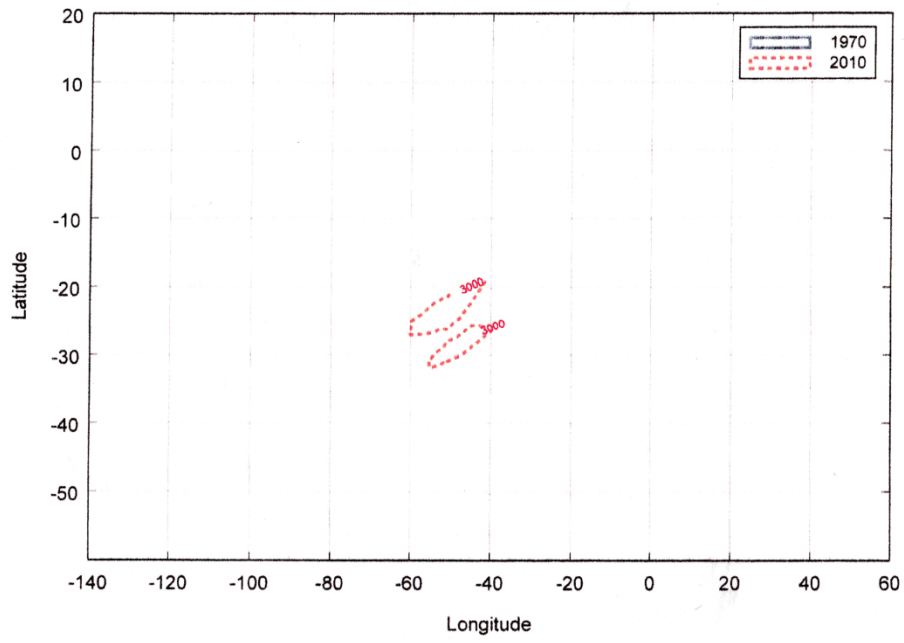
Figure 45: Location of E>100 MeV flux of 3000 protons at 800 km altitude for epochs 1960 and 2010.
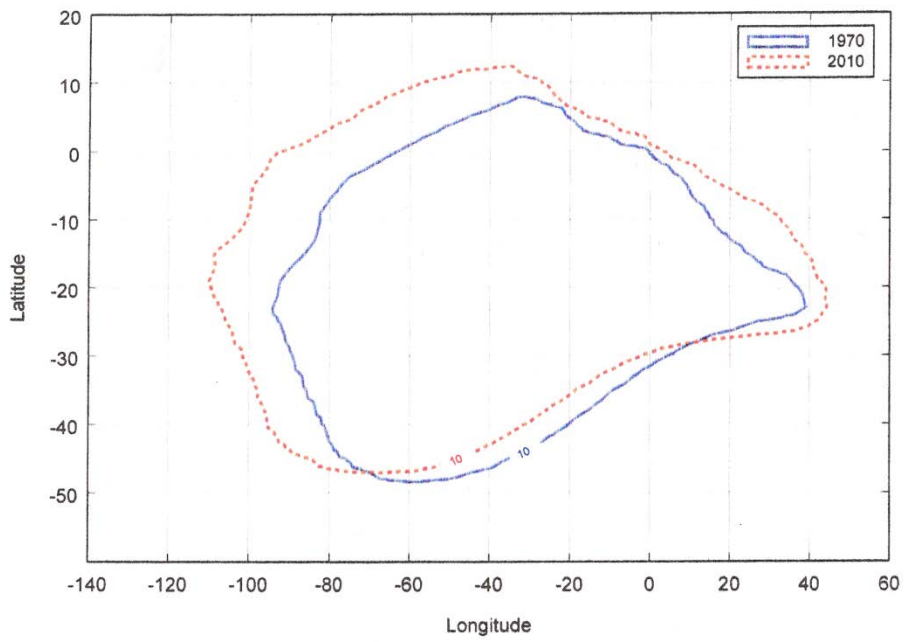
Figure 46: Location of E>200 MeV flux of 10 protons at 800 km altitude for epochs 1960 and 2010.
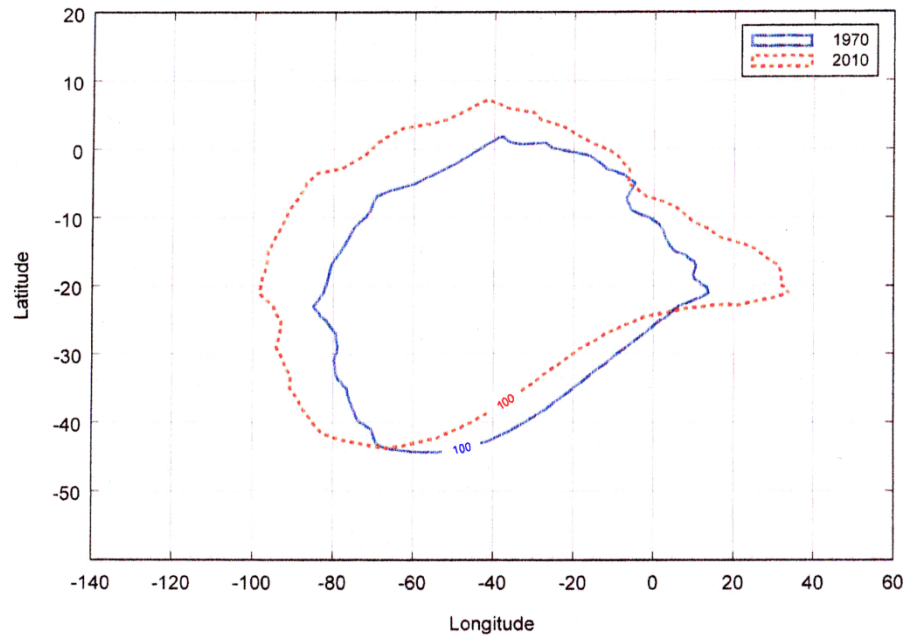
Figure 47: Location of E>200 MeV flux of 100 protons at 800 km altitude for epochs 1960 and 2010.
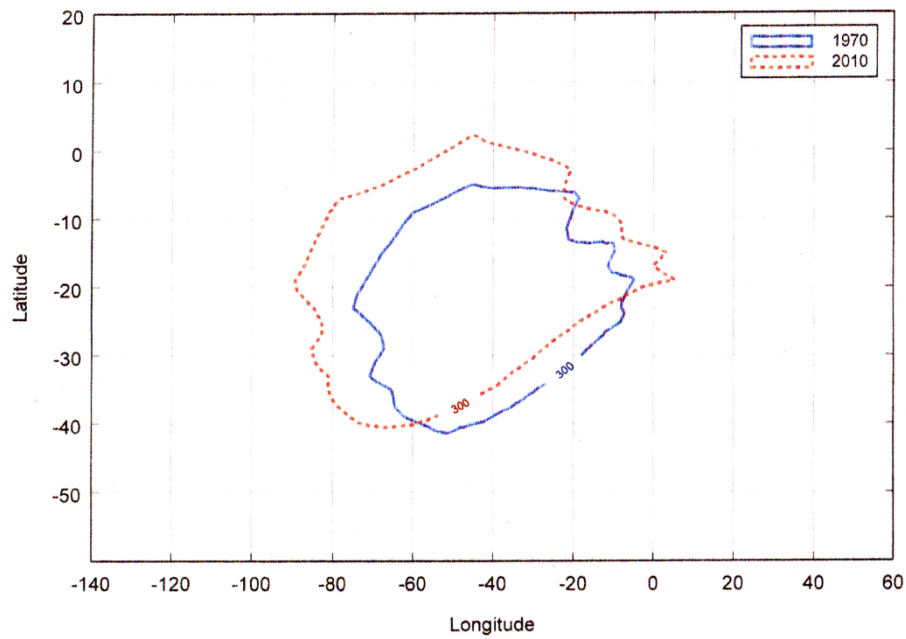
Figure 48: Location of E>200 MeV flux of 300 protons at 800 km altitude for epochs 1960 and 2010.
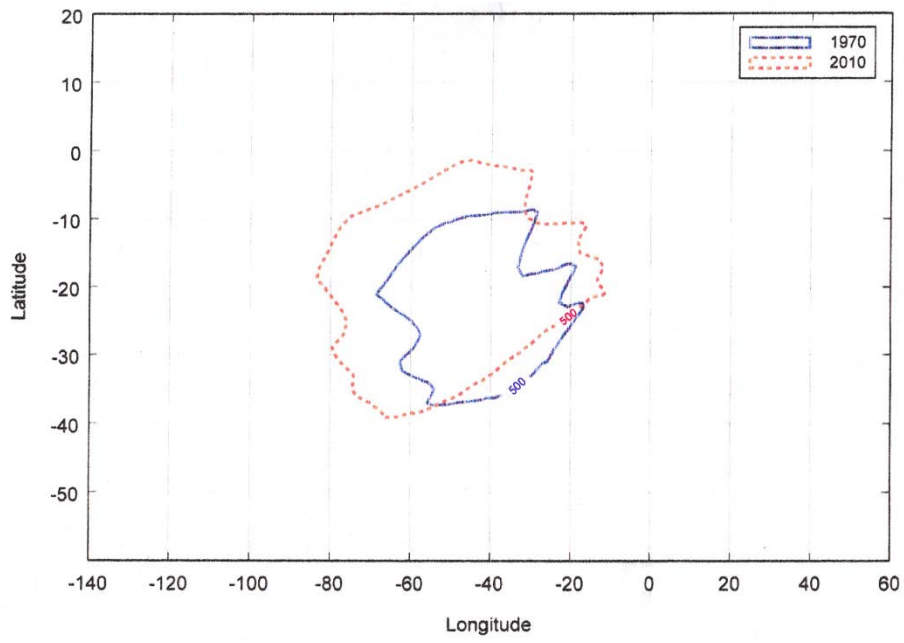
Figure 49: Location of E>200 MeV flux of 500 protons at 800 km altitude for epochs 1960 and 2010.
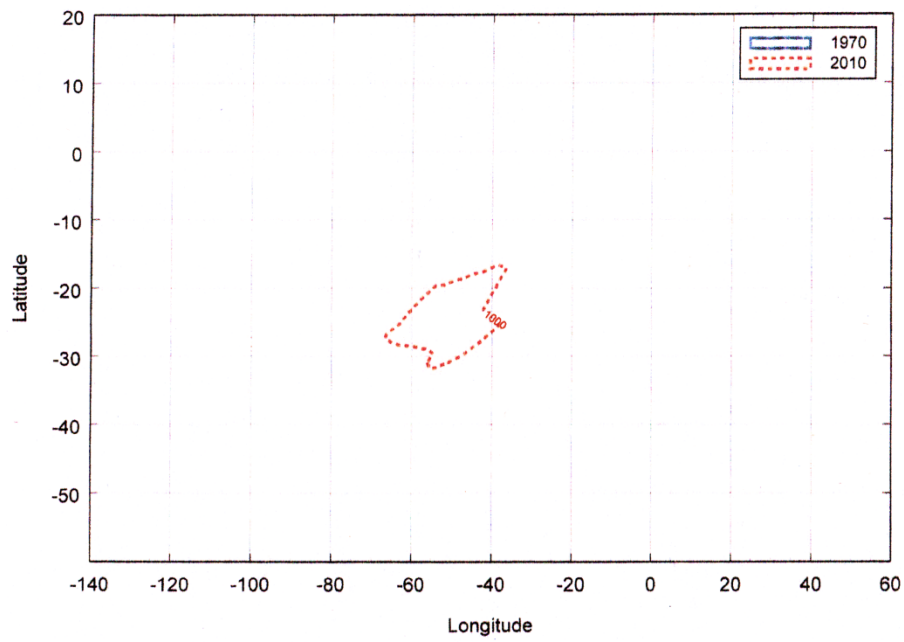
Figure 50: Location of E>200 MeV flux of 1000 protons at 800 km altitude for epochs 1960 and 2010.
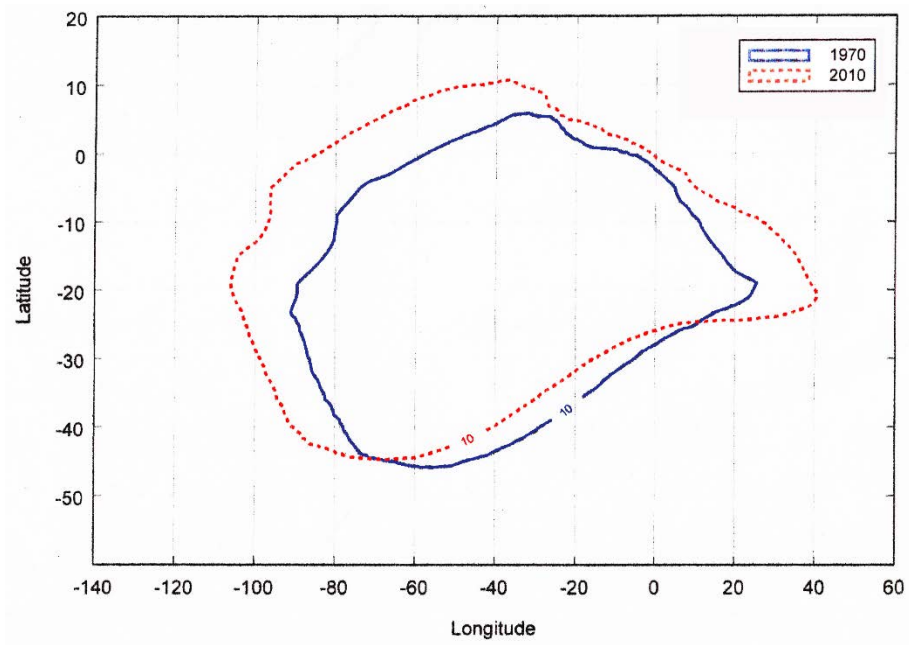
Figure 51: Location of E>300 MeV flux of 10 protons at 800 km altitude for epochs 1960 and 2010.
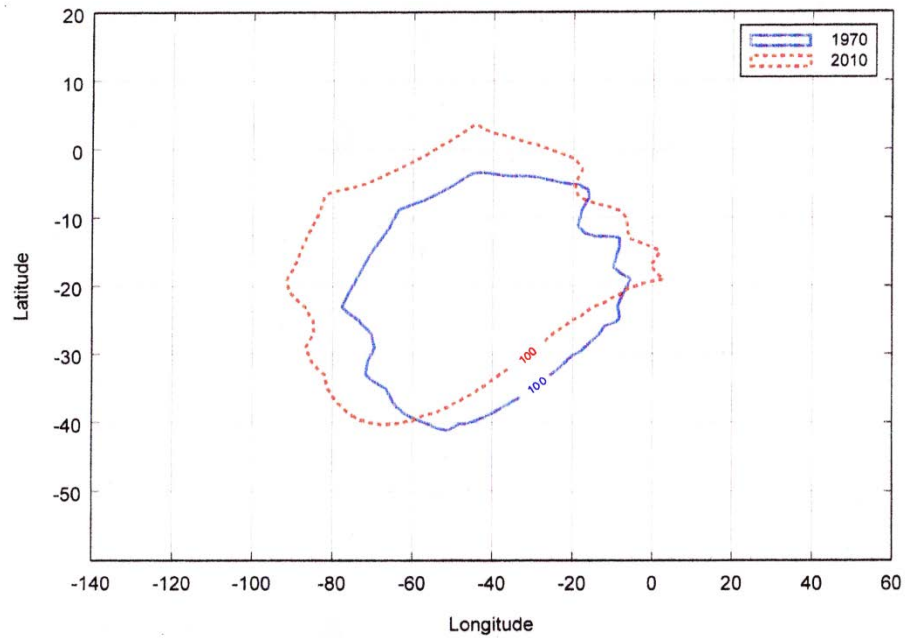
Figure 52: Location of E>300 MeV flux of 100 protons at 800 km altitude for epochs 1960 and 2010.
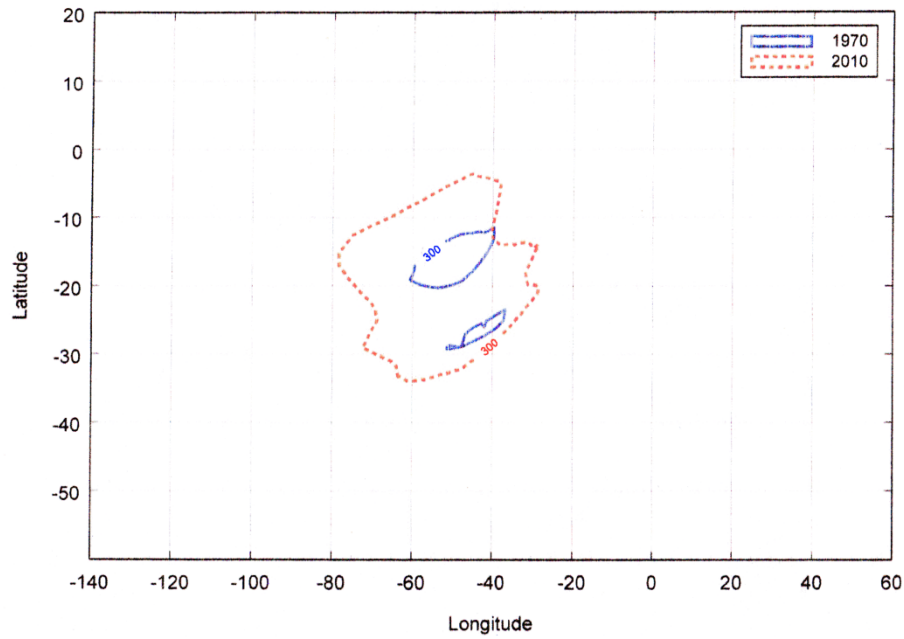
Figure 53: Location of E>300 MeV flux of 500 protons at 800 km altitude for epochs 1960 and 2010.

Table 3: Arrangement of Figures 31-53 by intensity and energy at 800 km altitude for epochs 1960 and 2010.

E(MeV):	> 50 MeV	> 100 MeV	> 200 MeV	> 300 MeV
Intensity (p/cm²-sec)	Figure Number			
10	1a	2a	3a	4a
100	1b	2b	3b	4b
300	1c	2c	3c	4c
500	1d	2d	3d	
1000	1e	2e	3e	
2000	1f	2f		
3000	1g	2g		
5000	1h			

48.   All plots indicate only minimal changes in the location of the southern boundary of the **SAA**, but display a substantial displacement in the west, north, and east directions. At all energies selected for plotting (>50 MeV, >100 MeV, >200 MeV, >300 MeV), significant expansion for all intensity levels occurs to the "north-northwest" and the "west-southwest" side of the **SAA**. Particularly noteworthy is the sharp protrusion mentioned before, that is most pronounced at the intensities displayed in Figures 32-35, 40-41, 47, and 51. As is to be expected, the areas occupied by the higher energy protons, are smaller in size than those of the lower energies. For increasing energies, the maximum intensity areas become progressively smaller, reflecting the drop in the proton spectrum.

49.   An important feature of the maps for epoch 2010 is the appearance of higher intensity contours in the center of the **SAA**, contours that either are not present in the maps for epoch 1970, or appear only as small "islands". In this case, the 2010 maps indicate a significant increase in the area occupied by these high intensities, as compared to the 1970 maps (see Figures 37-38, 42-43, 50, 53), correctly contributing to the increased flux and dose predictions, questioned by many of the models users. A more direct display of that observation is provided by a set of plots for particle energies of 10, 30, 50, 100, 200, and 300 MeV, respectively, in Figures 54 to 59, for the two epochs being compared (i.e. 1970 to 2010).
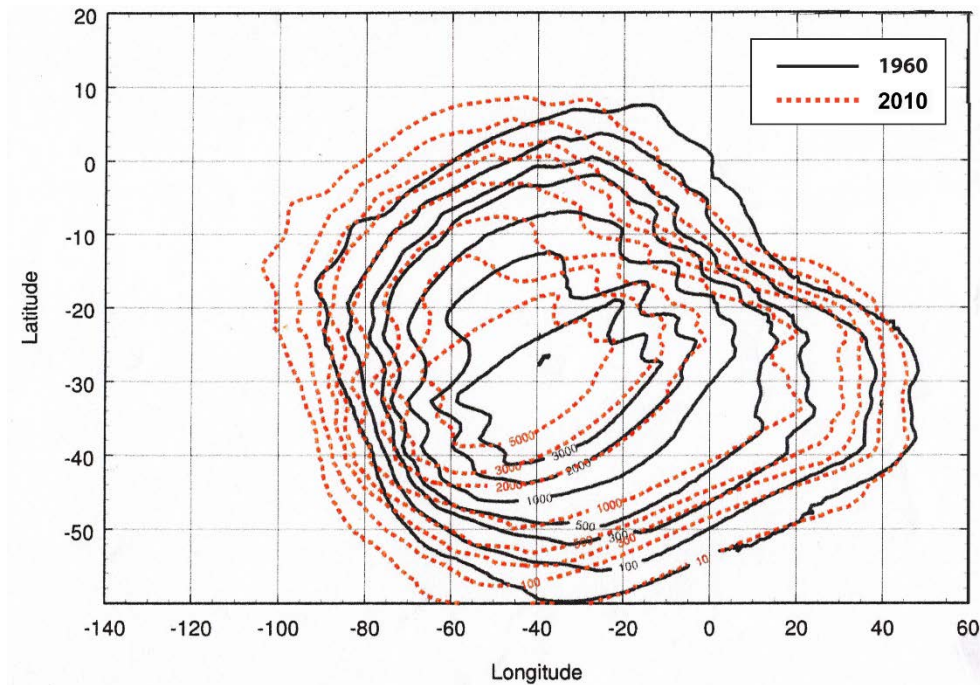
Figure 54: Comparison of proton fluxes of E>10 MeV for epochs 1960 and 2010 at 800 km altitude.
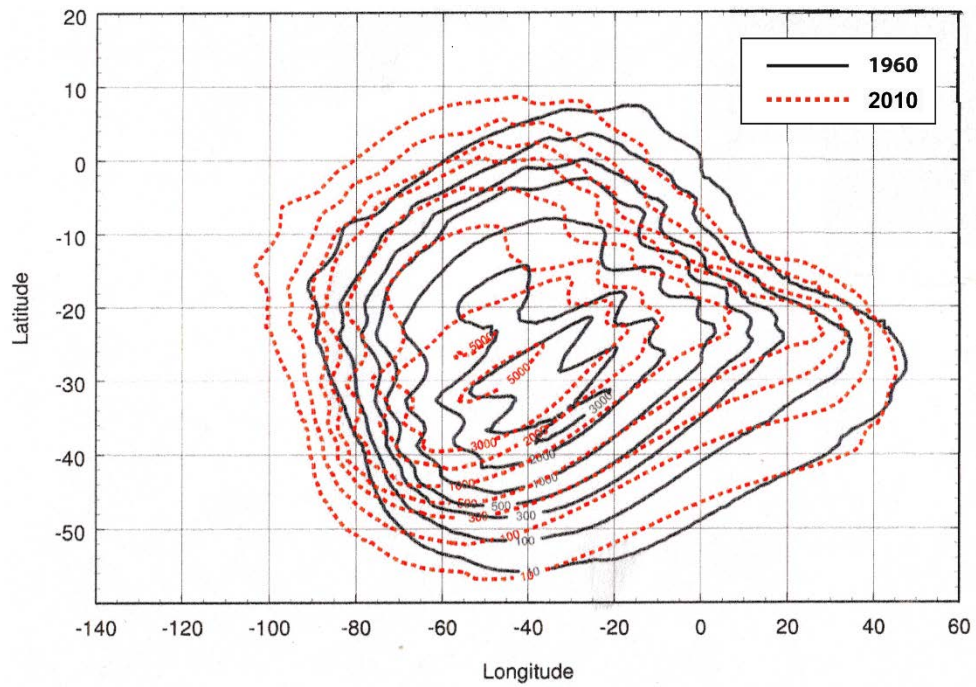
Figure 55: Comparison of proton fluxes of E>30 MeV for epochs 1960 and 2010 at 800 km altitude.
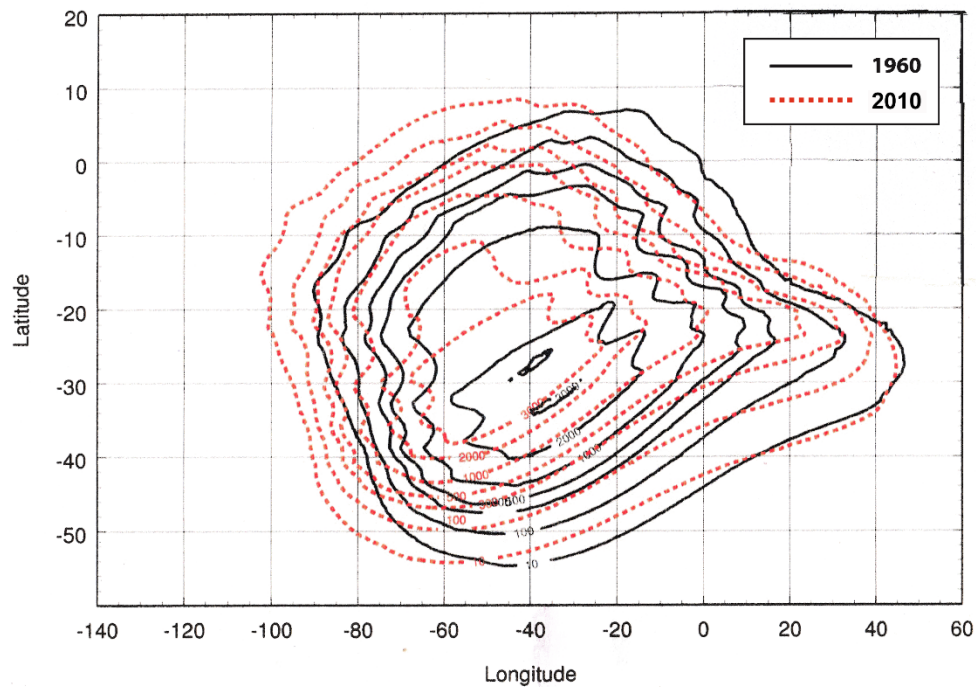
Figure 56: Comparison of proton fluxes of E>50 MeV for epochs 1960 and 2010 at 800 km altitude.
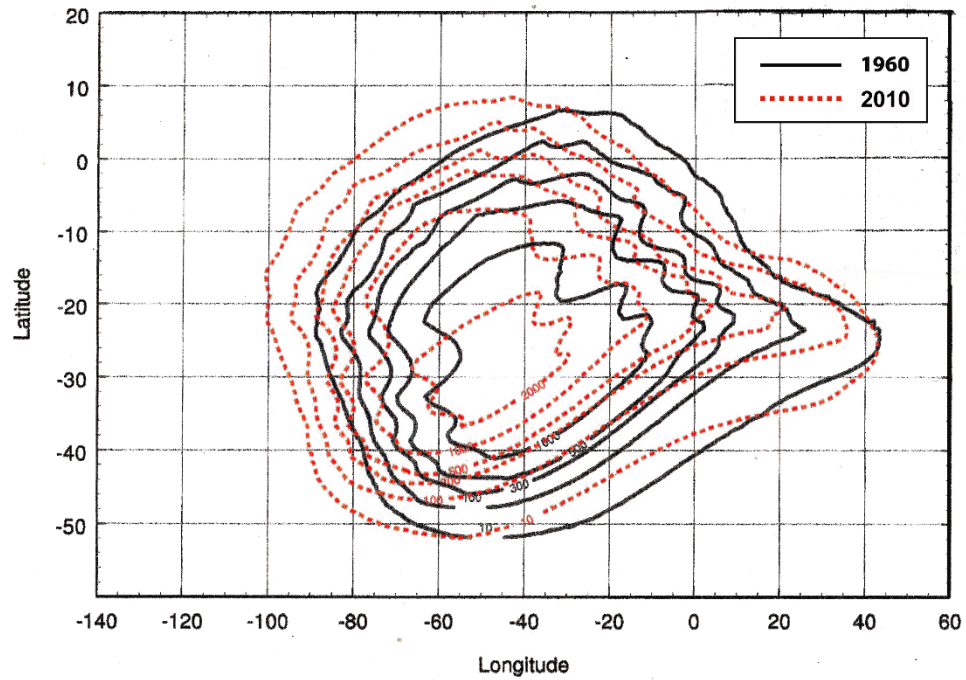
Figure 57: Comparison of proton fluxes of E>100 MeV for epochs 1960 and 2010 at 800 km altitude.
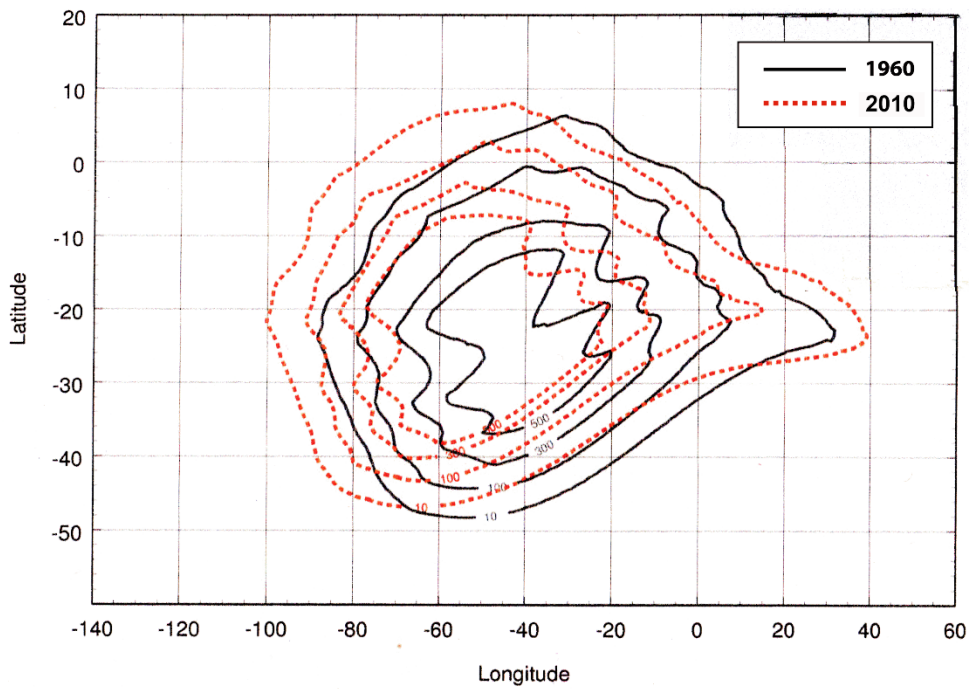
Figure 58: Comparison of proton fluxes of E>200 MeV for epochs 1960 and 2010 at 800 km altitude.
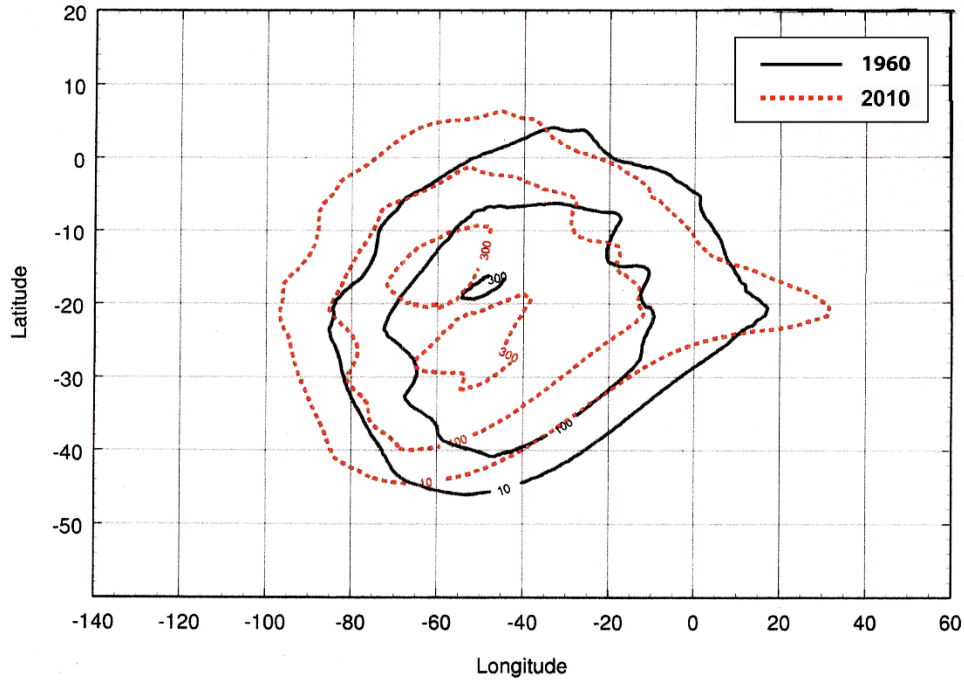
Figure 59: Comparison of proton fluxes of E>300 MeV for epochs 1960 and 2010 at 800 km altitude.

50.   Another way to show the effects of the field changes on the radiation evaluations for spacecraft is via the relative distribution of **B-L** points visited by the orbit. These results were obtained from the identical polar trajectory at 800 km altitude. Figures 60 to 63 list the **B-L** combinations experienced by the orbit during the years 1960 and 2010, for particles with energy of 10, 50, 100, and 300 MeV, respectively. The blue numbers reflect 1960, while the red numbers reflect 2010. The numbers indicate how many times each combination was encountered. As expected, it is apparent, that the same trajectory, for the same geographical positions, experienced, different combinations of **B-L** values at all orbit points in the 2010 calculations, but also encountered new combinations and dropped others. The quantity of points listed correlate with the size of the **SAA** area occupied by the particles of the indicated energy. Many of the dropped positions lie in the lower intensity regions of the model and many of the gained positions lie in the higher intensity regions.

Comparison Of SAA BL Bin Occurrences Of Data From The WorldMap Output Using A 1 By 1 Degree Grid Size (Calculated via RadBeltGrid)

Figure 60: Comparison of orbital **SAA B-L**-bins for epochs 1960 and 2010 of E>10 MeV protons.

Comparison Of SAA BL Bin Occurrences Of Data From The WorldMap Output Using A 1 By 1 Degree Grid Size (Calculated via RadBeltGrid)

B \ L	1.05	1.1	1.15	1.2	1.25	1.3	1.35	1.4	1.45	1.5	1.55	1.6	1.65	1.7	1.75	1.8	1.85	1.9	1.95	2	2.05	2.1	2.15	2.2	2.25	2.3	2.35	2.4	2.45	2.5	2.55	2.6	2.65	2.7	2.75	2.8	2.85	2.9	2.95	3	3.05	3.1	3.15
0.29																																											
0.285																																											
0.28																																											
0.275																																											
0.27																																											
0.265																																											
0.26																																											
0.255												2	5	5	5	6	2	8	3	2				1																			
0.25										4	7	8	7	10	10	4	10	4		8	7	4	2	6	5	3																	
0.245								4	12	10	8	9	12	5	11	6	9	8		10	9	10	8	4																			
0.24							7	12	13	9	12	11	10	11	8	9	10	9	8	10	11	13	11	13	3																		
0.235						9	19	14	16	12	13	17	10	13	11	12	12	14	13	17	13	17	27	29	17	4																	
0.23					10	21	23	17	19	15	19	10	17	14	15	18	15	17	20	23	34	24	10																				
0.225			4	3	17	21	23	22	19	18	16	18	19	15	17	19	19	24	34	33	18																						
0.22		4	32	23	25	21	19	21	17	20	17	17	20	20	24	30	40	26	7																								
0.215	1	62	47	23	26	20	23	17	20	19	26	24	26	34	42	22	2																										
0.21	13	61	110	31	27	26	21	18	24	25	22	26	33	42	23																												
0.205	78	187	105	37	29	28	25	26	24	24	36	47	24																														
0.2	50	239	94	36	31	26	29	28	34	35	37	2																															
0.195	37	234	76	37	34	34	36	47	57	13																																	
0.19		233	61	46	42	42	63	40																																			
0.185		195	80	60	65	82	21																																				
0.18		133	149	111	73	2																																					
0.175		136	39																																								
0.17		24	203	70	66	81	58	15																																			
0.165			121	101	56	4																																					
0.16																																											
0.155																																											
0.15																																											
0.145																																											
0.14																																											
0.135																																											
0.13																																											
0.125																																											
0.12																																											

Figure 61: Comparison of orbital **SAA B-L**-bins for epochs 1960 and 2010 of E>50 MeV protons.

Comparison Of SAA BL Bin Occurrences Of Data From The WorldMap Output Using A 1 By 1 Degree Grid Size (Calculated via RadBeltGrid)

Figure 62: Comparison of orbital **SAA B-L**-bins for epochs 1960 and 2010 of E>100 MeV protons.

Figure 63: B-L bin occurrence grid comparing epochs 1960 (blue/upper value) and 2010 (red/lower value) for E>300 MeV protons. B value in Gauss (vertical axis) versus L Value (horizontal axis).

B	Year	1.05	1.1	1.15	1.2	1.25	1.3	1.35	1.4	1.45	1.5	1.55	1.6	1.65
0.235	1960									5	8	3		
0.23	1960									11	23	17	10	
0.225	1960							2	12	23	22	19	18	4
0.225	2010									2	6	8	2	
0.22	1960				2	20	11	22	21	19	21	17	20	12
0.22	2010									4	12	10	14	7
0.215	1960		56	43	22	26	20	23	17	20	19	26	3	
0.215	2010			15	1	13	17	16	13	12	9	7		
0.21	1960	22	110	31	27	26	21	18	24	25	22	26	14	
0.21	2010		8	45	20	32	26	24	18	14	15	9		
0.205	1960	103	105	37	29	28	25	26	24	24	36	47	21	
0.205	2010	3	68	58	28	38	27	29	17	25	22	12		
0.2	1960	205	94	36	31	26	29	28	34	53	37	2		
0.2	2010	45	105	45	30	34	25	24	21	20	28	16	14	
0.195	1960	234	76	37	34	34	36	47	57	13				
0.195	2010	131	108	35	26	26	19	24	24	22	22	17	1	
0.19	1960	233	61	46	42	42	53	40						
0.19	2010	219	102	34	28	27	24	20	22	22	22	22	26	5
0.185	1960	199	80	60	65	82	21							
0.185	2010	180	100	36	30	25	26	25	24	26	25	28	35	27
0.18	1960	133	149	111	73	2								
0.18	2010	165	93	39	33	31	29	31	30	40	58	43	27	4
0.175	1960	136	39											
0.175	2010	145	102	51	43	40	43	61	57	33	3			
0.17	2010	24	203	70	66	81	58	15						
0.165	2010		121	101	58	4								

Figure 63: Comparison of orbital **SAA B-L**-bins for epochs 1960 and 2010 of E>300 MeV protons.

Solar Cycle and Events

51.   Frequently, the minimum and maximum activity phase of the solar cycle, and of the corresponding versions of the **AP8** and **AE8** models, are mentioned and invoked in the **SAA** literature **to explain the obtained data or justify the author's conclusions**, particularly in regards to environmental conditions and their effects on scientific instruments or measurements.

52.   Several topics are considered in this section: **(a)** solar cycles, **(b)** solar activity, and **(c)** effects on the **SAA** (radiation, size, location, drift). In modern times, when referring to solar cycles, the prevailing concept is to think of them in terms of a fixed 11-year duration, which is the typical average. The actual length of a solar cycle is unpredictable, however, and may vary from a short <9-year to a long >13-year period. There does not yet exist a sure and reliable way to accurately predict the duration of a future cycle.

53.   The active phase of a solar cycle is defined as a seven-year period, starting 2.5 years before the absolute maximum sunspot peak and ending 4.5 years after. The remaining time is classified as "solar minimum". Consequently, since the active phase is constant, and solar cycles vary in length, the solar minimum period is (by necessity) **a cycle variable.** A presentation of that solar cycle reality is provided in Figure 64 for the 5 most recent cycles, in which the cycles are numbered and the periods are indicated.
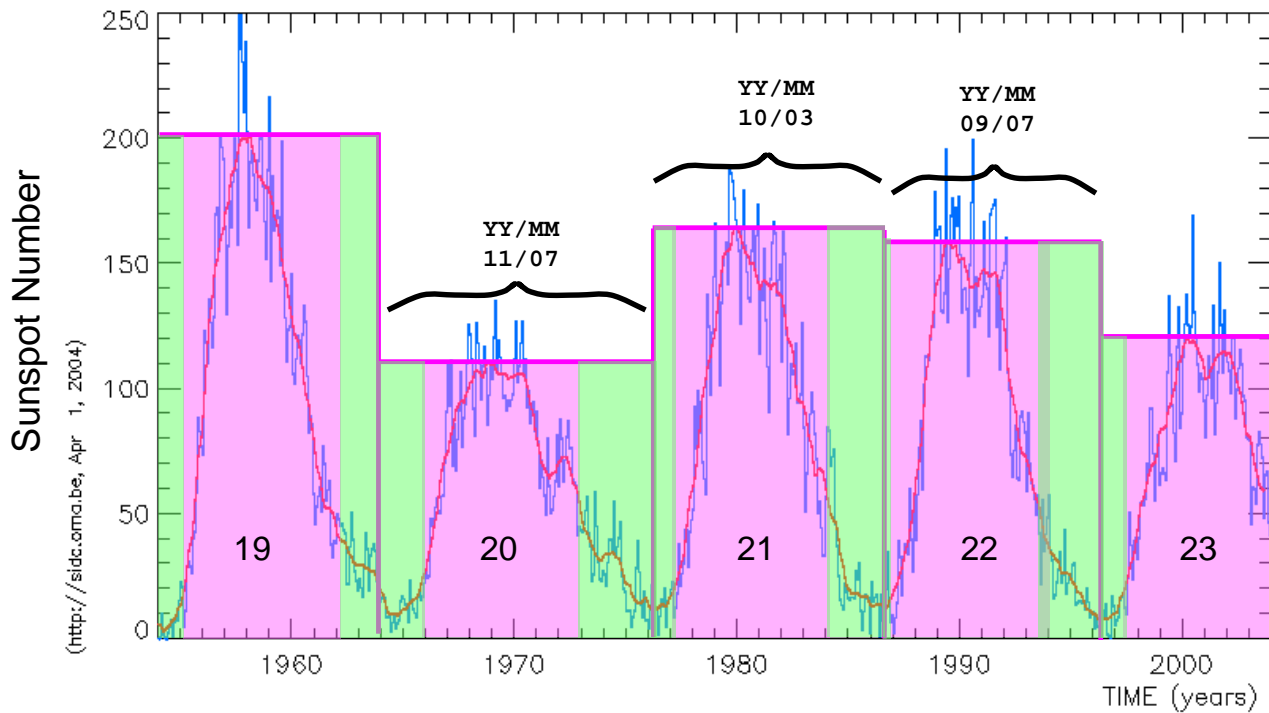
Figure 64: Activity and duration of solar cycles 19-23.

54.   Another aspect of solar cycles is their activity level. It is obvious from the recorded sunspot totals shown in Figure 64, that the activity level in each cycle is quite different. Historical records show a time at which no sun-spots appeared on the sun: the Maunder Minimum. This indicator of activity, however, did not exactly correspond to the occurrence of solar flare proton events (**SPE**) or coronal mass ejections (**CME**), which may have extended from small to extremely large in duration and intensity (**CME**'s happen predominantly during the active phase, although some **SPEs** do occur also in the quiet ["inactive"] phase). As mentioned before in paragraph 16, these events cannot be predicted with accuracy and confidence. A probabilistic statistical prediction approach was developed by King [14] as a function of **(a)** mission duration during the active period and **(b)** the confidence level that assumes a predicted number of extremely large events will not be exceeded.

55.   Subsequently, a new approach was developed based on the maximum entropy principle that accurately described the complete distribution of solar proton event magnitudes as a truncated power law (Xapsos [19]). This led, in conjunction with other statistical methods, to models of worst case events (Xapsos [20]), and cumulative fluences during missions for both protons (Xapsos [21]) and heavy ions (Xapsos [22]), In each case model inputs are the time period of the space mission and desired confidence level, as was the case for the King Model.

56.   A final concern regarding solar particle events, and their impact on the Earth's radiation environment, pertains to the penetration of solar protons into the **SAA,** especially from the occurrence of major flares or **CME**s. Typical spectra of extremely large proton events are shown in Figure 65, which indicates their steep decline: the spectra do not exceed energies greater than a few hundreds of MeVs protons, because of their charge, are being deflected by the magnetic field in a process that involves the ratio of their momentum-over-charge, i.e. the "magnetic rigidity". In order to overcome the magnetic rigidity and penetrate into the low altitude regime of the **SAA**, protons need to have at least an energy of about E = 2900 MeV (i.e. **2.9 GeV**). This rigidity relationship is illustrated in Figure 66.[14,15] It appears these GeV protons cannot be trapped in the Van Allen Belt.
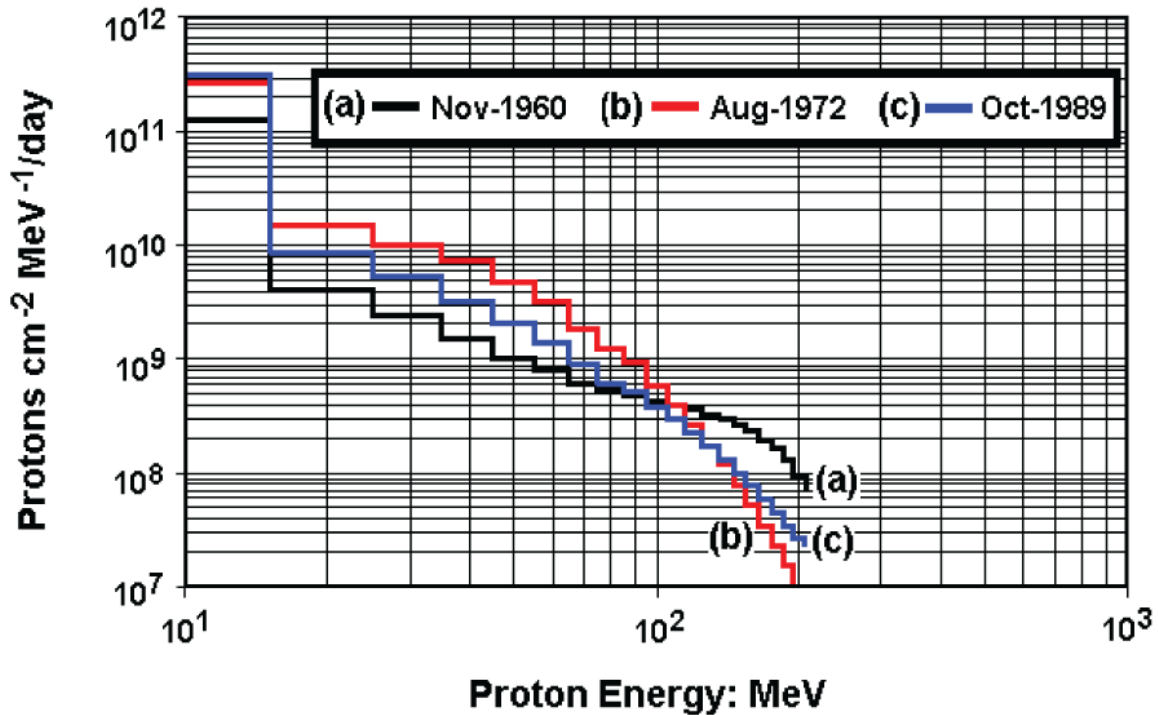
Figure 65: Typical spectra of extremely large solar proton events.

---

[14] Quote from APPENDIX A [4a]: *"In this region [SAA] the shielding effects of the geomagnetic field have been severely compromised, thus allowing high energy particles trapped in the Van Allen radiation belts to penetrate deep into the upper atmosphere to altitudes below 100 km."*

[15] Quote from APPENDIX A [13a]: *"However, other satellite missions, although designed for Earth observation, have also provided valuable information on solar flux. In fact, energetic particles (such as protons) reaching altitudes between 500 and 800 km produced signals by causing spikes (or outliers) in the measured radiances, as the case of NASA MOPITT ...."*.
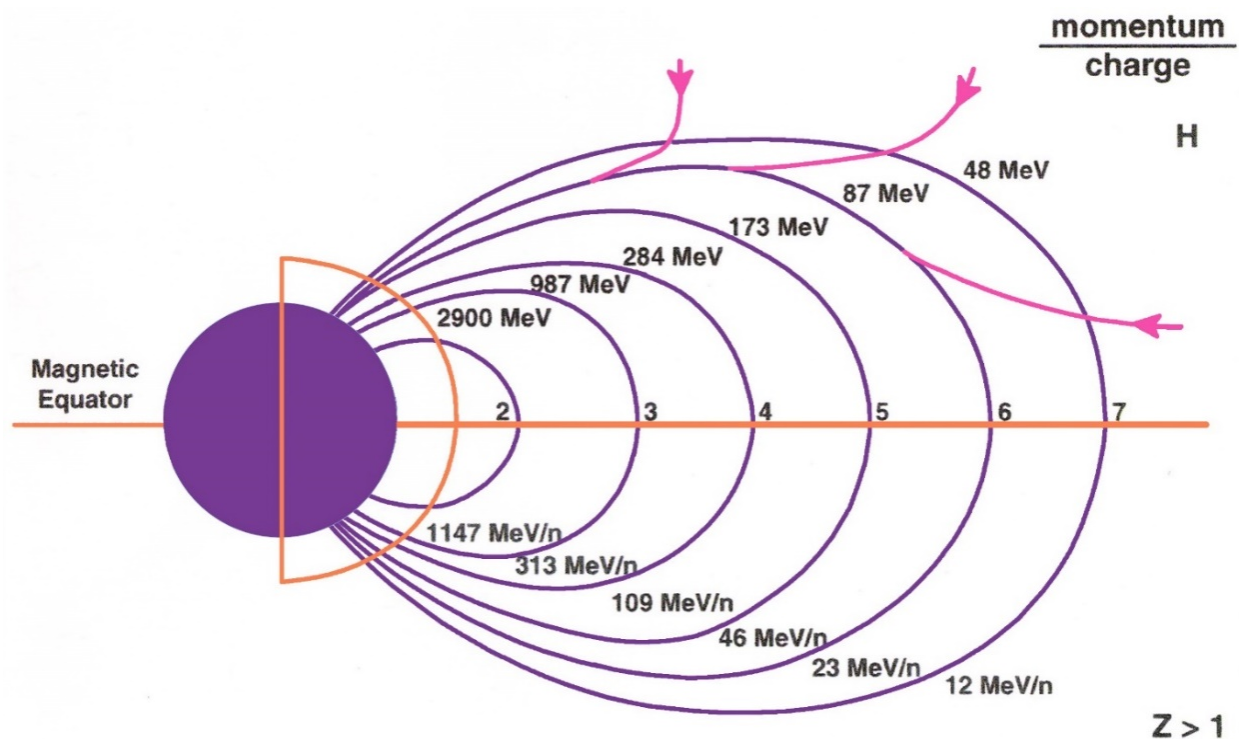
Figure 66: L-shell contours with rigidity imposed energy penetration limits.

57.   The question of energetic proton penetration into the inner zone of the Van Allen belts, and hence the **SAA**, is of particular importance because it is frequently mentioned in several publications, which claim that these particles affected their measurements in the **SAA** and had an impact on the **SAA**'s evolution. However, the "**rigidity principle**" applies to the inner zone of the radiation belts, and consequently the **SAA**; protons must have energies greater than **2.9 GeV** (as mentioned above) at least, to be able to reach the low altitude range of the anomaly.

Cosmic Rays

58.   A few papers mentioned concern about the penetration of cosmic rays into the **SAA** region. Solar and galactic cosmic rays are high-energy heavy ions: 90% hydrogen, 9% alpha particles, and 1% nuclei of heavier elements. In order for these particles to reach the inner zone of the Van Allen belts, and hence the **SAA**, they must have energies in excess of **1.15 GeV per nucleon**. All cosmic rays with lower energies are deflected by the Earth's magnetic field (rigidity cutoff). Most workers consider the galactic cosmic rays reaching the vicinity of the Earth (about 1 **AU**) as fully ionized, which means maximum deflection. As a consequence, very few of these particles reach the **SAA**. A solar cycle variation has been observed in the cosmic ray flux levels between solar minimum and solar maximum. During the active phase of the solar cycle, the cosmic ray intensities are about a factor of two or so lower than during solar minimum. It is obvious, considering Figure 66, that more cosmic rays have access to the higher latitude regions than near the equator, with a free unimpeded penetration over the poles, where open field lines connect directly to the interplanetary medium.[16]

---

[16] As a consequence of this shielding effect, neutrons, the cosmic ray daughter products in the atmosphere from collisions with the atmospheric constituents nitrogen and oxygen, are more numerous at high latitudes than near the equator [15].
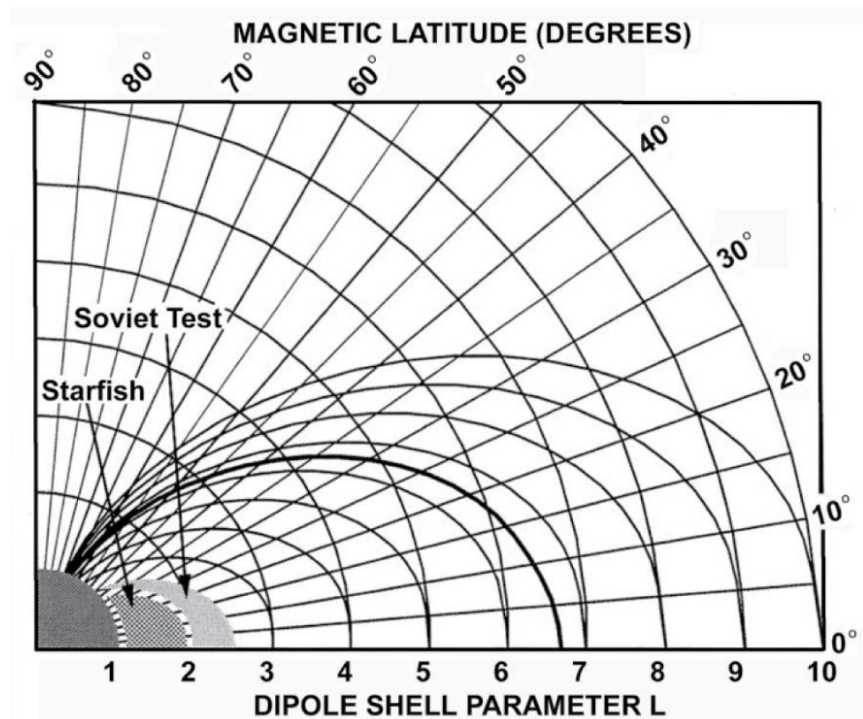
Figure 67: Schematic of the distribution of fission electrons from the STARFISH and Soviet tests in magnetic coordinates.

Artificial Radiation Belt

59.   A rare but serious threat to space missions travelling through the inner zone of the radiation belt, and especially the **SAA**, can be another exo-atmospheric explosion of a nuclear device, as for example, the famous **US "*STARFISH PRIME High Altitude Weapons Test*"** on July 9, 1962, over Johnston Island in the Pacific (at ~400 km altitude, 1.4 megaton yield) [16]. A similar Soviet high-altitude nuclear test was conducted over Semipalatinsk in Kazakstan on October 28, 1962. A schematic of the distribution of the fission electrons from those two tests is shown in Figure 67, in terms of the **L** parameter and the magnetic latitude. The **STARFISH** event injected about 10^{29} fission electrons into the magnetosphere, raising the intensity of the inner zone electron population by several orders of magnitude. Within the following six months, 10 satellites were lost from the effects of the increased radiation levels.

60.   A map of the **STARFISH** threshold-energy of E>0.28 MeV, as a function of magnetic shell parameter **L,** for the artificial electron cutoff times, is shown in Figure 68 [1**7**]. Figure 69 shows the integral STARFISH enhanced Van Allen belt electron fluxes before and after the Soviet event, in regions from **L** of ~1.8 – 4.0, for particles with energies of E>0.5 and E>1.9 MeV **[18].** The **STARFISH** electrons were mostly distributed over an **L**-range from 1.1 – 2.2 e_r, whereas the Soviet particles ranged from **L**=1.8-4.0, because of the higher test latitude. Significantly, the **STARFISH** 2-MeV electrons lasted about 8 years, before decaying back down to the natural background levels. Figure 70 shows the average lifetime of the 2 MeV fission electrons from the **STARFISH** and the Soviet experiments. The data suggest that longevity is maximum at low **L** values, decreases rapidly toward the slot region, and is in the range of weeks, and perhaps only days, at larger **L** values (approximately 10-12 days at Geostationary Earth Orbits [**GEO**]).
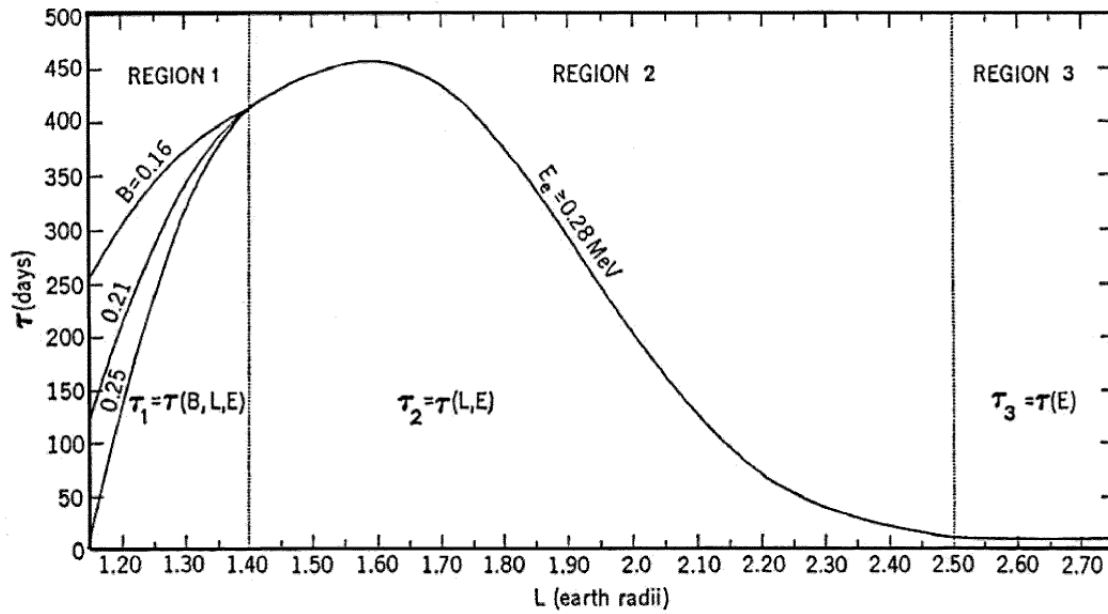
Figure 68: Decay cutoff times in months for the STARFISH model as a function of threshold energy and L paramets.
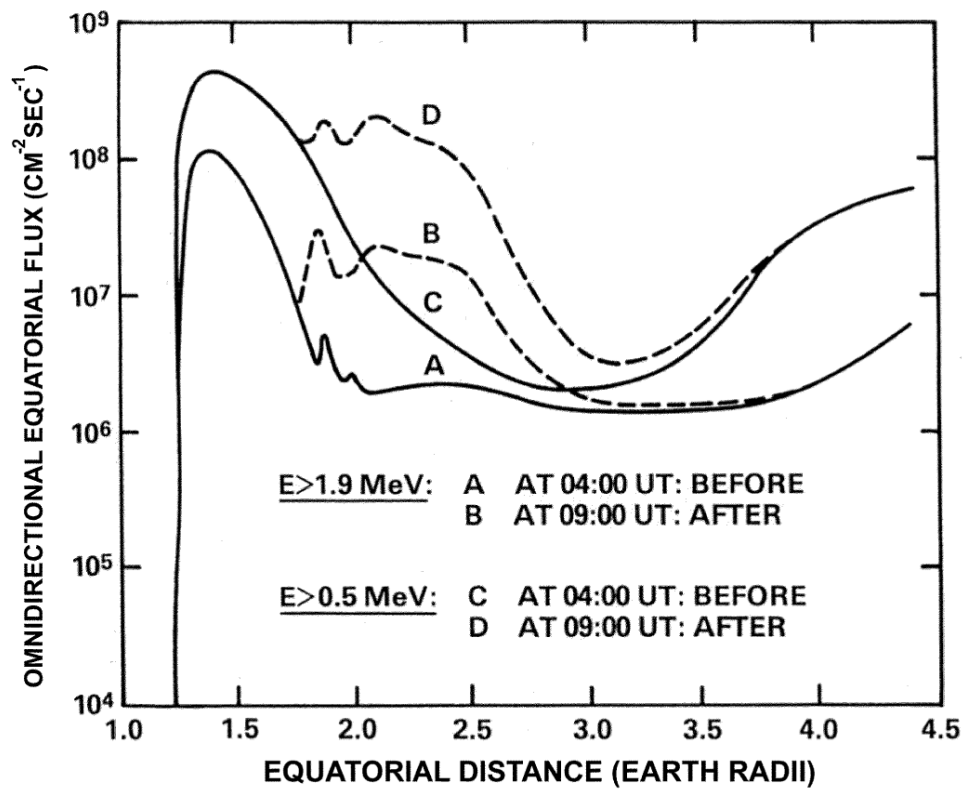
Figure 69: Integral Van Allen belt electrons before and after the Soviet event.
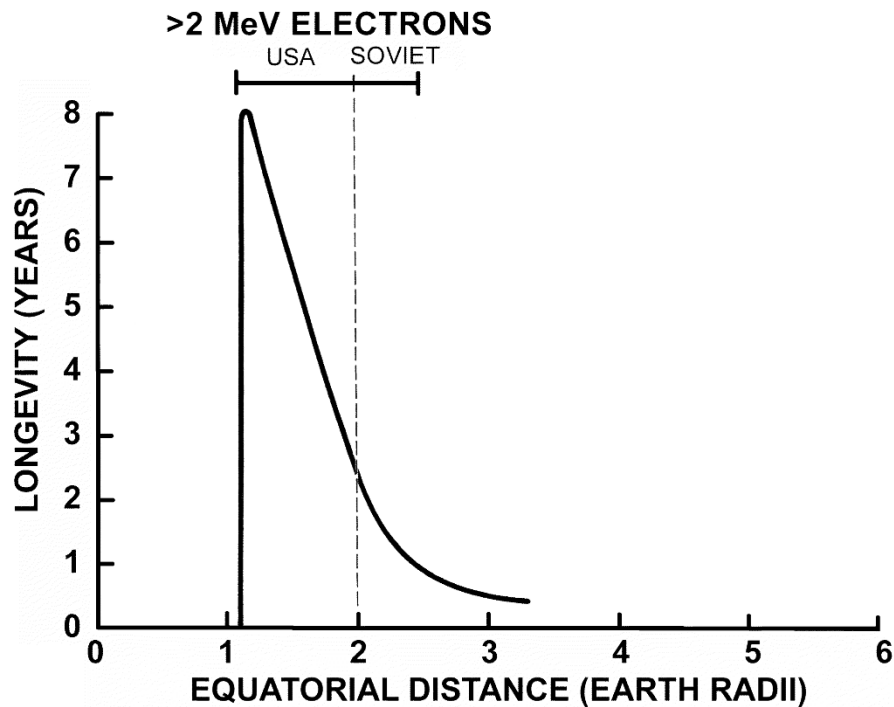
Figure 70: Comparison of the average lifetimes of E>2 MeV electrons for the STARFISH and Soviet tests.

<u>Conclusion</u>

61.   In conclusion, the effects of the differing radiation exposures experienced by satellites over long mission durations in near-Earth space, and particularly within the **SAA**, have to be expected, because the Earth's magnetic field will continue to change. A better approach to calculating intensity, exposure, and risk, would be to use a dynamic radiation model that takes into account and accommodates these natural field variations. Until a dynamic model becomes available, calculations performed with current models for later epochs (projections), will always yield higher values because of **(a)** the increasing size of the **SAA**, **(b)** the higher intensity patches that will appear and increase in size, and **(c)** longer exposure times during crossings of the larger area of the expanding anomaly.

62.   We only have two sets of models available that describe and define the near-Earth space environment: **(a)** geomagnetic field models, and **(b)** particle radiation models. In a process of evolution, these have been periodically updated and re-issued in an improved and/or expanded form, as new information is established and has been officially confirmed. In the meantime, whether perfect or not, we continue to use the current models for two reasons: **(a)** we have no other, better tools, and **(b)** they provide a common, acceptable base of reference for the entire international science community.

63.   It would be preferable and prudent to follow a more realistic and conservative approach in evaluating spacecraft radiation exposures, by using the latest existing models until better ones become available, even if that would involve possibly over-predicting the vehicle encountered particle fluences. It is better to be on the safe side, than to risk failure, by introducing makeshift remedies that don't correspond to the actual reality, and underestimate the vehicle-encountered radiation (Example: Table 2)

In Summary

64.   ***The drift of the SAA***: *In most papers from the **SAA** literature, data from experiments unrelated to the **SAA** were used. The primary interest and concern of the authors of these papers appeared to be the drift of the **SAA** and the effects of the **SAA's** radiation on **LEO** missions. As a result, an unexpectedly large spread in the derived **SAA** drift rates was observed. These unusual findings could be due to the great variety in acquisition methods, to the criteria used for the selection of data, and to the data processing techniques. The result is that the **SAA** drift values appear to be spread over an abnormally large range. Specifically, the minimum drift rate reported is **0.17^0/yr W** and **0.08^0/yr N**, and the maximum drift rate reported is **0.66^0/yr W** and **0.22^0/yr N**. The difference is almost a factor of **4** for the **W** direction, and approximately a factor of **3** for the **N** direction, which, in both directions, is much larger than expected, and which probably reflects an inconsistent approach, using non-specific data, to defining and describing the **SAA**. The corresponding data sources are listed in **Table 4**.*

65.   ***The Size of the SAA***: *In several publications authors' claim to have established the size of the **SAA** based on analyses of data from their unrelated experiments. In rare instances, the authors also imply that there is no altitude dependence. However, the accurate size of the "anomaly" cannot be defined in a single frame of reference from non-specific data, because the **SAA** has a different shape and occupies a different area at any given time, when plotted in reference to the variables (**a**) altitude, (**b**) particle species (electrons, protons), (**c**) particle energy (high, low), and (**d**) effects on electronics. Thus, many maps could be produced for temporally and spatially identical conditions, varying in the detail of the size and the shape of the **SAA**, depending on the type and quality of the data used.*

Table 4: SAA North and **W**est drift values reported in the literature.

	Author	Year	Experiment	Drift of SAA	
1.	Casadio	2010	ATSR	0.35°/yr W 0.22°/yr N	} in text
				0.30°/yr W 0.10°/yr N	} in Introduction
				0.35°/yr W 0.12°/yr N	} in Abstract & Conclusions
2.	Casadio	2011	ATSR	0.24°/yr W 0.12°/yr N	} average, in Conclusions
				0.17°/yr N	} in Analysis
				4.8°/20 yr W 2.4°/20 yr N	} in text
	Casadio	2011	SWIR	0.35°/yr W 0.12°/yr N	} in text
3.	Balhwar	1997	ISS	0.28°/yr W 0.08°/yr N	} between 1973-1995
4.	Konradi	1994	Shuttle	6.9°/20 yr W 3.4°/20 yr N	} in text
				6.7°/20 yr W	} in Discussion
5.	Ginet	2006	APEX	0.43°/yr W	} = 30 MeV protons
				0.50°/yr W	} = 60 MeV protons
6.	Hell	2010	RHESSI	0.66°/yr W	} in text and abstract
7.	Mullen	1988			
8.	Lauriente	1996	} SEU based }	0.19°/yr to 40°/yr W	} from experiments
9.	Adolphsen	1995			
10.	Fürst	2009	RXTE	0.248°/yr W	} in text
				0.27°/yr W	} calculations
				0.30°/yr W	} in Abstract

Minimum: 0.08°/yr N 0.19°/yr W
Maximum: 0.22°/yr N 0.66°/yr W
D factor of: ~3 ~3.5

Some Afterthoughts

Judged by the plethora of published papers in the topic, there is a very significant interest in the scientific community regarding the **SAA**. Concerns about the "anomaly" arise from a breadth of specialties.

Because all information to date has been obtained in a peripheral way, i.e. using opportunistic data from unrelated experiments, a large variety of opinions, results, and conclusions have been presented. These findings have sometimes been mutually contradictive, misleading, or confusing. What is needed is an independent research project specifically exploring the unknowns of the SAA, i.e. a dedicated in-depth study of the "anomaly".

A special exclusive examination of the **SAA**, with instruments specifically designed for that purpose, would focus primarily on its: **(a)** nature, **(b)** source, **(c)** dynamics, **(d)** evolution, **(e)** variability, and **(f)** its future, and would lead to a more reliable definition and model of the "anomaly".

Such research would also address the causes effecting slow (long range) and fast (short range) changes of the **SAA**, such as: **(1)** space weather events, **(2)** solar flares and **CME**s, **(3)** magnetic storms, **(4)** atmospheric conditions, **(5)** geomagnetic jerks and reversals, **(6)** solar cycle effects, **(7)** non-dipole contributions/effects, etc.

The currently available information on these topics is largely incomplete, inadequate, and inconsistent, having been collected by a variety of diverse instruments, on missions dedicated to other important scientific research, unrelated to the **SAA**. The data from these missions/instruments, and the concomitant conclusions drawn, are seriously undermined as a result of: **(a)** the type of instrument used and its sensitivity and calibration, **(b)** the quality of the measurements (contamination, noise), **(c)** the data analyses and processing methods (Weibull. Gaussian, Gumbel, etc.), **(d)** the environmental particle species (electrons, protons, cosmic rays), **(e)** the altitude in the **SAA** (200-1500 km), **(f)** the time- and epoch-effects on the measurements (day-night, solar cycle, diurnal, seasonal, etc.), and **(g)** the magnetic variations.

Finally, from the review of about two dozen publications about the SAA, it appears that frequently references are made to data, arguments, or statements in other similar documents, and opinions are being repeated, that are not based on sound scientific procedures or principles, thus promulgating unconfirmed assumptions and theories.

References

1. Kurnosova, Kolobianina, Logachev, Razorenov, Sirotkin, Fratkin, *"Discovery of radiation anomalies about South Atlantic at heights of 310-340 km"*, Planet. Space Sci., **9**, 513-516, August 1962.
2. International Geomagnetic Reference Field (IGRF), International Association of Geomagnetism and Aeronomy (IAGA), 1968.
3. Retrieved from: wdc.kugi.kyoto-u.ac.jp/igrf/anime/index.html
4. Fairfield, D.H. and G.D. Mead, *"Magnetospheric Mapping with a Quantitative Geomagnetic Field Model"*, J. Geophys. Res., **80**, 535, 1975.
5. Olson, W.P., and K.A. Pfitzer, *"A Quantitative Model of the Magnetospheric Magnetic Field"*, J. Geophys. Res. **79**, 3739, 1974.
6. Tsyganenko, N.A., *"A magnetospheric magnetic field model with a warped magnetic tail current sheet"*, Planet. Sci., v. 37 (1), pp. 5-20, 1989.
7. Tsyganenko, N.A., *"Modeling the Earth's Magnetospheric Magnetic Field Confined Within a Realistic Magnetopause"*, J. Geophys. Res., **100,** 5599-5612, 1995.
8. Seltzer, S.M., *"SHIELDOSE: A Computer Code for Space-Shielding Dose Calculations"*, National Bureau of Standards, NBS Technical Note 1116, US Government Printing Office, Washington, D.C., 1980.
9. Jordan, T., *"A Radiation Transport/Shielding Code: U*ser's *Guide"*, Experimental and Mathematical Physics Consultants, Gaithersburg, Maryland, 1987.
10. Agnostelli et al., *"GEANT4-A Simulation Tool Kit"*, Nuclear Instruments and Methods in Physics Research, Vol. A, No. 506, pp. 250-303, 2003.
11. Sawyer, D. and Vette, J., *"AP-8 trapped proton environment for solar maximum and solar minimum"*, National Space Science Data Center, Report 76-06, Greenbelt, Maryland, 1976.
12. McIlwain, C., *"Coordinates for mapping the distribution of magnetically trapped particles"*, J. Geophys. Res., **66**, 1961.
13. Vette, J.I., and Sawyer, D. M., *"Short Report on Radiation Belt Calculations"*, NSSDC, NASA-GSFC, Greenbelt, MD, 1986.
14. King, J.H., *"Solar Proton Fluences for 1977-1983 Space Missions"*, J. Spacecraft Rockets, **11**, 401, 1974.
15. Normand, E., and Baker, T. J., *"Altitude and latitude variations in avionics SEU and atmospheric neutrons."*, IEEE Trans. Nucl .Sci., 40, 6, 1993.
16. Hess, W.N., *"The Effects of High Altitude Nuclear Explosions"*, NASA TN D-2402, September 1964.
17. Stassinopoulos, E.G., and P. Verzariu, *"General formula for decay of STARFISH electrons"*, J. Geophys. Res, vol.76, pp. 1841-1844, 1971.
18. Barth, J.L., C.S. Dyer, and E.G. Stassinopoulos, *"Space, Atmospheric, and Terrestrial Radiation Environments"*, IEEE Trans. Nucl. Sci., vol. 50, no. 3, June 2003.
19. Xapsos, M.A., Summers, G.P., and Burke, E.A., *"Probability Model for Peak Fluxes of Solar Proton Events"*, IEEE Trans. Nucl. Sci., **45**, pg. 2948-2953, December 1998.
20. Xapsos, M.A., Summers, G.P., Barth, J.L., Stassinopoulos, E.G., and Burke, E.A., *"Probability Model for Worst Case Solar Proton Event Fluences"*, IEEE Trans. Nucl. Sci., **46**, pg. 1481-1485, December 1999.
21. Xapsos, M.A., Summers, G.P., Barth, J.L., Stassinopoulos, E.G., and Burke, E.A., *"Probability model for Cumulative Solar Proton Event Fluences"*, IEEE Trans. Nucl. Sci., **47,** pg. 486-490, June 2000.

22. Xapsos, M.A., Stauffer, C., Jordan, T., Barth, J.L., and Mewaldt, A., *"Model for Cumulative Solar Heavy Ion and Linear Energy Transfer Spectra",* IEEE Trans. Nucl. Sci., **54,** pg. 1985-1989, December 2007.
23. Ginet, G.P., et al., *"AE9/AP9 and SPM: New Models for Specifying the Trapped Energetic Particle and Plasma Environment",* Space Sci. Rev., **179,** pg. 579-615, 2013.
24. Huston, S.L., *"Space Environments and Effects: Trapped Proton Model",* Report NAS8-98218, The Boeing Co., Huntington Beach, CA, January 2002.

List of Projects, Instruments, Missions
(mentioned in SAA papers (re: source of data used by authors)

a. AMPTE = University of Surrey Satellite (UK)

b. ATSR = Along Track Scanning Radiometer (ESA)

c. CEASE = Compact Environment Anomaly Sensor (USAF)

d. CREDO = Cosmic Radiation Environment and Dosimetry (UK)

e. DEMETER = Detection of Electro-Magnetic Emissions Transmitted from Earthquake Regions (CNES)

f. DMI = Doppler Michelson Interferometer (SWIFT, Canada)

g. DORIS = Doppler Orbitography and Radiopositioning Integrator by Satellite (CNES)

h. DSLP = Dual Segmented Langmuir Probe (ESA)

i. ENVISAT = Environmental Satellite (ESA)

j. ISIRO = ???

k. JASON == Ocean Surface Topology Mission (NASA-CNES)

l. MEPED = Medium Energy Proton and Electron Transport Studies (CANADA)

m. MODIS = Moderate-Resolution Imaging Spectroradiometer (NASA)

n. MOPITT = Measurement of Pollution in the Troposphere (NASA)

o. NYULIN = Dosimeter on Board MIR Space Station (Bulgarian)

p. OERSTED = Geomagnetic Research Satellite

q. PAMELA = Payload for Antimatter Exploration and Light-nuclei Astrophysics (Russia, Germany, Italy, Sweden)

r. POES = Polar Operational Environmental Satellite (NOAA)

s. PROBA-2 = Project for Onboard Autonomy (ESA)

t. RHESSI = Ramaty High Energy Solar Particle Spectroscopic Imager (NASA)

u. SAMPEX = Solar Anomalous and Magnetospheric Particle Explorer (NASA)

v. SEM-2 = Space Environment Monitor (NOAA)

w. SREM = Space Radiation Environment Monitor (India)

x. SWIR = Short Wave Infrared Sensor (ESA)

y. TED = Total Energy Detector (POES)

z. TERRA = Earth Observing Satellite (NASA)

aa. TPMU = Thermal Plasma Measurement Unit (ESA)

bb. TSX-5 = Tri-Service Experiment (USAF)

cc. UARS = Upper Atmosphere Research (UK)

dd. UoSAT = University of Surrey Satellite (UK)

Appendix A.

Important Statements

Good or Bad --- Right or Wrong

1. **Hell, Natalie**, *"The Evolution of the South Atlantic Anomaly Measured by RHESSI"*, Erlanger Centre for Astroparticle Physics, Dr. Remeis-Sternwarte Bamberg, Friedrich-Alexander-Universitaet, Erlangen-Nuernberg, Germany, 2010

   a) **Quote:** "The position of **RHESSI** in latitude, longitude, and altitude is calculated via two different algorithms. **The first algorithm has three faults**: **(a)** sometimes **no numerical value is given** at all, **(b)** on other occasions, the derived altitude is suggested to be constant, equal to 6378.13 km for a while, **being obviously wrong**, **(c) the third defect is much more delicate**: the satellite seems to **jump occasionally from its orbit at 540 km to 600 km to less than 500 km and back again** within short time, which is a rather unrealistic behavior for a spacecraft. In contrast, **the second algorithm** produces no such outliers for three months in 2006: **from March to May the position calculation completely failed, claiming an altitude of minus earth radius**."

2. **Smart, D.F. and M.A. Shea**, "*Comment on the use of GOES solar proton data and spectra in solar proton dose calculations"*, Radiation Measurements, **30**, 327-335, 1999

   a) **Quote: "Appendix**: **Conversion from CD-ROM high energy proton flux data to corrected proton flux** developed by Sauer (1995): Procedure: **Convert data back to counts**, **correct for side penetration** and **apply new geometric factors** to obtain **corrected flux**. **Calibration: The greatest** unresolved problem is the response of the HEPD instrument. The threshold energy adjustment and the geometric factor adjustment proposed by Sauer (1995) are a good step. These are helpful resolving some of the discrepancies in **P8**, **P9**, and **P10** data".

3. **Fuerst et al.,** "*Temporal Variations of Strength and Location of the South Atlantic Anomaly as Measured by RXTE*", Earth and Planetary Science Letters, 10 February 2009

   a) **Quote:** "The **AP8/AE8** models are based on data taken with **older instruments which were not necessarily as sophisticated as modern devices".**

   b) **Quote:** "On shorter time scales, solar coronal mass ejections **(CME)** can cause geomagnetic storms and **inject electrons and protons into the atmosphere**. Asikainen and Mursula (2005) have shown that during the great storm of March 21, 2001 **electrons became trapped in the SAA and drifted around the Earth with the SAA."**

   c) **Quote:** "The **drift rate** [of the SAA] depends strongly on the **accuracy of the models** [AP8/AE8]'.

   d) **Quote:** "We note that while some properties of the **SAA** are altitude dependent, in the following we will concentrate on the **shape** and **position** of the **SAA**, **which have been shown to be independent of altitude."**

4. **Mozzoni, David**, "*The Changing Geomagnetic Field from the Ionosphere to the Core-Mantle Boundary"*, GeoForschungs Zentrum Potsdam (GFC), Scientific Technical Report STR08/02.

   a) **Quote:** "In this region [= the SAA] the shielding effects of the geomagnetic field have been severely **compromised**, thus **allowing** high energy particles trapped in the Van Allen radiation belt **to penetrate deep** into the upper atmosphere **to altitudes below 100 km.**
   Compromise = a change that makes something worse and that is not done for a good reason

   b) **Quote:** "**The anomaly arises from the eccentric displacement** between the magnetic and geographic **poles** of the Earth …"

c) **Quote:** "The lack of the natural shelter afforded by the geomagnetic field is more than simply a curiosity of the region. It represents a **real hazard,** which can be and does have direct impact on spacecraft, orbiting the Earth **with inclinations between 35^0 to 60^0**, exposing them to **long periods (several minutes)** of stronger than usual radiation **during each orbit**.

d) **Quote:** "In fact orbiting spacecraft, while traversing the region, may be bombarded by particles **with energies up to 10 MeV**, at rates as **high as 3000 cm^{-2} sec^{-1}**, but it only takes particle energies **of 1 MeV** to have the potential to **cause spacecraft damage**.

e) **Quote:** "Humans orbiting in the **ISS** or in spacecraft (like the shuttle), as a result, are potentially subject to **increased** ionizing radiation dose rates as well, which can be biologically harmful.

f) **Quote: "**The effect can be shown to a lesser degree**, even on airplanes that fly through the region."**
   [= the SAA]

5. **Grigorian, O.R., A.N. Petrov, V.V. Romashova,** *"On the Drift of the South Atlantic Anomaly",* WDS'05 Proceedings of Contributed Papers, Part II, 251-256, 2005

   a) **Quote: "Conclusions**: **1. Heinderickx (1996)** calculation of high-energy proton flux in the **SAA** region **do not coincide** with experimental results obtained on board the MIR station". **2.** Experimental distribution of high-energy proton fluxes **obtained onboard the MIR** station **agrees with a magnetic field distribution obtained at the same station experimentally**." **3.** Comparison of the position of **SAA** using dose rate and proton flux distribution in the **SAA** region **shows that positions of these distributions do not correspond."**

6. **Grigorian, O.R., V.V. Romashova, A.N. Petrov**, *"SAA drift: Experimental Results",* Advances in Space Research 41 (2008) 76-78

   a) **Quote: "Conclusions:** and **summarising** the observations onboard various satellites [**COSMOS-484**, 1972; **Intercosmos-24**, 1990] and orbital stations [**SALUT-6**, 1979; **MIR** 1991 & 1998; **ISS**, 2002], we can formulate the following conclusions: **1**., **2**. The comparison of electron fluxes **reveals** that there is a **northward** drift of the **SAA** at the same time with **westward**. **The northward drift of the SAA protons is not observed according our data**."

7. **Dyer, C., A. Sims, C. Underwood,** *"Radiation Belt Observations From CREAM and CREDO",* American Geophysical Union, Geophysical Monograph 97, 1996

   a) **Quote: "Abstract:** The **LEO** observations have shown the drift of the **SAA** and an **altitude dependence** of trapped protons **which is at variance with the AP8".**

   b) **Quote: "Discussion: 1., 2**. The increase in the **SAA** protons with altitude **is less than predicted by the AP-8 model".**

   c) **Quote:** "**Trapped Proton Results**: It was noted that certain **SAA** passes (e.g. orbit **23** of **STS-48** and orbit **40** of **STS-44**) were not predicted when **using the recommended technique of employing the field model pertaining to the data from which the models were created** (i.e. 1970). However, **use of the 1991 geomagnetic field does predict peaks for these orbits** as it accounts for the steady drift of the **SAA** contours to the west due to evolution of the geomagnetic field (**Fig. 1** = 1970 field [orbit misses SAA], **Fig. 2** = 1991 field [orbit intersects SAA])."

   d) **Quote: "Trapped Proton Results: Encouraging agreement** is obtained between the three experiments **despite the different design**. For the region of the **SAA**, the **LET**-spectra observed from **KITSAT** and **POSAT** have been compared with each other and **with predictions based on the AP8 model** for solar minimum, allowing for protons stopping and slowing in the detector. **Figure 4** shows that **agreement is good** considering that uncertainties of a factor of two are inherent in allowing for spacecraft shielding and particle atmospheres."

61

8. **Underwood, C., N.K. Oldfield, C.S. Dyer, A.J. Sims,** *"Long-term Trends in the LEO Radiation Environment as Measured by Radiation Monitors On-board Three UoSAT-Class Micro- Satellires",* ESA Symposium Proceedings on "Environment Modeling for Space-based Applications", ESTEC, Noordwijk, NL, 18-20 September 1996.

    a) **Quote: "**The **AP8 model predictions** were found to be **in good agreement with the flight data**. **Figure 11** shows that the fit between the **AP8MIN** model predictions and the **KITSAT-1 CRE** [800 km] flight data **is very good**. Similarly, the fit between the AP8MIN predictions and flight results for **PoSAT-1** [1330 km] **is good**, although here the predicted flux is slightly low.'

    b) **Quote: "**The **CRE** measurements of the trapped proton environment in the **SAA**, generally, **show good agreement** with the predictions of the **AP8MIN** model, provided the proper account is taken of the very high-**LET**, low-energy protons, slowing and stopping in the detector."

    c) **Quote:** "It would therefore appear **that the AP8 model gives a reasonable basis for modeling the trapped proton environment** of these low-Earth orbits in order to make predictions of single-event effect rates -- at least to within a factor of two".
       Editor: which is the value of the uncertainty factor of the model.

9. **Ginet, G.P., Dan Madden, B.K. Dichter, D.H. Brautigam**, *"Energetic Proton Maps for the South Atlantic Anomaly",* AFRL-RV-HA-TR-2008-1060.

    a) **Quote:** "Proton **beam calibration** for the telescope**, validating** the computer model of the telescope**, have not yet been performed."**

    b) **Quote:** "Our simple application of the **Monte Carlo** results **assumes** an incident isotropic flux **which is not necessarily consistent with observation."**

    c) **Quote**: "**Uncertainties** in the **geometric factor** and **threshold energies** due to the sensor modeling process, **were estimated** by using different characterizations of the proton spectrum when integrating the channel response functions".

    d) **Quote:** "Given the **disparity** in geometric factors it **is reasonable to assume** that the response in the anomaly is predominantly from protons".

10. **Casadio, S., and O. A**rino, *"Monitoring the South Atlantic Anomaly using ATSR Instrument Series",* Advances in Space Research, Vol. 48, Issue 6, pp.1056-1066, 2011.

    a) **Quote: "**The comparison results, reported in **Table 2**, show that the **SAA area** and **strength** are essentially **insensitive to the presence of** fires while the **SAA peak location** is shifted westward by 1^0 and northward by **1.4^0**. Thus the **SAA peak coordinates** evaluated from **SWIR** data **are expected to be biased** by similar amounts with repsect the **VIS** retrievals".

11. **Konradi, A., G.D. Badhwar, L.A. Braby,** *"Recent Space Shuttle Observations of the South Atlantic Anomaly and the Belt Models",* **Advances in Space Res., Vol. 14, No. 10, pp. 911-921, 1994.**

    a) **Quote: "** We know from both part exposure and the current data set that the radiation is very **anisotropic** since it not only has highly peaked pitch angle distribution, but also exhibits **a strong east-west effect**. This, combined with the **uneven shielding distribution** around the spacecraft from pass to pass, **may produce different measured dose** rates **even for identical space points sampled at different times."**

12. **Konradi, A., A.C. Hardy, W. Atwell,** *"Radiation Environment Models and the Atmospheric Cutoff",* **JGR, Vol. 24, No. 3, May-June 1987.**

    a) **Quote:** "The calculations presented here will be based on the **IGRF** for **1975** and fluxes of protons with energies **above 30 MeV** as represented by **AP8MIN**. ----- **Figure 1** shows **B** and **L** contours in the **SAA** at 500 km altitude for epochs **1965(a), 1995(b),** and **2025(c).**

b) **Quote: "**The above described use of the trapped radiation environment models is also based on the assumption that **B** and **L**, <u>**being derived from the first and second adiabatic nvariants,**</u> are themselves invariant. In a <u>**static magnetic field**</u>, this is certainly true and this coordinate system is very successful in ordering particle data and is, therefore, incorporated into the models of the Earth's trapped radiation environment. However**, <u>since the Earth's dipole is decreasing</u>** with a characteristic time of about 1000 years, when calculating particle flux transformations, <u>**all three adiabatic invariants have to be taken into account properly.**</u>

c) **Quote:** "Since the gradient within the geomagnetic cutoff is very steep, within a short time period the order of magnitude flux increases and <u>**even subterranean fluxes are predicted**</u>." ---- "Not only does the flux increase with time, but also increases <u>**disproportionally**</u> at low altitudes and <u>**even below the Earth's surface**</u>, If real, such an increase would have implications <u>**far beyond any one's imagination**</u>."

13. **Casadio, S.O., O. Arino, O. Serpe,** *"Monitoring the South Atlantic Anomaly Using ATSR",* **Living Planet Symposium, 27 June – 2 July, 2010, Bergen, Norway**

a) **Quote:** "However, other satellite missions, <u>**although designed for Earth observation**</u>, have also provided valuable information <u>**on solar flux**</u>. In fact, energetic particles <u>**(such as protons)**</u> <u>**reaching altitudes between 500 and 800**</u> km produce detectable signals by <u>causing spikes</u> (or outliers) in the measured radiances, as the cases of the <u>**NASA MOPITT**</u> instrument on **TERRA** and **DORIS** on **JASON-1**."

b) **Quote:** "Monitoring the <u>**solar particle flux**</u> <u>**reaching the inner belt**</u> of the Earth's magnetic field and **<u>in particular in correspondence of the SAA</u>**.

c) **Quote:** "Regarding the <u>**accessibility**</u> of <u>**solar energetic particles**</u> <u>**to the SAA**</u>."

d) **Quote: "RHESSI, SAMPEX, NYULIN, DMI, ISIRO, PROBA, SREM, SEM-2, POES, MEPED, PROBA-2, TPMU, DSLP:** <u>all these satellite missions</u> <u>**are dedicated**</u> to the **detection and characterization of <u>extraterrestrial particles</u> <u>reaching the inner belt</u>** of the Earth's magnetic field.**

14. **Heirtzler, J.R., "Future Radiation Damage in Space Due to the South Atlantiv Anomaly". Laboratory for Terrestrial Physics, NASA GSFC, Greenbelt, MD 20771, 2000**

a) **Quote: "**The <u>**geographic limits**</u> of the South Atlantic Anomaly**,** as <u>**defined by radiation damage**</u>, are compared to contours if geomagnetic total field intensity, as **defined by the <u>1995 IGRF</u>**, for the <u>**present and recent past**</u>.

b) **Quote: "**The <u>**most likely**</u> **secular variation** of the geomagnetic field <u>**is estimated and used**</u> to <u>extrapolate the geomagnetic field</u> to <u>**the year 2100**</u>.

c) **Quote: "**The **SAA** <u>**greatly influences**</u> the <u>shape</u> of the <u>**geomagnetic field lines**</u>.**"**

d) **Quote:** "The radiation environment causes several types of **hazards**, but here we will look at <u>**one of the most common.**</u> This is the <u>**Sudden Event Upset**</u> **(SEU),** where, apparently, a single particle causes a piece of equipment to malfunction.

e) **Quote: "**If the map of secular change <u>**from the IGRF coefficients**</u> (**Figure 6**) is used to <u>**extrapolate back**</u> from <u>**1995**</u> to <u>**1922**</u> the charts <u>**compare favorably in the South Atlantic**</u>.**"**

15. **Csaadio, S.O., and O. Arino, "Monitoring the South Atlantic Anomaly using ATSR historical data sets", 2013**

a) **Quote: "**The **ATSR's provided consistent SWIR** measurements. The **SWIR** data could be used for fire detection. **But how to <u>discriminate fires</u> from the SAA noise**? <u>**Not easily**</u>, because the **SAA** <u>**"spikes"**</u> <u>**cannot be unambiguously distinguished**</u> from that of the fires."

Etc. etc. etc.

Appendix B

Comments on Appendix A

1. **Hell 2010**: problems with <u>orbit generator</u> (**trajectory calculations**)

2. **Smart and Shea 1999**: problems with <u>data processing</u> and <u>instrument calibration</u> (**geometric factor**, **threshold energy**)

3. **Fuerst 2009**: (a) <u>old vs. new</u> instruments (**sophistication of devices**)

    (b) electrons from the **CME**, trapped in the **SAA**, <u>**drift around**</u> <u>**the Earth**</u> with the **SAA**

    (c) drift rate [= of SAA] **depends strongly** on the <u>accuracy of the models</u>

4. **Mozzoni ????**: (a) <u>proton penetration</u> to **altitudes below 100 km**

    (b) the **SAA** <u>arises from the displacement</u> of the **magnetic and geographic poles**

5. **Grigorian 2005**: (a) **SPENVIS** High energy proton calculations <u>don't coincide</u> with **experiment results** on **MIR**

    (b) <u>position of **SAA** does not correspond</u> **to dose rate and flux distribution**

6. **Grigorian 2008**:

    (a) <u>the North drift of **SAA**'s protons</u> **is not observed** in their data <u>from many satellites</u>

    (b) the <u>altitude dependence</u> of protons **is at variance** with the **AP8** model

7. **Dyer 1996**:

    (a) <u>increase of **SAA'**s protons</u> **with altitude** is **less than produced** by the **AP8** model

    (b) certain shuttle **SAA** passes **were not predicted** when using <u>recommended techniques for using the field model of **1970**</u> [= SPENVIS], however, <u>use of the **1991**</u> model does [=correctly] <u>predict peaks</u>, as it **accounts for the drift**, due to the evolution of the field from **1970** to **1991**

    (c) trapped proton results from **KITSAT** and **POSAT** compared with <u>predictions</u> from **AP8-MIN show good agreement**

8. **Underwood 1996**:

    (a) **AP8** <u>predictions</u> **are in <u>good</u> agreement with flight data**

    (b) **KITSAT-1 CRE** <u>proton measurements in the **SAA**</u> show <u>**very good agreement**</u> with **AP8-MIN** predictions

    (c) it appears the **AP8** gives a **reasonable basis** for trapped proton modeling on **LEO**

9. **Ginet 2008:** (a) **instrument calibration** <u>was not performed</u> for telescope

    (b) **assumed** <u>indirect isotropic</u> **flux** **not consistent with observations**

10. **Cassadio 2011**: **SAA** peak coordinates from **SWIR** data <u>expected to be</u> **biased**

11. **Konradi 1994**: radiation in **SAA** is <u>anisotropic</u>, and uneven shielding around spacecraft <u>from pass to pass may yield different doses</u>, **even for identical points, sampled different times**

12. **Konradi 1987**:

    (a) field calculations for **1965**, **1995**, and **2025** were performed with the **IGRF 1975** model

    (b) expressed concern about **adiabatic invariants**: <u>seams not to be aware</u> that the **IGRF** models are **<u>static</u>** over their 5-year validity period and <u>that all 3 adiabatic invariants are valid</u>

13. **Casadio 2010**:

   (a) solar flux **reaching** altitudes **between 500 and 800** km in the SAA

   (b) monitoring solar particle flux **reaching** the inner belt**, in particular the SAA**

   (c) regarding the accessibility of solar energetic particles to the **SAA**

   (d) **RHESSI, SAMPEX, NYULIN, DMI, ISIRO, PROBA, SREM**, **SEM-2, MEPED, PROBA-2, TPMU, DSLP: all dedicated to the detection and characterization** of *extraterrestrial particles reaching the inner belt of the magnetic field*

14. **Heirtzler, J.R.**

   (a) the geographic limits of the **SAA, as defined by radiation damage**

   (b) the **most likely** secular variation of the geomagnetic field **is estimated** and **used to extrapolate the field** to **2100 [!!!!]**

   (c) the **SAA greatly influences the shape** of the geomagnetic **field lines**

   (d) the radiation environment causes several types of hazards, but here we will look at one of the most common. This is the **SUDDEN Event Upset** (SEU) **[SUDDEN ????]**

   (e) if the map of secular change **from the IGRF coefficients** (Figure 6) is used to **extrapolate back** from **1995** to **1922** the charts **compare favorably in the South Atlantic**. **[!!!!]**

Appendix C

Some Special Comments on the Reviewed Publications

1.   Data concerning the **SAA**, collected by different instruments at different times, have yielded different results, for similar conditions, even when measured at identical points in space. The causes include: **(a)** the large variety of instruments, **(b)** their specific sensitivity and response, **(c)** their calibration and geometric factors, **(d)** their threshold energy, **(e)** their contamination by noise/interference, and **(f)** their accuracy. Contributing could also be the differences in processing and analyzing the data, the relevance and interpretation of the data, and the assumptions made may also contribute to this great variety of results. The examples below highlight some of the challenges faced when using varied instruments and peripheral data.

The listed examples refer to the items contained in section Appendix A.

Example: #2 Smart and Shea
Quote: "*Appendix: **Conversion** from CD-ROM high energy proton flux data <u>to **corrected** proton</u> flux developed by **Sauer (1995**): Procedure: **Convert data back to counts**, <u>correct for side penetration</u> and **<u>apply new geometric factors</u>** to obtain **corrected** flux. Calibration: The greatest unresolved problem is the response of the **HEPD** instrument. The **<u>threshold energy adjustment</u>** and the **<u>geometric factor adjustment</u>** proposed by **Sauer (1995)** are a good step. These are helpful <u>resolving some of the discrepancies in **P8**, **P9**, and **P10** data</u>*".

Example: #3 Fuerst et al.
Quote: "*The AP8/AE8** models <u>are based on data **taken with older instruments**</u> which <u>were not necessarily **as sophisticated as modern devices**</u>.*"

Example: #9 Ginet 2008
Quote: "*Proton **beam** <u>calibration</u> for the telescope, **<u>validating</u> the <u>computer model of the telescope</u>, <u>have not yet been performed</u>".***

Quote: "<u>Uncertainties</u> in the <u>geometric factor</u> and <u>threshold energies</u> due to the <u>sensor modeling process, **were estimated**</u> by <u>using different characterizations</u> of the proton spectrum when integrating **<u>the channel response functions</u>**.*"

Quote: *Given the **<u>disparity</u>** in **<u>geometric factors</u>** it is **reasonable to <u>assume</u>** that the <u>response in</u> the <u>anomaly</u> is predominantly from protons."*

2.   Based on the assumptions presented in some of the of **SAA** related publications, not all authors may be familiar with the special physics, the processes, and the conditions involved with the **SAA** and its origin, area, size, drift, strength, evolution, and accessibility to solar energetic particles. Publications that mention "extraterrestrial energetic particles", solar or galactic in origin, that are supposedly capable of reaching (i.e. penetrating) the **SAA**, to altitudes below 100 km, within the inner zone of the Van Allen belts, may not be considering the current understanding of atmospheric cutoff and magnetic rigidity.

Example: #4 Mozzoni, David
Quote: "In this region **[= the SAA]** <u>the shielding effects of the geomagnetic field have been severely compromised</u>**, thus allowing high energy particles trapped in the Van Allen radiation belt to <u>penetrate deep into the upper atmosphere to altitudes below 100 km.</u>"**

3.   The **SAA**, when first detected, was considered an "anomaly" of the field, an aberration. But the SAA is really not an anomaly at all, just an apparent locally weaker area of the Earth's magnetic field over Brazil. This area is the consequence of simple geometry, namely the tilt, the eccentricity, and the displacement of the dipole axis by about 500 km toward the North Pacific. As a result, the magnetic unit sphere lies outside the northern physical Earth over the Pacific, and therefore has a higher local field strength at the surface of the globe, because it is closer to the dipole center, it lies inside the physical Earth over the South Atlantic and has a lower local field strength at the surface of the globe, because it is farther away from the center of the dipole.

Apparently, though, there is still prevailing some confusion in the community about this topic, judging by the following statement:

Example: #4 Mozzoni, David
Quote: "*The anomaly **arises** from the **eccentric displacement** between the magnetic and geographic **poles** of the Earth ….."*.

4.   Regarding the geomagnetic field models, the internationally accepted and widely used **IGRF** model is being updated and re-issued every 5 years. It has accounted for long scale changes of the field, which occurred during each 5-year time period. The secular variation terms, accompanying every new 5-year version, however, should not be used to extrapolate the field into the future for more than the 5 years, maximum.

Example: #12 Konradi, A., A.C. Hardy, W. Atwell
Quote: *"The calculations presented here will be based on the **IGRF** for 1975 and fluxes of protons with energies above 30 MeV as represented by **AP8MIN**. ---- **Figure 1** shows **B** and **L** contours in the **SAA** at 500 km altitude **for epochs 1965(a), 1995(b), and 2025(c).***

Example: #14 Heirtzler, J.R.
Quote: *"The most likely secular variation of the geomagnetic field **is estimated** and used to **extrapolate** the geomagnetic field **to the year 2100**."*

Quote: *"If the map of secular change from the **IGRF coefficients** (Figure 6) **is used to extrapolate back from 1995 to 1922** the charts compare favorably in the South Atlantic."*

5.   The adiabatic invariants, that are the basis for McIlwain's magnetic shell parameter "**L**", require a static magnetic field for all three to be valid. In the case of the **IGRF** models, all changes in the field over the 5-year period of each new model issued, have been accounted for; the field is indeed static over that time, and its use is perfectly safe and correct, in terms of the three adiabatic invariants.

Example: #11 Konradi, A., A.C. Hardy, W. Atwell
Quote: *"The above-described use of the trapped radiation environment models is also based on the assumption that **B** and **L**, **being derived from the first and second adiabatic invariants**, are **themselves invariant**. In a static magnetic field, this is certainly true and this coordinate system is very successful in ordering particle data and is, therefore, incorporated into the models of the Earth's trapped radiation environment. However, **since the Earth's dipole is decreasing** with a characteristic time of about 1000 years, when calculating particle flux transformations, **all three** adiabatic invariants have to be taken into account properly*."

6. The **SAA** is nothing more than an integral part of the inner zone of the Van Allen belts. It is not an independent, separate, or special entity. All the rules that apply to the inner zone, apply also to the **SAA**. It has the same atmospheric cutoff, the same intensity and distribution of trapped particles, the same magnetic field effects, and experiences the same penetration of very high energy cosmic rays. Specifically, most solar-flare and **CME** protons, being deflected by the magnetic field (rigidity), cannot reach a major part of the inner zone, and hence the **SAA**, because in order to do so they need to have energies in excess of **2.9 GeV**. These energies have not been detected in such events.

Example: #13 Casadio et al.
Quote: *"Monitoring the **solar particle flux** **reaching** the inner belt of the Earth's magnetic field and in particular in correspondence of the SAA*.

7. Although trapped electrons and protons drift around the Earth in opposite directions, the drift of the **SAA** is strictly a local phenomenon, centered at the South Atlantic over Brazil.

Example: #3 Fuerst et al.
Quote: *"On shorter time scales, solar coronal mass ejections (CME) can cause geomagnetic storms and inject electrons and protons into the atmosphere. Asikainen and Mursula (2005) have shown that during the great storm of March 21, 2001, **electrons became trapped** in the SAA and **drifted around the Earth** **with the SAA.**"*

8. Incorrect assertions about the **SAA** may stem from using data from unrelated spacecraft missions, and their instruments , and measurements. In the examples below **none** of these **missions/satellites** were either **dedicated**, **designed**, **qualified**, or **intended** for a study of the **SAA**. Page 58 lists many unrelated projects, frequently referenced in the reviewed literature, and describes their correct mission definitions.

Example: #13 Casadio et al. 2010
Quote: *" **RGESSI, SAMPEX, NIULIN, DEMETER, DMI, ISIRO, PROSA, SREM, SEM-2, POES, MEPED, TPMU, DSLP = all these satellites** are **dedicated** to the **detection and characterization** of extraterrestrial energetic particles **reaching the inner belts of the Earth's magnetic field**."*

Quote: *"However, other satellite missions, **although designed for Earth** observation, have also provided valuable information **on solar flux**. In fact, **energetic particles** (**such as protons**) **reaching altitudes between 500 and 800 km** prodiuce detectable signals by causing spikes (or outliers) in the measured radiances, as the cases of the **NASA MOPITT** instrument on **TERRA** and **DORIS** on **JASON-1**."*

9. A far more serious and potentially dangerous, misrepresentation is the issue of solar proton event particles penetrating the inner zone of the Van Allen belts (aka: the **SAA**), and reaching altitudes below 100 km. One paper claims effects on airplanes that fly through the **SAA, an impossibility.**

Example: #4 Mozzoni, David
Quote: *"In this region [= the SAA] the shielding effects of the geomagnetic field have been severely compromised, thus allowing high energy particles trapped in the Van Allen radiation belt **to penetrate deep into the upper atmosphere to altitudes below 100 km.**"*
Quote: *"**The effect can be shown** to a lesser degree, **even on airplanes that fly through the region.**"*

Example: #13 Casadio et al.
Quote: *"Regarding the **accessibility of solar energetic particles** **to the SAA**."*

Quote: *"However, other satellite missions, **although designed for Earth** observation, have also provided valuable information **on solar flux**. In fact, **energetic particles** (**such as protons**) **reaching altitudes between 500 and 800 km** prodiuce detectable signals by causing spikes (or outliers) in the measured radiances, as the cases of the **NASA MOPITT** instrument on **TERRA** and **DORIS** on **JASON-1**."*

Quote: *"Monitoring the <u>**solar particle flux reaching**</u> the inner belt of the Earth's magnetic field and **in particular in <u>correspondence of the SAA</u>**."*

10. Some authors are confused as to the nature of the **SAA** and of the inner zone of the Van Allen belts, which in most cases are considered two different entities that interact with and influence each other. It is not understood that the **SAA** and the inner zone of the Van Allen belts are one and the same, with no physical differences, having only different names. The fact that the **SAA** is, in essence, not even a true anomaly, is often overlooked.

<u>Example</u>: #14 Heirtzler, J.R.
<u>Quote</u>: "*The SAA <u>**greatly influences the shape**</u> of the geomagnetic field lines*.**"**

<u>Example</u>: #4 Mozzoni, David
<u>Quote</u>: *"<u>The anomaly arises</u> from the <u>**eccentric displacement**</u> **between the magnetic and geographic <u>poles</u>** of the Earth … ".*

Quote: *"The main feature visible in Figure 3.1 is represented by the large red region, <u>indicating an elevated proton flux count</u> **corresponding to the SAA**, <u>which arises</u> **from the relative proximity of the <u>inner radiation belt.</u>"***

11. Another challenging feature of the **SAA** is that both its <u>shape</u> and <u>size</u>, as well as its position, are very much **altitude dependent**. This fact is easily demonstrated with any field model used, any proton model considered, any energy selected, and for any time period involved: in each case the shape of the **SAA** is different at <u>every altitude</u>.

<u>Example</u>: #3 Fuerst et al.
<u>Quote</u>: *"We note that while some properties of the SAA are altitude dependent, in the following we will concentrate on the <u>**shape**</u> and <u>**position**</u> of the SAA, **which have been shown to be <u>independent</u> of altitude."***

12. The use of peripheral data from unrelated experiments cannot accurately **<u>define</u>** uniquely the **real size and shape** of the **SAA**. As stated before, the anomaly can have (<u>at the same time</u>), multiple, **varying shapes and sizes**, depending on the parameters selected for plotting (e.g. the field model, the particle model, the particle energy, the altitude, or special data sets from an unrelated experiment, etc.).

<u>Example</u>: #14 Heirtzler, J.R.
<u>Quote</u>: *"The <u>**geographic limits**</u> of the South Atlantic Anomaly, <u>**as defined by radiation damage**</u>, are ……".*

13. A further misconception is the assumption that the **SAA** , which is just a name defining a region, has influence and power that can impact physical processes, as the quotation below implies. In reality, the opposite is true, i.e. the geomagnetic field lines influence the shape of the **SAA** (in essence: the dipole field)
<u>Example</u>: #14 Heirtzler, J.R.
<u>Quote</u>: "*The SAA <u>**greatly influences the shape**</u> of the geomagnetic field lines*".

Appendix D

Future Evolution of the Earth's Magnetic Field

A special study was performed with data obtained from the officially established "International Geomagnetic Reference Field" (**IGRF**), issued in updated form every 5 years by the "International Association of Geomagnetism and Aeronomy" **(IAGA).**

The model is equipped with first and second order time derivatives, describing the secular variation of the field. Each new 5-year issue is based on current global measurements of the field.

The geomagnetic field is composed of a major dipole term and of additional lesser non-dipole terms (quadrupole and higher).

The field experiences two significant variations that are not constant in time: (a) the drift of the magnetic poles and (b) the gradual decline in the field strength.

The study was based on eleven versions of the **IGRF**, from 1960 to 2010, using data calculated with the secular variation terms in each model period.

All these field models are widely being used in research and application, involving the radiation of the Van Allen belt particle models, where a primary concern is the use of the parameters **B** and B_0, as obtained from the updated **IGRF** field, at epochs later then the construction dates of the particle models.

B_0 is the field strength at the point where the magnetic field-line intersects the magnetic equator, but it is not necessarily the location of the absolute minimum **B** value on that field-line, which may be off the equator. (Figure 1)

Specifically, the exact values are respectively:
B(1960) = 21300.4 nT,   B(2010) = 19358.7 nT,   Differ. = 1941.7 nT

B_0(1960) = 18267.9 nT
B_0(2010) = 16819.0 nT
Differ. = 1448.9 nT

Thus: 1941.7 – 1448.9 = **492.8 nT**: is the relative decrease of **B** vs B_0 in 50 years

Then: 19358.7 ÷ 492.8 = **39.283**: is the number of 50-year periods to reach equal values

And: 39.283 × 50 = **1964.15**: is the number of years, when **B** will be equal to B_0.

Assuming that the change in the field remains constant during this time, which is questionable, these calculations imply a disappearance of the field, i.e. a possibility magnetic reversal, as experienced many times before on geologic scales.
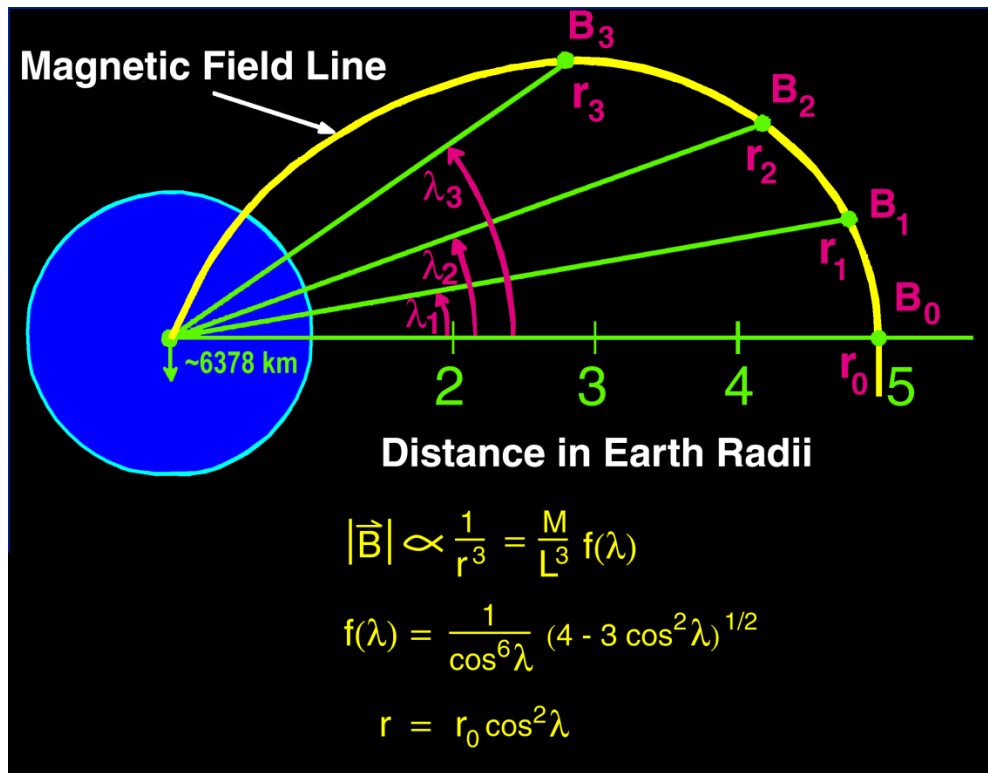
Figure 1: Magnetic coordinate system.

A plot of the **B** and **B₀** intensities from 1960 to 2010 (Figure 2), obtained from the corresponding eleven **IGRF** 5-year models, clearly indicates a gradual convergence of the positional field strength to the relative **B₀** value. It is obvious that **B** decreases faster than **B₀** by about **500 nT** in 50 years.
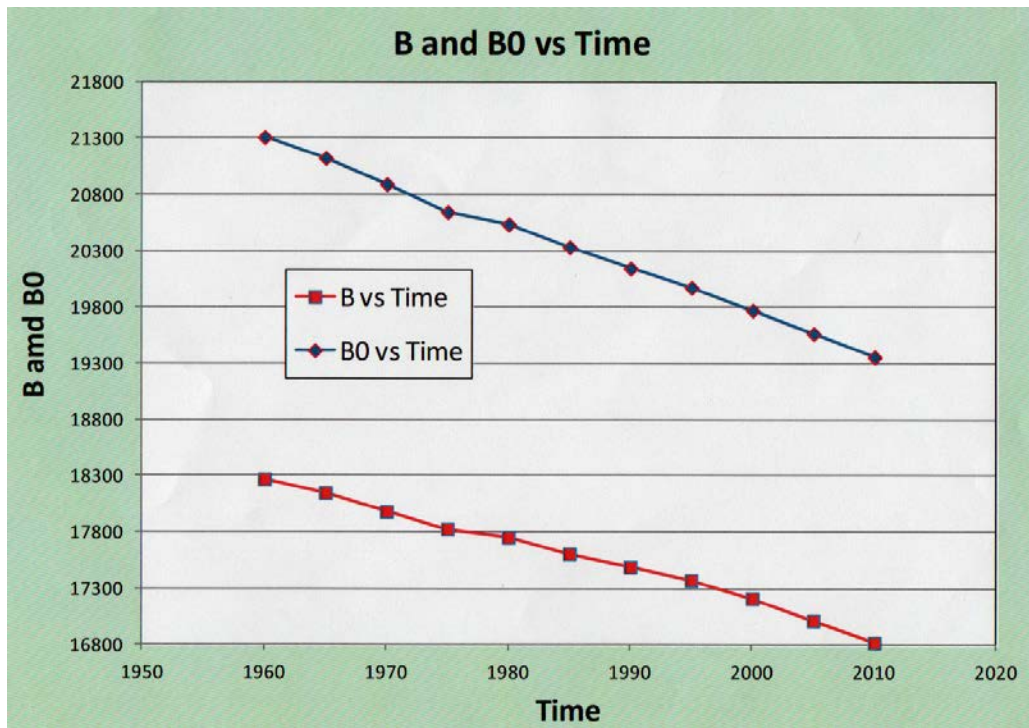

Figure 2: B and B0 magnetic field intensities from 1960 to 2010.

Appendix E

General Information on SAA Radiation

Inclination Dependence

- Greatest flux is experienced in the inclination range $0^0 < i < 35^0$.
- For $i > 35^0$, fluxes rise gradually until about $i = 60^0$.
- Over $i = 60_0$, inclination has little effect on flux levels.

Altitude Dependence

- Largest fluxes occur between 200-600 km, increasing as altitude rises.
- For altitudes $h > 600$ k m, fluxes increase more gradually.
- Over about 1500 km, orbits are essentially outside the SAA.

Peak Flux Positions

- Location of peak fluxes depends on particle energy, for both electrons & protons.

Magnetic Rigidity Protection

- Shielding by geomagnetic field from cosmic rays and solar event particles is dependent more on <u>inclination</u> than on <u>altitude.</u> The degree of <u>inclination</u> is most important for shielding from these particles.
- Inclinations up to about 45^0 are almost totally shielded.
- Inclinations greater than 45^0 experience progressively larger exposures.
- As inclinations reach 90^0, the satellite is outside the closed magnetic field lines and is fully exposed to cosmic rays and solar event particles in the polar regions.
- During major solar particle events or magnetic storms, satellites with inclinations below ~45^0 may not be completely shielded, due to the compression of the field lines, resulting in solar flare and cosmic ray particles reaching previously unattainable altitudes and inclinations.
- As <u>altitude</u> increases the regions of space accessible to cosmic rays and solar event particles gradually increase also.

Systemic Changes

- Solar cycle variations
- Seasonal variations
- Diurnal variations
- Magnetic field secular variations

Occasional Variations

- Solar events (flares, CMEs)
- Magnetic storms
- Geomagnetic jerks
- Space weather effects